R. & M. No. 3692

MINISTRY OF DEFENCE (PROCUREMENT EXECUTIVE)
AERONAUTICAL RESEARCH COUNCIL
REPORTS AND MEMORANDA

Calculations of the Effect of Blowing from the Leading Edges of a Slender Delta Wing

By J. E. BARSBY

LONDON: HER MAJESTY'S STATIONERY OFFICE
1972

£2·75 NET

Calculations of the Effect of Blowing from the Leading Edges of a Slender Delta Wing

By J. E. BARSBY†

Reports and Memoranda No. 3692†
April, 1971

Summary.

The thin-jet model, applied by Spence to the study of the jet flap, is combined with the vortex-sheet model, applied by Mangler and Smith to the study of leading-edge separation, to study the effect of blowing from the leading edges of a delta wing at incidence. A jet-vortex sheet, supporting a pressure difference related to the curvature of the streamlines in it, leaves the leading edge in a direction tangential to the wing plane and rolls up into a spiral above the wing. The inner part of the spiral is replaced by an asymptotic representation and the properties of this configuration are calculated by slender-body theory for the case of conical flow. The effects of the three basic parameters—the coefficient of blowing momentum, the initial angle between the jet streamlines and the leading edge and the ratio of the angle of incidence to the apex angle of the wing—are covered in the calculations.

Blowing is shown to increase the lift on the wing and to increase the circulation about the vortex, while displacing it upwards and outboard. The limited comparisons which can be made with experimental results are encouraging.

*Replaces RAE Technical Report 71077 – A.R.C. 33 029.

†School of Mathematics and Physics, University of East Anglia. This work was carried out under a research agreement between the University and the Ministry of Defence (Aviation Supply), monitored by Aerodynamics Department, RAE.

LIST OF CONTENTS

1. *Introduction.*

When a slender delta wing is placed at incidence to a uniform stream, the shear layers which separate from the leading edge roll up to form two strong vortex cores close to the upper surface of the wing. One feature of such concentrated vortices is the very low pressures that can be included in their core regions. Such low pressure regions existing just above the wing upper surface can contribute an appreciable amount to the lift.

In this Report we calculate the effect on such a flow, of a thin jet of air blown out from the leading edges of a flat plate delta wing, the initial direction of the jet being in the plane of the wing. We shall show that in general there is an increase in the normal force on the wing, and a tendency for the vortex to strengthen and to move both outboard and upward. Solutions have been found for different jet strengths and directions, and for various incidences, for a flat plate delta wing with a semi-apex angle of 20 degrees.

The Report is divided into six sections. In this section we first outline the formulation of the problem and discuss the use of a vortex-sheet model for the flow, then follow with the approximations that are necessary to enable us to find a solution, and conclude with a brief discussion of the results. In Section 2 the mathematical problem of constructing a velocity potential in terms of the unknown position and strength of the two jet-vortex* sheets is formulated, together with the boundary conditions that the potential must satisfy. In Section 3 the iterative numerical technique for calculating the position and strength of the two vortex sheets is described. The programming techniques used are outlined in Section 4 where the range of solutions obtained, and the role of the tolerances allowed in satisfying the boundary conditions in the iterative procedure is also discussed. Section 5 contains a discussion of the results and in Section 6 comparisons are made with previously obtained experimental results.

1.1. *Previous Solutions for the Leading-edge Vortex Problem.*

The general three-dimensional flow problem described above has, as yet, proved intractable, and the solution attempts that have been made so far have relied upon certain simplifying assumptions suggested by experimental features. The assumptions which have been made in general take the flow to be inviscid and conical, and incorporate a slender-body approximation. A conical flow is one in which the velocity of the fluid is constant along any half-line through the apex of the delta wing.

Early calculations for the leading-edge vortex problem were performed by Legendre[1,2], Brown and Michael[3], and Mangler and Smith[4]. The models for the flow proposed by these authors involved condensing all the vorticity contained in the flow field onto singular lines and surfaces and treating the rest of the flow field as irrotational. The assumptions of conicality and of slender-body theory reduced the problem to one of solving a two-dimensional Laplace equation in a plane normal to the wing centre line, the cross-flow plane. The feeding of vorticity from the leading edge to the vortex core was not represented sufficiently well for these models to produce good agreement with experimental results.

Smith[5] proposed an improved numerical technique whereby the boundary conditions which are to be satisfied on the vortex sheet, and which represent the feeding of vorticity, can be applied at as many points as is deemed necessary. Thus the flow near the leading edge can be more accurately represented than in the earlier works referred to above. The results obtained show better agreement with experiment.

Further analysis has been carried out by Stewartson and Hall[6] on the structure of the core region of a leading-edge vortex, where an inviscid outer solution has been found and matched with a viscous inner solution. Mangler and Weber[7] investigated the structure of a core region for a tightly rolled vortex sheet where some of the assumptions of slender-body theory that are used in this Report are violated. A significant result of Mangler and Weber's work was that the leading terms of the velocity components in the expansion given for the core region agree with those of Hall[8], who considered a vortex core with distributed vorticity. An inviscid compressible leading-edge vortex core problem has been investigated by Brown[9] and a more general study of vortex cores has been carried out by Küchemann and Weber[10].

1.2. *Assumptions.*

The method used for the solution of the title problem is an adaptation of the numerical technique

*Defined in Section 2.

developed by Smith[5], incorporating the thin-jet approximation exploited by Spence[11] in his treatment of the jet flap. The basic assumptions made for the flow include those made by Smith and are mentioned only briefly below. For further discussions of the implications of these assumptions reference may be made to the work of Smith. The assumptions made include,

(i) The effects of viscosity are ignored and an inviscid model studied. Although viscosity is important in establishing the flow, its effects are confined to the very small regions near the core centre, along the viscous shear layers, and in the boundary layers on the wing surface. These regions are considered to be small enough for viscosity to be neglected throughout. We shall also ignore the effects of the smaller vortex that can form owing to the secondary separation of the flow as it is swept outboard under the main vortex.

(ii) All the vorticity in the fluid is assumed to be condensed onto two vortex sheets originating at the leading edges. In the numerical treatment of the model the inner parts of these vortex sheets which represent the core region of the vortex are replaced by two line vortices. The shear layer which springs from the leading edge is thus represented by a finite vortex sheet. Apart from these singular lines and surfaces the flow is assumed to be irrotational.

(iii) Experimental flow studies indicate that the flow over the forward part of a delta wing is approximately conical. The assumption of conical flow which we make, simplifies the problem greatly by reducing the number of independent variables from three to two.

(iv) The equation for the velocity potential in compressible inviscid isentropic flow is highly non-linear. Since a flat plate delta wing of small semi-apex angle at low incidence is considered, we can reduce the three-dimensional non-linear equation to a two-dimensional Laplace equation in the cross-flow plane by making the assumptions of the slender-body theory of Munk, Jones and Ward. This approximation becomes exact in the limit as the incidence and semi-apex angle tend to zero in constant proportion.

(v) The effects of the jet blowing air out from the leading edge are calculated using the thin jet flap approximation of Spence[11]. The jet is considered to have width δ and is separated from the main flow by two vortex sheets. These vortex sheets must from Helmholtz's theorem form stream surfaces in the inviscid flow. Any entrainment of fluid from the main stream into the jet is not represented in the model and the magnitude of the momentum flux in a jet streamtube remains constant. The flow in the jet between these two vortex sheets is considered to be inviscid and irrotational, and from these assumptions we can calculate the pressure jump across the jet. If we define J to be the momentum flux in the jet per unit length, then we have that $J = \delta\rho_J V^2$ where ρ_J is the density and V the speed of the jet fluid. It can be shown that the pressure difference across the jet at any point is proportional to the product of the momentum flux J and the curvature of the jet streamline at that point. Finally we take the double limit $\delta \to O$, $V \to \infty$ keeping J constant. The limit effectively reduces the jet of air to a singular surface originating from the leading edge. This new surface is coincident with the vortex sheet, forming a combined sheet called a jet-vortex sheet. A jet-vortex sheet is a vortex sheet which carries a pressure difference across its surface. The presence of this pressure difference across the jet-vortex sheet contributes to the distribution of vorticity on the sheet. The mass flux in this jet-vortex sheet is equal to $\lim_{\delta \to 0} \delta\rho_j V$ which is, of course, zero. However, the source effect of a thin jet is usually negligible compared with the effects of the momentum flux in the jet.

The effect of the assumptions (i) to (v) outlined above is to reduce the problem to that of solving a free boundary value problem for the two-dimensional Laplace equation in the cross-flow plane. Boundary conditions have to be satisfied on the wing surface, at infinity, and on the jet-vortex sheets which spring from the two leading edges of the wing. As in the case with no blowing, we have to calculate the position and strength of a singular jet-vortex sheet embedded in the fluid. In the absence of blowing, the pressure difference across the sheet is zero, the effect of the jet is to enable the surface to sustain a pressure jump. The pressure jump across the sheet is calculated as a function of the sheet shape which is unknown *a priori*.

Morgado and Craven[12] attempted a solution to the leading-edge blowing problem by assuming that in the thin-jet limit as $\delta \to 0$, the jet streamlines could be considered to lie in the cross-flow plane, and hence the momentum flux of the jet along the trace of the sheet in the cross-flow plane is constant.

However Maskell[13] pointed out that in an inviscid fluid the fluid particles in a thin jet will only experience a force due to the pressure difference across the sheet. Consequently the direction of acceleration of these particles, which lies along the principal normal to the path which they follow, must also lie along the surface normal of the sheet. Hence the principal normal of the path of a particle in the jet must coincide with the surface normal of the sheet. This is the condition for the particle path to be a geodesic line in the sheet surface.

The assumption of conical flow implies that the sheet is a conical surface, and so the calculation of the geodesic lines is relatively straightforward. Also since conical surfaces are developable, a useful overall picture of the jet-vortex sheet is available as follows. A developable surface is one which can be 'unrolled' or 'rolled' without stretching or tearing the surface. The jet-vortex sheet can, therefore, be 'unrolled' into a plane surface. The geodesics, since they are lines of shortest distance in the sheet, become straight lines in this 'unrolled' plane. If we consider Figs. 1 and 2 we see that the particles of fluid issuing from the leading edge to form the jet only extend a finite distance along the trace of the vortex sheet in the cross-flow plane. The distance the jet extends along the sheet clearly depends on the angle between the initial direction of the jet and the wing centre line, but is independent of the jet strength.

Since the calculations described below are carried out in the cross-flow plane, we need to know the pressure jump across the trace of the sheet in this plane. The pressure jump is a function of the curvature of the jet streamline at the point under consideration, and of the jet strength. Hence as we follow the trace of the sheet around in the cross-flow plane we calculate the curvature of separate geodesics as they intersect this plane. The last such geodesic on the trace is the one that originates from the apex. This geodesic is a straight line in the vortex sheet and hence has zero curvature. In a conical theory we must have a conical jet, thus the strength of the jet increases linearly as we move away from the apex, and the strength of the jet geodesic originating from the apex is zero. In the calculation, the curvature and pressure jump are calculated along the trace until the curvature reaches zero at which point the pressure jump across the sheet becomes zero, as in the case of no blowing.

1.3. *Solution Procedure.*

The calculation described in Section 2 is carried out in the cross-flow plane. The simplifying assumptions which we make reduce the problem to the solution of a two-dimensional Laplace equation, and thus a transformation of the cross-flow plane can be made to simplify the problem. Since the position of the jet-vortex sheet on which boundary conditions are prescribed is unknown, it is not possible to use a transformation which will transform the sheet into some simple, known curve. However, it is possible to transform the plane so that the wing centre line becomes part of the line of symmetry, and in that way we can automatically satisfy the boundary condition on the wing.

The jet-vortex sheet is split into two parts, the inner part is represented by an isolated line vortex, and is joined to the end of the finite outer part of the sheet by a cut which renders the dynamic variables single-valued. The position and strength of the finite outer part of the vortex sheet is determined numerically by its position and strength at n discrete 'pivotal' points along its length. The length of the finite outer part of the sheet can be varied and the number of pivotal points that specify it can also be varied. This allows a more accurate representation of the jet-vortex sheet using either a longer finite part or perhaps an increase in the number of pivotal points or both. The positions of these pivotal points are measured in polar coordinate form in the transformed plane with the isolated vortex as origin. The polar angles are held fixed throughout the whole calculation, thus the n polar distances, the n values for the strength of the sheet, and the position and strength of the isolated vortex, form a set of $2n+3$ unknowns to be determined.

The length of the part of the jet-vortex sheet which carries momentum depends primarily on the angle β, the angle between the initial direction of the jet and the wing centre line. For sufficiently large β the jet streamlines or geodesics may extend beyond the end of the finite representation, or outer part of the vortex sheet, in the cross-flow plane. The position of the inner part of the jet sheet is calculated using an asymptotic method not dissimilar to that of Mangler and Smith[4]. The effect of the pressure jump across this inner part of the jet sheet is represented as a force which has to be sustained by the vortex and cut. Hence the force on the vortex and cut is only zero, as in the case without blowing, when the angle β

is small enough to keep the effect of the jet within the length of the finite outer part of the jet-vortex sheet.

The calculation procedure outlined below determines the $2n+3$ unknowns subject to the following $2n+3$ conditions.

(i) A Kutta-Joukowski condition that the velocity is finite at the leading edge.

(ii) A condition that the force sustained by the vortex and cut is equal to the force arising from the pressure difference across the inner part of the jet sheet. Since the two components of the force must vanish separately, this represents two conditions.

(iii) A pressure condition that the pressure jump across the sheet is prescribed as a function of its shape. This condition is applied at n intermediate points on the sheet, that is at the $n-1$ points halfway between the pivotal points and at one point between the first pivotal point and the leading edge.

(iv) A velocity condition that the velocity at the surface of the sheet is consistent with the sheet being a stream surface in the three-dimensional flow. This condition is also applied at the n intermediate points.

The determination of the $2n+3$ unknowns is iterative and follows closely the successful procedure devised by Smith[5] in the case where there is no blowing. A good approximation to the solution to start the procedure is necessary to ensure rapid convergence. The calculation consists, essentially, of three separate nested iterations. For convenience we label these three iterations A, B, C.

Iteration A first calculates the pressure jump across the jet-vortex sheet at the n intermediate points using the initial approximation for the shape of the sheet. With the isolated vortex and sheet position fixed, it then calculates new values for the strengths of the isolated vortex and the finite part of the vortex sheet at the n pivotal points by satisfying the pressure condition and the Kutta condition. The equations involved are non-linear and an iterative method is used for their solution. Since the iteration scheme does not change the shape of the sheet, the pressure jump due to the jet need only be calculated at the beginning of this iteration. The new values obtained for the strengths are used as the new approximation and the process repeated until the maximum change in any of the strengths is less than a prescribed tolerance.

The pressure and Kutta conditions thus satisfied, iteration B finds a vortex position which satisfies the force condition on the vortex and cut. With the new values for the strengths replacing the old in the initial approximation, iteration B calculates the force due to the inner part of the jet sheet and then the force on the vortex and cut due to the flow field. The difference between these two forces is stored. The isolated vortex is moved to a new position and the polar distances of the pivotal points are adjusted since they are measured from the isolated vortex. The adjustments are made so that the end of the finite part of the sheet moves with the vortex, and the end near the leading edge still joins the leading edge smoothly. Iteration A is recalled and a new set of strengths for the isolated vortex and the jet-vortex sheet are calculated for this new vortex position. The second force difference is calculated and stored. The vortex is then moved to a third trial position, the sheet shape is adjusted, and iteration A calculates a third set of sheet and vortex strengths. The third force difference is calculated and stored. We now have the values for this force difference for the vortex in three trial positions, in each case with the pressure and Kutta conditions satisfied. We use the method, proposed by Warner[14], as used by Levinsky, Wei and Strand[15] which assumes that the correct vortex position, which satisfies the prescribed force condition, is a linear function of the force difference. The three trial positions give six equations from which the true vortex position can be estimated. The vortex is moved to this new position, the sheet adjusted, and iteration A calculates the vortex and vortex-sheet strengths associated with this position. A test is applied to check if the absolute value of the square of the new force difference is less than a prescribed tolerance. If this is not the case the 'worst' trial position is then replaced by the new one, and another vortex position is calculated. The iteration is repeated until a vortex position is found for which the absolute value of the square of the force difference is less than the prescribed tolerance.

With the pressure conditions, Kutta condition, and the force conditions satisfied iteration C calculates the changes required in the n pivotal distances for the sheet to satisfy the velocity condition. If these changes are found to be greater than a prescribed tolerance, it is necessary to scale down the changes before they are added to the polar distances, in order to prevent the procedure becoming unstable. When the shape of the sheet has been adjusted in this way the pressure, Kutta, and total force conditions will no longer necessarily still be satisfied and the whole procedure is now repeated from the beginning.

This continues until the changes in the polar distances are less than some prescribed tolerance at which point a solution is said to have been found.

1.4. *Results.*

Attention has mainly been centred upon the lift increments, or more correctly the normal force increments ΔC_N, that can be obtained by blowing with different strengths in various directions. This normal force increment is the increase in the normal force on the wing obtained for a particular configuration, in excess of that obtained for the same configuration without blowing. For a fixed blowing coefficient C_μ the normal force increment ΔC_N increases steadily with the blowing angle β until it reaches a maximum for a blowing direction approximately normal to the leading edge. This contrasts with an experimental survey by Alexander[16] whose results suggested that the lift increment was approximately constant for various blowing directions, only falling to zero when the blowing direction was close to the leading edge. Comparison of the magnitude of ΔC_N can more appropriately be made with the results of Trebble[19], who employed a slot of conical geometry on a delta wing. If the calculated increment in normal force is reduced to allow for the effect of the trailing edge in the same proportion as the basic normal force is reduced, then reasonably close agreement is obtained with the measured variation of ΔC_N with C_μ. The relevance of the experimental results is discussed in more detail in Section 6.

As the effect of the blowing increases (by increasing the momentum flux J or the inclination of the jet, β), the vortex system moves outboard and upwards. At the leading edge the curvature of the jet-vortex sheet decreases, and towards the core region it becomes less tightly rolled. The circulation about the isolated vortex is shown to increase as the blowing angle increases, but the circulation about the part of the sheet near the leading edge decreases. The net effect is one of increased total circulation associated with the positive normal force increment. The variation of total circulation with blowing angle shows the same general characteristics as the variation of ΔC_N with blowing angle. The above general features of the changes in the flow field which take place as the blowing angle increases for a fixed blowing coefficient are reflected in the surface pressure distribution. These show that the suction peak is larger than for the case of no blowing and that it is displaced outboard. Since the pressure difference across the wing surface does not now fall to zero at the leading edge, the effect of the presence of the jet is somewhat similar to an end-plate effect.

2. *Mathematical Treatment of the Model.*

2.1. *Governing Equations.*

With reference to Fig. 3 we introduce a right-handed coordinate system $0xyz$ with origin 0 at the apex of the delta wing, x-axis along the wing centre line, z-axis normal to the wing surface, and y-axis to starboard. Let the wing apex angle be 2γ, and the initial direction of the jet issuing from the leading edge in the plane of the delta wing be at angle β to the wing centre line. The wing incidence α to a uniform stream U is assumed to be small, as is γ, so α/γ is 0(1). We write the velocity potential for the flow as

$$Ux+\Phi \tag{1}$$

where, since $\cos\alpha \simeq 1$, Φ represents the potential of the disturbances introduced by the wing in a uniform stream U, together with the z-component $U\sin\alpha$ of the uniform stream. From the assumptions which we make, and which have been described in Section 1.2, Φ can be shown to satisfy the two-dimensional Laplace equation,

$$\Phi_{yy}+\Phi_{zz}=0\,, \tag{2}$$

with boundary conditions

$$\Phi_z=0 \text{ on the wing, } z=0,\ |y|\leqslant s\,, \tag{3}$$

$$\Phi\to Uz\alpha \qquad \text{as } Z=y+iz\to\infty\,, \tag{4}$$

together with conditions on the jet-vortex sheet itself. The calculation takes place in the cross-flow plane in which the wing semi-span is of length $s = x \tan \gamma$.

The potential Φ can be written as the real part of a complex analytical function $W(Z)$ in which x enters as a parameter. Z is defined in equation (4), and is a complex representation of the cross-flow plane.

We now consider the conditions on the jet-vortex sheets. The trace of the sheet in the cross-flow plane is shown in Figs. 3 and 4. Let s denote the wing semi-span, σ the arc length of the trace, let n be the unit normal to the trace, and let the radius vector from the origin have length $\tilde{r}_1$ and be at angle θ_1 to the y-axis. The angle ϕ_1 is defined as the angle between the radius vector $\tilde{r}_1$ to a point on the trace and the tangent to the trace at that point. From the condition that the jet-vortex sheet, given by $S(x, \tilde{r}_1, \theta_1) = 0$, is a stream surface in the flow, which is required by Helmholtz's theorem, we must have

$$\underline{V}.\nabla S = 0\,, \tag{5}$$

where $\underline{V} = U\underline{i} + \nabla\Phi$, or

$$US_x + \Phi_{\tilde{r}_1} S_{\tilde{r}_1} + \Phi_{\theta_1} \frac{S_{\theta_1}}{\tilde{r}_1^2} = 0\,. \tag{6}$$

Now in the cross-flow plane we have

$$\frac{S_{\theta_1}}{S_{\tilde{r}_1}} = -\frac{d\tilde{r}_1}{d\theta_1} = -\tilde{r}_1 \cot \phi_1\,, \tag{7}$$

and hence the condition (5) that S is a stream surface reduces to

$$\Phi_n = \frac{1}{\tilde{r}_1} \Phi_{\theta_1} \cos \phi_1 - \Phi_{\tilde{r}_1} \sin \phi_1 = U \sin \phi_1 \frac{S_x}{S_{\tilde{r}_1}}\,, \tag{8}$$

where Φ_n is the component of velocity in the cross-flow plane normal to the trace of the sheet. If we let $r_1 = \tilde{r}_1/s$, then since for a conical surface $S_x/S_{\tilde{r}_1} = -\tilde{r}_1/x$ equation (8) reduces to

$$\Phi_n = -U \tan \gamma\, r_1 \sin \phi_1\,. \tag{9}$$

This is the same condition as was derived in Ref. 5.

Consider now the pressure condition. The pressure coefficient is given from Bernoulli's theorem, according to slender-body theory, as

$$C_p = -2\Phi_x/U - (\Phi_y^2 + \Phi_z^2)/U^2 + \alpha^2\,, \tag{10}$$

where the higher order term (Φ_x^2/U^2) is neglected. For conical flow Φ must be homogeneous of order one, and by Euler's theorem on homogeneous functions

$$\Phi = x\Phi_x + y\Phi_y + z\Phi_z\,, \tag{11}$$

therefore

$$C_p = 2(y\Phi_y + z\Phi_z - \Phi)/Ux - (\Phi_y^2 + \Phi_z^2)/U^2 + \alpha^2\,. \tag{12}$$

Let $\tilde{\Delta}$ denote the difference operator across the sheet so that $\tilde{\Delta}C_p$ is the pressure jump across the sheet (inside minus outside). Then from equation (9) we have that $\tilde{\Delta}\Phi_n=0$ and thus

$$\tilde{\Delta}(y\Phi_y+z\Phi_z)=yy_\sigma\tilde{\Delta}\Phi_\sigma+zz_\sigma\tilde{\Delta}\Phi_\sigma=r_1 s\cos\phi_1\,\tilde{\Delta}\Phi_\sigma \tag{13}$$

and

$$\tilde{\Delta}(\Phi_y^2+\Phi_z^2)=\tilde{\Delta}(\Phi_\sigma^2)=2\Phi_{\sigma_m}\tilde{\Delta}\Phi_\sigma\,, \tag{14}$$

where Φ_{σ_m} is the mean of the tangential velocities on either side of the sheet. Operating with $\tilde{\Delta}$ on equation (12) and using equations (13) and (14) we have

$$\tilde{\Delta}C_p=2(r_1 s\cos\phi_1\,\tilde{\Delta}\Phi_\sigma-\tilde{\Delta}\Phi)/Ux-2\Phi_{\sigma_m}\tilde{\Delta}\Phi_\sigma/U^2\,. \tag{15}$$

The pressure condition which we must satisfy on the jet-vortex sheet is that the jump in pressure across the sheet is prescribed in our model according to the jet flap theory of Spence[11]. With the pressure jump given, we may write the pressure condition from equation (16) as a condition on the jump in Φ across the sheet, thus

$$\tilde{\Delta}\Phi=\tilde{\Delta}\Phi_\sigma(r_1 s\cos\phi_1-s\phi_{\sigma_m}/U\tan\gamma)-\tilde{\Delta}C_p Us/2\tan\gamma\,. \tag{16}$$

If $\tilde{\Delta}C_p=0$, this reduces to the condition derived in Ref. 5.

The Kutta condition can be written simply in terms of the complex potential $W(Z)$, thus

$$\frac{dW}{dZ}\text{ is finite for }Z=\pm s\,. \tag{17}$$

This Kutta condition implies that the initial blowing direction must lie in the plane of the delta wing.

In order to apply equation (16) we must now calculate the pressure jump $\tilde{\Delta}C_p$. If we consider a jet of air width δ, velocity $\underline{V}$, density ρ_J issuing from the leading edge then the magnitude of the momentum flux in the jet per unit length measured normal to $\underline{V}$ is given by

$$J=\rho_J\delta\underline{V}.\underline{V}=\rho_J\delta V^2\,. \tag{18}$$

If we take the limit as $\delta\to 0$, $V\to\infty$, keeping J fixed as in the jet flap theory, the pressure jump across the sheet is given by the equation

$$\tilde{\Delta}C_p=-\kappa J/(\tfrac{1}{2}\rho U^2)\,, \tag{19}$$

where κ is the curvature of the jet geodesic. In a conical theory the shape of the jet must be conical and the pressure difference across it must be constant along its generators. The momentum flux of the jet from the leading edge varies linearly with the distance from the apex, and the magnitude of the momentum flux along the streamline which emerges, say, from the point with wing semi-span $s=s_0$ remains constant along that streamline, and is given by

$$J=Ms_0 \tag{20}$$

where M is a constant. We recall that the jet streamlines will be geodesics in the jet-vortex sheet. If we then follow the trace of the jet-vortex sheet in the cross-flow plane round from the leading edge, the magnitude of the momentum flux decreases, since each geodesic streamline in the jet originates at a point closer to the apex, at which point $s_0=0$.

The magnitude of the flux of momentum from a length dl of one leading edge is, by the definition of J,

$$Jdl \sin(\beta-\gamma).$$

Hence, using the proportionality of J to x represented by (20), we find the magnitude of the momentum flux from one leading edge by integration as

$$\tfrac{1}{2}M \sec\gamma \sin(\beta-\gamma)\,(\text{wing area}).$$

So, defining a coefficient of blowing momentum C_μ by referring the sum of the magnitudes of the momentum fluxes from both edges to the wing area and the free-stream kinetic pressure, we have:

$$C_\mu = \frac{2M \sin(\beta-\gamma)}{\rho U^2 \cos\gamma}. \tag{21}$$

The static axial thrust coefficient is then $C_\mu \cos\beta$. In terms of the blowing coefficient C_μ, and using equation (19), equation (16) can be written as

$$\frac{\tilde{\Delta}\Phi}{Us\tan\gamma} = \frac{\tilde{\Delta}\Phi_\sigma(r_1\cos\phi_1 - \Phi_{\sigma_m}/(U\tan\gamma))}{U\tan\gamma} + \frac{\kappa s_0 C_\mu \cos\gamma}{2\sin(\beta-\gamma)\tan^2\gamma}. \tag{22}$$

The quantity κs_0 may be conveniently calculated in terms of the shape of the trace of the jet-vortex sheet in the cross-flow plane at the station s. We note that as we move along the trace of the sheet in the cross-flow plane both the curvature κ and the quantity s_0 tend to zero, as we approach the point where the geodesic from the apex intersects the cross-flow plane. Beyond this point $\tilde{\Delta}C_p = 0$.

An expression for κs_0 is derived in this section, as equation (43) below, where it is seen, through (27) and (29), to depend explicitly upon the sheet shape and the quantity $w(\theta) = s_0/\bar{s}(\theta)$ associated with the geodesics, where $\bar{s}$ is the wing semi-span at any station. In Appendix II a geometrical construction is given which yields the quantity w directly, and it is shown that κs_0 tends to zero like the cube of the polar angle from the end of the jet sheet measured at the vortex centre in the cross-flow plane. We here pursue an analytical development for the geodesic lines in the conical jet-vortex sheet.

With reference to Fig. 4 let $r = f(\theta)$ be the equation of the trace of the jet-vortex sheet in the cross-flow plane, where rs is the radial distance from the isolated vortex to a point on the trace of the jet-vortex sheet. Let the vortex centre in the cross-flow plane in which we work be at position $y = \lambda_1 s$ and $z = \lambda_2 s$ and let ε be the angle between the line joining the vortex to the leading edge and the y-axis. Then if $\bar{s}$ is the wing semi-span at any station, the equation for the conical jet-vortex sheet is given by

$$\left.\begin{aligned} y(\bar{s},\theta) &= (\lambda_1 + f(\theta)\cos(\theta-\varepsilon))\bar{s}, \\ z(\bar{s},\theta) &= (\lambda_2 + f(\theta)\sin(\theta-\varepsilon))\bar{s} \end{aligned}\right\} \tag{23}$$

and

$$x(\bar{s},\theta) = \bar{s}\cot\gamma,$$

where

$$\tan\varepsilon = \frac{\lambda_2}{1-\lambda_1}, \text{ and } f(0) = \sqrt{(1-2\lambda_1+\lambda_1^2+\lambda_2^2)}. \tag{24}$$

Thus $\underline{R}(\bar{s},\theta) = x\underline{i} + y\underline{j} + z\underline{k}$ with x,y,z defined by equations (23), and $\underline{i},\underline{j},\underline{k}$ unit vectors parallel to $0x$, $0y$ and $0z$, is the vector equation describing the conical jet-vortex sheet. If we further restrict $\bar{s}$, θ such that $\bar{s} = \bar{s}(\tau)$ and $\theta = \theta(\tau)$ are functions of a single parameter τ, then $\underline{R}$ traces out a curve in the jet-vortex sheet

as τ varies. Now if a dot denotes differentiation with respect to τ, and a dash denotes differentiation with respect to θ, the condition that $\underline{R}$ traces out a geodesic as τ varies if given by (*see* Willmore[17])

$$\left(\frac{d}{d\tau}\left(\frac{\partial T}{\partial \dot{\bar{s}}}-\frac{\partial T}{\partial \bar{s}}\right)\right)\frac{\partial T}{\partial \dot{\theta}}-\left(\frac{d}{d\tau}\left(\frac{\partial T}{\partial \dot{\theta}}-\frac{\partial T}{\partial \theta}\right)\right)\frac{\partial T}{\partial \dot{\bar{s}}}=0\,, \tag{25}$$

where

$$T(\bar{s},\dot{\bar{s}},\theta,\dot{\theta})=\tfrac{1}{2}(a(\theta)\dot{\bar{s}}^2+2b(\theta)\bar{s}\dot{\bar{s}}\dot{\theta}+c(\theta)\bar{s}^2\dot{\theta}^2)\,, \tag{26}$$

with

$$\left.\begin{aligned} a(\theta)&=\frac{\partial \underline{R}}{\partial \bar{s}}\cdot\frac{\partial \underline{R}}{\partial \bar{s}}=\cot^2\gamma+\lambda_1^2+\lambda_2^2+2f(\theta)\,(\lambda_1\cos(\theta-\varepsilon)+\lambda_2\sin(\theta-\varepsilon))+f^2(\theta)\,,\\ b(\theta)&=\frac{1}{\bar{s}}\frac{\partial \underline{R}}{\partial \bar{s}}\cdot\frac{\partial \underline{R}}{\partial \theta}=\lambda_1(f'(\theta)\cos(\theta-\varepsilon)-f(\theta)\sin(\theta-\varepsilon))+\\ &\quad+\lambda_2(f'(\theta)\sin(\theta-\varepsilon)+f(\theta)\cos(\theta-\varepsilon))+f(\theta)f'(\theta) \end{aligned}\right\} \tag{27}$$

and

$$c(\theta)=\frac{1}{\bar{s}^2}\frac{\partial \underline{R}}{\partial \theta}\cdot\frac{\partial \underline{R}}{\partial \theta}=f^2(\theta)+f'^2(\theta)\,.$$

The differential equation (25) determines one of the two functions $\bar{s}(\tau)$, $\theta(\tau)$ and since the equation for the geodesic has been written in a parametric form we are free to choose the other. In particular if we let $\theta=\tau$ and hence $\bar{s}=\bar{s}(\theta)$, then the differential equation (25) eventually reduces to

$$q\bar{s}\bar{s}''-2q\bar{s}'^2-\tfrac{1}{2}q'\bar{s}\bar{s}'+p\bar{s}^2=0\,, \tag{28}$$

where

$$\left.\begin{aligned} q(\theta)&=a(\theta)c(\theta)-b^2(\theta)\\ \text{and}\qquad p(\theta)&=c(\theta)b'(\theta)-c^2(\theta)-\tfrac{1}{2}b(\theta)c'(\theta)\,. \end{aligned}\right\} \tag{29}$$

The two boundary conditions required to determine $\bar{s}(\theta)$ from the second order differential equation (28) are given by the value s_0 of $\bar{s}$ in the cross-flow plane from which the geodesic originated at the leading edge $\theta=0$, and the initial direction of the geodesic streamline at this station. Thus at $\theta=0$

$$\bar{s}(0)=s_0\,, \tag{30}$$

and

$$\left.\frac{\dot{y}}{\dot{x}}\right|_{\theta=0}=\tan\beta\,, \tag{31}$$

where x and y are defined by equations (23). These conditions reduce to

$$\bar{s}(0)=s_0 \tag{32}$$

and

$$\bar{s}'(0)=\frac{s_0 f(0)\tan\gamma}{(\tan\beta-\tan\gamma)\sin\varepsilon}, \tag{33}$$

where the condition that the sheet is tangential to the wing has been used. It is convenient to make the transformation

$$w(\theta)=\frac{s_0}{\bar{s}(\theta)}, \tag{34}$$

so that the equation (28) becomes the linear equation

$$w''=\frac{1}{2}\frac{q'}{q}w'+\frac{p}{q}w, \tag{35}$$

with boundary conditions

$$w(0)=1 \tag{36}$$

and

$$w'(0)=-\frac{f(0)\tan\gamma}{(\tan\beta-\tan\gamma)\sin\varepsilon}. \tag{37}$$

As we have already indicated, the geometrical construction for w, obtained in Appendix II, provides us with a solution of equation (35), subject to (36) and (37); it is simply

$$w=\frac{\sin\gamma}{\sin(\beta-\gamma)}\sqrt{a}\sin(\beta-\gamma-v)$$

where $\dfrac{dv}{d\theta}=\dfrac{\sqrt{q}}{a}$, which may be verified by direct substitution into (35). Unfortunately, at the time when the results presented in this Report were obtained this simple solution of (35) was not available, and the differential equation was integrated using a Runge-Kutta method. The details of the procedure adopted are discussed later.

To find the curvature of the geodesic we proceed as follows. Let $\underline{t}^\alpha$ and $\underline{n}^\alpha$ be unit vectors along the tangent and principal normal to the geodesic. Then, if σ denotes the arc length along the geodesic, the curvature, κ, is given by

$$d\underline{t}^\alpha/d\sigma=\kappa\underline{n}^\alpha,$$

so that

$$\kappa=\underline{n}^\alpha\cdot\frac{d\underline{t}^\alpha}{d\sigma}.$$

Now

$$\underline{t}^\alpha=d\underline{R}/d\sigma=\frac{d\underline{R}/d\tau}{d\sigma/d\tau},$$

so that

$$\frac{d\sigma}{d\tau}=\left|\frac{d\underline{R}}{d\tau}\right|=\sqrt{2T},\quad\text{by}\quad(26),$$

and

$$\frac{d\underline{t}^{\alpha}}{d\sigma}=\frac{d^2\underline{R}}{d\tau^2}\Big/\left(\frac{d\sigma}{d\tau}\right)^2-\frac{d\underline{R}}{d\tau}\frac{d^2\sigma}{d\tau^2}\Big/\left(\frac{d\sigma}{d\tau}\right)^3.$$

Since $\underline{n}^{\alpha}$ is normal to $\underline{t}^{\alpha}$, $\underline{n}^{\alpha}\cdot\frac{d\underline{R}}{d\tau}=0$ and

$$\kappa=\underline{n}^{\alpha}\cdot\frac{d^2\underline{R}}{d\tau^2}\Big/\left(\frac{d\sigma}{d\tau}\right)^2=\underline{n}^{\alpha}\cdot\frac{d^2\underline{R}}{d\tau^2}\Big/2T. \tag{38}$$

Since $\underline{n}^{\alpha}$ is the principal normal to the geodesic, it is also the surface normal. Hence it is normal to any two vectors in the tangent plane. In particular:

$$\underline{n}^{\alpha}=\left[\frac{\partial\underline{R}}{\partial\bar{s}}\Lambda\frac{\partial\underline{R}}{\partial\theta}\right]\Big/\left|\frac{\partial\underline{R}}{\partial\bar{s}}\Lambda\frac{\partial\underline{R}}{\partial\theta}\right|.$$

By (23), $\underline{R}=\bar{s}\underline{F}(\theta)$ and so

$$\frac{\partial^2\underline{R}}{\partial\bar{s}^2}=0 \text{ and } \frac{\partial^2\underline{R}}{\partial\theta\partial\bar{s}}=\frac{1}{\bar{s}}\frac{\partial\underline{R}}{\partial\theta}.$$

Hence

$$\underline{n}^{\alpha}\cdot\frac{d^2\underline{R}}{d\tau^2}=\underline{n}^{\alpha}\cdot\left(\frac{\partial^2\underline{R}}{\partial\bar{s}^2}\dot{\bar{s}}^2+2\frac{\partial^2\underline{R}}{\partial\theta\partial\bar{s}}\dot{\bar{s}}\dot{\theta}+\frac{\partial^2\underline{R}}{\partial\theta^2}\dot{\theta}^2\right)=\underline{n}^{\alpha}\cdot\frac{\partial^2\underline{R}}{\partial\theta^2}\dot{\theta}^2,$$

since $\underline{n}^{\alpha}$ is normal to $\partial\underline{R}/\partial\theta$. With $\tau\equiv\theta$, $\dot{\theta}=1$, and so, by (38),

$$\kappa=\frac{(\underline{R}_{\bar{s}},\underline{R}_{\theta},\underline{R}_{\theta\theta})}{2T|\underline{R}_{\bar{s}}\Lambda R_{\theta}|}=\frac{\bar{s}(\underline{F},\underline{F}',\underline{F}'')}{2T|\underline{F}\Lambda\underline{F}'|}, \tag{39}$$

where the numerator is a triple scalar product. This can be evaluated from (23) and the determinantal expression for the triple product as

$$(\underline{F},\underline{F}',\underline{F}'')=\cot\gamma\,(2f'^2-ff''+f^2). \tag{40}$$

To express the denominator, we note that

$$\begin{aligned}[\underline{F}\Lambda\underline{F}']\,.\,[\underline{F}\Lambda\underline{F}']&=(\underline{F}\Lambda\underline{F}',\underline{F},\underline{F}')=([\underline{F}\Lambda\underline{F}']\Lambda\underline{F})\,.\,\underline{F}'\\&=((\underline{F}\,.\,\underline{F})\underline{F}'-(\underline{F}\,.\,\underline{F}')\underline{F})\,.\,\underline{F}'=(\underline{F}\,.\,\underline{F})\,(\underline{F}'.\,\underline{F}')-(\underline{F}\,.\,\underline{F}')^2\\&=ac-b^2=q\text{, by (27) and (29).}\end{aligned} \tag{41}$$

By (26) and (34)

$$2T=s_0^2(aw'^2-2bww'+cw^2)/w^4 \tag{42}$$

and so, by (39), (40), (41) and (42):

$$\kappa s_0=\frac{\cot\gamma\,(2f'^2-ff''+f^2)w^3}{(aw'^2-2bww'+cw^2)\sqrt{q}} \tag{43}$$

Thus given s_0 we can determine w, $\bar{s}$, κ as functions of θ, and we require in equation (22) κs_0 for the separate geodesic lines in the cross-flow plane $\bar{s}=s$. However, from the simplifying assumption of conical flow, w and κs_0 are functions of θ only and so the same for all cross-flow planes. Hence κs_0 is given by equation (43) as a function of θ in the plane $\bar{s}=s$, in terms of the shape of the trace of the jet-vortex sheet and the solution $w(\theta)$ of equation (35).

The shape of the sheet is represented in the solution procedure by its distance from the vortex centre at n discrete pivotal points. However, since we use a Runge-Kutta method to solve the differential equation (35) for $w(\theta)$ we need a smooth representation for $f(\theta)$, the shape of the sheet in the cross-flow plane. We obtain this by fitting a low order polynomial to the discrete points which represent the shape of the sheet in the cross-flow plane. A cubic polynomial has proved satisfactory and is used throughout the solution procedure. For values of θ between the leading edge and the first pivotal point the cubic was fitted to the leading edge and the first two points of the sheet. The fourth condition on the cubic is provided by the fact that the blowing direction is in the plane of the wing, so that the sheet must merge smoothly onto the leading edge at $\theta=0$. For other values of θ, the four points necessary to determine the cubic are used in such a way that two points lie on either side of the value of θ at which f, f', f'' are required. The last four points are used for values of θ between the last two points specifying the sheet.

2.2. *Construction of the Velocity Potential.*

In the absence of a transformation which allows a simplified treatment of the conditions on the jet-vortex sheet of unknown shape, the cross-flow plane is transformed so that the wing boundary conditions are automatically satisfied. Such a transformation is given by

$$Z^{*2}=Z^2-s^2\,. \tag{44}$$

The leading edges are transformed into the origin of this Z^*-plane and the wing into a finite part of the imaginary axis. The symmetry of the flow about the imaginary axis of the cross-flow plane has been preserved by this transformation so that the wing boundary condition of zero normal velocity on the wing surface is now automatically satisfied. Furthermore the condition at infinity is left unchanged by this transformation. In Fig. 5 let $Z^*=Z^*(\theta^*)$ be the equation of the starboard jet-vortex sheet in the transformed plane. The angle θ^* is the polar angle between the line joining the centre of the jet-vortex spiral to a point on the spiral and the line joining the centre of the jet-vortex spiral to the origin. The complex velocity potential $W(Z^*)$ can be constructed from the upward component of the uniform freestream U sin α, together with the contribution from the two jet-vortex sheets given by the equations $Z^*=Z^*(\theta^*)$ and $Z^*=-\bar{Z}^*(\theta^*)$. Thus

$$\frac{dW}{dZ^*}=-iU\alpha+\int_0^\infty\left(-\frac{1}{2\pi i}\frac{d\Delta\Phi}{d\theta^*}\right)\left(\frac{1}{Z^*-Z^*(\theta^*)}-\frac{1}{Z^*+\bar{Z}^*(\theta^*)}\right)d\theta^*\,, \tag{45}$$

since $\sin\alpha\simeq\alpha$, and $d\Delta\Phi/d\theta^*$ is a measure of the strength of the vortex sheet at each point. The velocity components in the cross-flow plane are given by

$$\frac{dW}{dZ}=\frac{Z}{Z^*}\frac{dW}{dZ^*}\,. \tag{46}$$

The mean tangential and normal velocity components along the sheet itself are given from the following equation, where the singular integral involved in the calculation is interpreted as a Cauchy Principal Value,

$$\Phi_{\sigma_m}-i\Phi_n=\frac{dW}{d\sigma}=\frac{dW}{dZ}\frac{dZ}{d\sigma}=\left|\frac{Z}{Z^*}\right|\frac{dZ^*}{d\sigma^*}\frac{dW}{dZ^*}\,. \tag{47}$$

The transformation and form of the velocity are as given in Ref. 5.

To summarise, the problem now is to determine the strength and position of the jet-vortex sheets springing from the leading edges of the wing so that the complex velocity potential (45) satisfies (i) the pressure condition (22), (ii) the Kutta condition (17), and (iii) the normal velocity condition (9). The wing boundary condition and the condition at infinity are already satisfied by the expression for dW/dZ^* in equation (45).

2.3. *Representation of the Inner Part of the Jet-Vortex Sheet.*

In Section 1.2 we stated that the inner part of the jet-vortex sheet would be represented by a line vortex and cut, since the numerical representation of an infinite angular spiral, with which we are concerned, is too complicated. Thus we represent the jet-vortex sheet by an outer part, a jet-vortex sheet of finite angular extent springing from the leading edge; and an inner part, an isolated line vortex with a cut joining the end of the finite outer part of the jet-vortex sheet to this line vortex. If the strengths of these two isolated vortices are Γ and $-\Gamma$ and they are at positions $Z^* = Z_V^*$ and $Z^* = -\bar{Z}_V^*$, then equation (45) for the complex velocities can be rewritten

$$\frac{dW}{dZ^*} = -iU\alpha + \frac{\Gamma}{2\pi i}\left(\frac{1}{Z^* - Z_V^*} - \frac{1}{Z^* + \bar{Z}_V^*}\right) + \\ + \int_0^{\theta_0^*} \left(-\frac{1}{2\pi i}\frac{d\Delta\Phi}{d\theta^*}\right)\left(\frac{1}{Z^* - Z^*(\theta^*)} - \frac{1}{Z^* + \bar{Z}^*(\theta^*)}\right) d\theta^*, \tag{48}$$

where θ_0^* is the value of the angle θ^* at the end of the finite outer part of the jet-vortex sheet.

The conditions to be applied to the isolated vortex and cut are derived from the conditions that would have been applied to the inner part of the complete jet-vortex sheet. For cases when the extent of the jet, blown from the leading edge, exceeds the length of the finite outer part of the sheet in the cross-flow plane there is a force on the fluid which is to be represented in some way as a condition on the vortex and cut. To do this we estimate from an asymptotic analysis, the position of the inner jet-vortex sheet and the pressure jump across it. This pressure jump can then be integrated along the length of the inner jet-vortex sheet and the force, per unit length in the x-direction, sustained by it can be deduced. The condition that is applied on the vortex and cut is that the force to be sustained by the vortex and cut is equal to the force sustained by the inner jet-vortex sheet. The asymptotic method used to calculate the shape of this inner sheet is similar to that of Mangler and Smith[4] for the case when there is no blowing. The details of the calculation of this force are omitted here and can be found in Appendix I. The shape of the sheet is obtained as the solution of a differential equation; in the case when the blowing coefficient is zero the solution is given explicitly as

$$f(\theta) = \frac{k_1}{k_2 + \theta}, \; k_1, k_2 \text{ constants}, \tag{49}$$

which is the solution obtained by Mangler and Smith. For $C_\mu \neq 0$ the differential equation is solved numerically and the curvature and pressure jump along it are calculated. As outlined in Section 1.2 these two quantities tend to zero as the effect of the jet extends only a finite distance along the jet-vortex sheet in the cross-flow plane. Thus the non-dimensional force $F = F^y + iF^z$ (F^y, F^z are the components in the y- and z-directions) is given by the integral of the pressure jump along the asymptotic solution for the inner part of the jet-vortex sheet. Thus the integration commences at the value of $\theta (= \theta_0)$ corresponding to the end of the finite outer part of the jet-vortex sheet and terminates at the value of $\theta (= \theta_m)$ where the curvature falls to zero. In the case when the blowing coefficient is zero, or when the blowing angle β is small enough for the effect of the jet to be contained within the outer finite part of the jet-vortex sheet, then the force to be sustained by the vortex and cut reduces to the zero force condition used by Smith[5].

Using the complex representation of the cross-flow plane, let $Z = Z_E$ be the position of the end of the

starboard finite jet-vortex sheet, and $Z=Z_V$ be the starboard vortex position. Now since Φ_y and Φ_z are continuous across the cut, the pressure difference across the cut is given from equation (15) as

$$\Delta p_s=\tfrac{1}{2}\rho U^2\Delta C_p=-\rho U\Gamma/x\,, \tag{50}$$

where $\Gamma(=\Delta\Phi)$ is the circulation about the starboard isolated vortex. Since the pressure difference is independent of the shape of the cut, the force on the cut, per unit length in the x-direction, is given by

$$-i(Z_V-Z_E)\Delta p_s=i\rho U\tan\gamma\,\Gamma(Z_V-Z_E)/s\,. \tag{51}$$

The force on the vortex is given from the Joukowski formula and is equal to

$$-i\rho\Gamma N\,, \tag{52}$$

where N is the component of velocity normal to the line vortex $Z=Z_V$, and can be written as

$$N=-U\tan\gamma\,Z_V/s+\overline{\lim_{Z\to Z_V}\left(\frac{dW}{dZ}-\frac{\Gamma}{2\pi i}\frac{1}{(Z-Z_V)}\right)}\,. \tag{53}$$

Thus the condition that the force sustained by the vortex and cut be equal to the force obtained by integrating the pressure jump across the inner part of the jet sheet can be written

$$\begin{aligned}\tfrac{1}{2}\rho U^2\tan^2\gamma\,sF=-i\rho\Gamma\Bigg(&-U\tan\gamma\,Z_V/s+\overline{\lim_{Z\to Z_V}\left(\frac{dW}{dZ}-\frac{\Gamma}{2\pi i}\frac{1}{(Z-Z_V)}\right)}+\\&+i\rho U\tan\gamma\,\Gamma(Z_V-Z_E)/s\Bigg),\end{aligned} \tag{54}$$

where the force F on the part of the jet beyond the finite part of the sheet is given by equation (I.26) of Appendix I.

2.4. *Finite Difference Representation.*

The position of the finite outer part of the sheet is represented by the distance and angular displacement of n pivotal points on the sheet relative to the isolated vortex in the transformed plane. In Fig. 5 the quantities

$$d_2, d_4, \ldots, d_{2n}\,, \tag{55}$$

are the values of the distance of the pivotal points on the sheet from the isolated vortex, divided by the wing semi-span s. The corresponding polar angles measured from the line between the isolated vortex and the origin in the transformed plane are given by

$$h_1, h_2, \ldots, h_n\,. \tag{56}$$

The $2n$ quantities $d_{2i}, h_i\,(i=1,\ldots,n)$ define uniquely the position of the finite outer part of the sheet. For simplicity the intermediate points where the sheet boundary conditions are to be applied are at polar angles given by

$$\tfrac{1}{2}h_1, \tfrac{1}{2}(h_1+h_2), \ldots, \tfrac{1}{2}(h_{n-1}+h_n)\,, \tag{57}$$

and at polar distances given by

$$d_1=\tfrac{1}{2}(d_0+d_2),\ d_3=\tfrac{1}{2}(d_2+d_4),\ \ldots,\ d_{2n-1}=\tfrac{1}{2}(d_{2n-2}+d_{2n}), \tag{58}$$

where d_0 is the non-dimensional distance from the vortex to the origin. The strength of the jet-vortex sheet at the pivotal points is represented by the quantities

$$g_j=\frac{-1}{Us\tan\gamma}\frac{d\Delta\Phi}{d\theta^*}\Bigg|_{\theta^*=h_j} \qquad j=1,\ldots,n. \tag{59}$$

The strength and position of the isolated vortex are represented by the quantities

$$g=\Gamma/Us\tan\gamma \tag{60}$$

and

$$\bar{y}+i\bar{z}=Z_V^*/s. \tag{61}$$

The non-dimensional cartesian coordinates $(y^*/s, z^*/s)$ of the pivotal and intermediate points in the transformed plane are represented by

$$\left.\begin{aligned} y_{2j}^*+iz_{2j}^*&=\bar{y}+i\bar{z}-d_{2j}e^{i(b+h_j)}\\ \text{and}\qquad y_{2j-1}^*+iz_{2j-1}^*&=\bar{y}+i\bar{z}-d_{2j-1}e^{i(b+0.5(h_{j-1}+h_j))}\end{aligned}\right\} \quad j=1,\ldots,n, \tag{62}$$

where

$$b=\arg(\bar{y}+i\bar{z}). \tag{63}$$

The non-dimensional polar coordinates of the pivotal and intermediate points in the cross-flow plane relative to the wing semi-span, with wing centre line as polar origin are given by b_j and c_j and can be written using equation (44)

$$b_j^2e^{2ic_j}=(y_j^*+iz_j^*)^2+1 \qquad j=1,\ldots,2n. \tag{64}$$

The vortex position Z_V and the end of the jet-vortex sheet Z_E are represented in the cross-flow plane by the quantities

$$\left.\begin{aligned} a_0+ia_1&=Z_V/s=\sqrt{((\bar{y}+i\bar{z})^2+1)}\\ \text{and}\qquad a_2+ia_3&=Z_E/s=\sqrt{((y_{2n}^*+iz_{2n}^*)^2+1)}.\end{aligned}\right\} \tag{65}$$

The derivatives along the sheet at the intermediate points which are needed to evaluate the various boundary conditions on the sheet are given by the following formulae, which represent the simplest choice possible.

$$\left.\begin{aligned}
\frac{1}{s}\frac{d\tilde{r}_1}{d\theta^*} &= \frac{b_{2j}-b_{2j-2}}{h_j-h_{j-1}} &&= f_{2j-1}\,,\\
\frac{d\theta_1}{d\theta^*} &= \frac{c_{2j}-c_{2j-2}}{h_j-h_{j-1}} &&= f_{2j}\quad,\\
\frac{1}{s}\frac{dr^*}{d\theta^*} &= \frac{d_{2j}-d_{2j-2}}{h_j-h_{j-1}} &&= e_{2j-1}\\
\frac{1}{s}\frac{d\sigma^*}{d\theta^*} &= (d_{2j-1}^2+e_{2j-1}^2)^{\frac{1}{2}} &&= e_{2j}
\end{aligned}\right\}\quad j=1,\ldots,n\,, \tag{66}$$

and

where

$$b_0=1,\ c_0=0,\ \text{and}\ h_0=0\,. \tag{67}$$

For the complex velocity given by equation (48) we use the trapezium rule to evaluate the integral, and thus using the above notation

$$\begin{aligned}
\frac{1}{U\tan\gamma}\frac{dW}{dZ^*} = -ia+\frac{g}{2\pi i}\left(\frac{1}{(Z^*/s-\bar{y}-i\bar{z})}-\frac{1}{(Z^*/s+\bar{y}-i\bar{z})}\right)+\\
+\frac{1}{4\pi i}\sum_{j=1}^{n} g_j(h_{j+1}-h_{j-1})\left(\frac{1}{(Z^*/s-y_{2j}^*-iz_{2j}^*)}-\frac{1}{(Z^*/s+y_{2j}^*-iz_{2j}^*)}\right)
\end{aligned} \tag{68}$$

where

$$h_{n+1}=h_n \text{ and } a=\alpha/\tan\gamma\,. \tag{69}$$

We have assumed that the integrand vanishes at $\theta^*=0$. This assumption is correct for all $Z^*\neq 0$ since the Kutta condition (17) implies that $d\Delta\Phi/d\theta^*$ vanishes at $\theta^*=0$. The special case $Z^*=0$ is evaluated when we use the Kutta condition in the next section.

3. *Solution Procedure.*

The procedure splits up into three nested iterations. The first calculates the strengths of the sheet and the isolated vortex from the pressure and Kutta conditions, the second calculates the vortex position from the force condition, and the third calculates the sheet shape from the normal velocity condition. A good approximation to the $2n+3$ unknowns is needed to obtain a solution, for example for small β or C_μ calculations may be commenced using the solutions of Smith[5] for $C_\mu=0$.

3.1. *Determination of the Strength of the Sheet and Isolated Vortex from the Pressure and Kutta Conditions.*

The $n+1$ values for the strength of the isolated vortex and the strength of the sheet at the n pivotal points are calculated by applying the pressure condition (22) at the n intermediate points and the Kutta condition (17) at the leading edge. We calculate the pressure jump $\tilde{A}C_p$ across the sheet from equation (19), using the initial approximation, and linearise the non-linear term $\tilde{A}\Phi_\sigma\Phi_{\sigma_m}$ in equation (22) by also calculating Φ_{σ_m} numerically in terms of the initial approximation. The equations then reduce to a set of n linear equations in terms of the vortex strength g and the n values for the sheet strength at the intermediate points. The equations are solved for the sheet strength at the intermediate points in terms

of the vortex strength g. The sheet strengths at the pivotal points are found in terms of g by interpolation. The unknown vortex strength g is then calculated by substituting the values for the sheet strength into the equation obtained from the Kutta condition, thus determining a new set of strengths g and g_j $(j=1,\ldots,n)$.

In order to find $\tilde{\Delta}C_p$, we need the curvature of the geodesic. This is given by equation (43), where w is the solution of equation (35) subject to the boundary conditions (36) and (37), or is found by the method of Appendix II. Using the initial approximation and a given C_μ we can calculate β_j, the last term in equation (22), at the n intermediate points as

$$\beta_j=\frac{\kappa s_0 C_\mu \cos\gamma}{2\sin(\beta-\gamma)\tan^2\gamma}\Bigg|_{\text{jth intermediate point}} \qquad j=1,2,\ldots,n. \tag{70}$$

For the coefficient of $\Delta\Phi_\sigma/U\tan\gamma$ in the second term of equation (22) we introduce α_j, writing it in terms of the initial approximation:

$$\begin{aligned}\alpha_j&=s\frac{d\theta^*}{d\sigma}(\Phi_{\sigma_m}/U\tan\gamma-r_1\cos\phi_1)\Big|_{\text{jth intermediate point}}\\&=\frac{b_{2j-1}^2}{e_{2j}(y_{2j-1}^{*2}+z_{2j-1}^{*2})}\left(\frac{\Phi_{\sigma_m}}{U\tan\gamma}\frac{(y_{2j-1}^{*2}+z_{2j-1}^{*2})^{\frac{1}{2}}}{b_{2j-1}}-\frac{b_{2j-1}f_{2j-1}}{e_{2j}}\right)\end{aligned} \tag{71}$$

for $j=1,\ldots,n$, where Φ_{σ_m} is given at the jth intermediate point as

$$\begin{aligned}\left[\frac{\Phi_{\sigma_m}}{U\tan\gamma}\right]_{\text{jth intermediate point}}&\frac{(y_{2j-1}^{*2}+z_{2j-1}^{*2})^{\frac{1}{2}}}{b_{2j-1}}=\\=\mathscr{R}\Bigg\{(u_j+iv_j)\Bigg(&-ia+\frac{g\bar{y}}{\pi i(y_{2j-1}^*+iz_{2j-1}^*-\bar{y}-i\bar{z})(y_{2j-1}^*+iz_{2j-1}^*+\bar{y}-i\bar{z})}+\\&+\sum_{k=1}^{n}\frac{g_k y_{2k}^*(h_{k+1}-h_{k-1})}{2\pi i(y_{2j-1}^*+iz_{2j-1}^*-y_{2k}^*-iz_{2k}^*)(y_{2j-1}^*+iz_{2j-1}^*+y_{2k}^*-iz_{2k}^*)}\end{aligned} \tag{72}$$

and where

$$\begin{aligned}u_j+iv_j&=\frac{dZ^*}{d\sigma^*}=\frac{d\theta^*}{d\sigma^*}\left(\frac{Z^*-s(\bar{y}+i\bar{z})}{r^*}\right)\left(\frac{dr^*}{d\theta^*}+ir^*\right)\\&=\frac{(y_{2j-1}^*+iz_{2j-1}^*-\bar{y}-i\bar{z})(e_{2j-1}+id_{2j-1})}{d_{2j-1}e_{2j}}.\end{aligned} \tag{73}$$

Thus the quantities $\alpha_j, \beta_j\,(j=1,\ldots,n)$ just defined are calculated in terms of the initial approximation. The jump in Φ across the sheet can be written as

$$\tilde{\Delta}\Phi=\Gamma-\int_0^{\theta_0^*}\frac{d\tilde{\Delta}\Phi}{d\theta^*}\,d\theta^*. \tag{74}$$

Employing the trapezium rule for the integration, we have

$$\left[\frac{\tilde{\Delta}\Phi}{Us\tan\gamma}\right]_{\text{jth intermediate point}} = g + \sum_{k=1}^{n} L_{jk}\gamma_k \qquad j=1,\ldots,n, \tag{75}$$

where

$$\gamma_k = \left[-\frac{1}{Us\tan\gamma}\frac{d\Delta\Phi}{d\theta^*}\right]_{\text{kth intermediate point}} \tag{76}$$

is the value of the strength of the jet-vortex sheet at the kth intermediate point, and

$$\left.\begin{aligned} L_{jk} &= 0 && j>k, \\ &= \tfrac{1}{4}(h_{j+1}-h_{j-1}) && j=k, \\ &= \tfrac{1}{4}(h_{k+1}+h_k-h_{k-1}-h_{k-2}) && j<k, \end{aligned}\right\} \tag{77}$$

with

$$h_0 = 0, \text{ and } h_{n+1} = 2h_n - h_{n-1}.$$

The pressure equation (22) may now be written

$$g + \sum_{k=1}^{n} L_{jk}\gamma_k = \alpha_j\gamma_j + \beta_j \;, \; j=1,\ldots,n, \tag{78}$$

where for our iteration scheme α_j, β_j are given from the initial approximation, and g, γ_j are the unknowns to be calculated. The equations (78) are solved for the quantities γ_j in terms of the unknown g. The values for the strength of the sheet g_j at the pivotal points are then calculated in terms of the vortex strength g by interpolation between the quantities γ_j. To finally calculate the unknown vortex strength g, we use the Kutta condition (17) which can be written in terms of the transformed plane as

$$\frac{dW}{dZ^*} = 0 \text{ at } Z^* = 0. \tag{79}$$

The integrand in equation (48) is not determined at the point $\theta^* = 0$ when $Z^* = 0$. We assume, therefore, that its value is a linear function of θ^* at this point, and hence we can extrapolate to find its value I_0 at $\theta^* = 0$ in terms of its value I_1 at $\theta^* = h_1$ and its value I_2 at $\theta^* = h_2$.

Thus

$$I_0 = (h_2 I_1 - h_1 I_2)/(h_2 - h_1). \tag{80}$$

The real part of dW/dZ^* at $Z^* = 0$ is zero by symmetry and setting the imaginary part to zero and using equation (80), the Kutta condition reduces to

$$2\pi a = \frac{2g\bar{y}}{\bar{y}^2+\bar{z}^2} + \frac{h_2^2 y_2^* g_1}{(h_2-h_1)(y_2^{*2}+z_2^{*2})} + \left(h_3 - \frac{h_1 h_2}{(h_2-h_1)}\right)\frac{y_4^* g_2}{(y_4^{*2}+z_4^{*2})} +$$

$$+ \sum_{k=3}^{n} (h_{k+1}-h_{k-1})\frac{y_{2k}^* g_k}{(y_{2k}^{*2}+z_{2k}^{*2})}, \tag{81}$$

where $h_{n+1}=h_n$. The values g_j in terms of g obtained by interpolation from the solution of (78) are substituted into equation (81) to determine the value of g. The new values obtained in this way for the g and g_j are used to recalculate the quantities α_j in equations (71), (72) and (73). The quantities β_j remain unchanged since the shape of the sheet has not been changed in the calculation just described. A further approximation to the g and g_j can now be obtained and the process continued until the maximum change from one iteration to the next in any of the g and g_j is less than a prescribed tolerance ε_1.

At this stage we have, for the initial approximation to the vortex position and the sheet shape, the values of the g and g_j which satisfy the Kutta condition (17) and the pressure condition (22).

3.2. *Determination of the Vortex Position from the Total Force Condition.*

With the pressure condition satisfied for a particular configuration, we have now to find a vortex position which satisfies the force condition (54). Thus using the fact that

$$\lim_{Z\to Z_V}\left(\frac{Z}{Z^*}\frac{1}{(Z^*-Z_V^*)}-\frac{1}{(Z-Z_V)}\right)=\frac{-s^2}{2Z_VZ_V^{*2}}, \tag{82}$$

the total force condition (54) can be written as the equation

$$P=0, \tag{83}$$

where

$$P=\frac{(\bar{y}+i\bar{z})(2a_0-2ia_1-a_2+ia_3)}{a_0+ia_1}+ia-\frac{ig}{4\pi}\left(\frac{1}{\bar{y}}+\frac{1}{(a_0+ia_1)^2(\bar{y}+i\bar{z})}\right)+$$

$$+\frac{i}{2\pi}\sum_{j=1}^{n}g_j(h_{j+1}-h_{j-1})\frac{y_{2j}^*}{(\bar{y}-y_{2j}^*+i\bar{z}-iz_{2j}^*)(\bar{y}+y_{2j}^*+i\bar{z}-iz_{2j}^*)}-\frac{iF(\bar{y}+i\bar{z})}{2g(a_0+ia_1)}. \tag{84}$$

The quantity P is complex and equation (83) represents two conditions from which the vortex position can be found. With the isolated vortex at the position of the initial approximation and the pressure condition satisfied as outlined in Section 3.1, the force F is calculated as described in Appendix I. The value of P corresponding to this vortex position can then be found and if $|P^2|$ is greater than a prescribed tolerance ε_2, a new vortex position has to be found. We denote the real and imaginary parts of P by δP_1^y and δP_1^z for a first trial vortex position. The vortex is now moved to a second position $(\bar{y}_2, \bar{z}_2)$. To maintain a realistic representation of the vortex system, the finite part of the sheet must also, at least in part, be moved. However, since the sheet coordinates are measured from the isolated vortex position, the polar distances of that part of the sheet near the leading edge must be adjusted so as to ensure that the sheet still joins the leading edge smoothly. The following transformation is thus applied to the polar distances

$$\left.\begin{aligned}&[d_{2j}]_{\text{new}}=[d_{2j}]_{\text{old}}+(h_k-h_j)(d'_0-d_0)/h_k \qquad j\leqslant k\\ &[d_{2j}]_{\text{new}}=[d_{2j}]_{\text{old}} \qquad\qquad\qquad\qquad\quad j>k\end{aligned}\right\} \tag{85}$$

and

where $d_0=(\bar{y}^2+\bar{z}^2)^{\frac{1}{2}}$, $d'_0=(\bar{y}_2^2+\bar{z}_2^2)^{\frac{1}{2}}$.

From the kth pivotal point onwards the sheet moves with the vortex, as it is considered to be part of the core region.

With the isolated vortex and the inner part of the finite outer part of the jet-vortex sheet in a new position, the whole of the first part of the calculation, including the calculation of the curvatures, is

repeated and a second set of g and g_j obtained. The values δP_2^y, δP_2^z are stored. The procedure is repeated for a third trial vortex position. Let $\bar{y}_j + i\bar{z}_j$ $j=1,2,3$ denote the three trial vortex positions used, and δP_j^y, δP_j^z j $=1,2,3$ be the corresponding values of the force difference P. The vortex position $\bar{y}_4 + i\bar{z}_4$ which satisfies the force condition is assumed to be a linear function of δP^y and δP^z. Hence

and

$$\left.\begin{aligned} \bar{y} &= \bar{y}_4 + \left(\frac{\partial \bar{y}}{\partial P^y}\right)_4 \delta P^y + \left(\frac{\partial \bar{y}}{\partial P^z}\right)_4 \delta P^z \\ \bar{z} &= \bar{z}_4 + \left(\frac{\partial \bar{z}}{\partial P^y}\right)_4 \delta P^y + \left(\frac{\partial \bar{z}}{\partial P^z}\right)_4 \delta P^z \end{aligned}\right\} \tag{86}$$

Using the three trial vortex positions we have six equations given in matrix form as

$$\begin{pmatrix} \delta P_1^y & \delta P_1^z & 1 \\ \delta P_2^y & \delta P_2^z & 1 \\ \delta P_3^y & \delta P_3^z & 1 \end{pmatrix} \begin{pmatrix} \left(\frac{\partial \bar{y}}{\partial P^y}\right)_4 & \left(\frac{\partial \bar{z}}{\partial P^y}\right)_4 \\ \left(\frac{\partial \bar{y}}{\partial P^z}\right)_4 & \left(\frac{\partial \bar{y}}{\partial P^z}\right)_4 \\ \bar{y}_4 & \bar{z}_4 \end{pmatrix} = \begin{pmatrix} \bar{y}_1 & \bar{z}_1 \\ \bar{y}_2 & \bar{z}_2 \\ \bar{y}_3 & \bar{z}_3 \end{pmatrix}, \tag{87}$$

from which $\bar{y}_4 + i\bar{z}_4$ can be easily found. The vortex is then moved to this new position and using transformation (85) the sheet is adjusted accordingly. A new set of g and g_j are found. If for this new vortex position $|P^2| > \varepsilon_2$, where ε_2 is some prescribed tolerance, then that trial vortex position with the maximum value of $|P^2|$ is abandoned in favour of the newly calculated position $\bar{y}_4 + i\bar{z}_4$ and a further position is calculated as above. If the value of $|P^2|$ at $\bar{y}_4 + i\bar{z}_4$ is larger than that at any of the three trial positions, the calculation of $\bar{y}_4$ and $\bar{z}_4$ is repeated using a new set of trial positions which are spaced more widely. If $|P^2| < \varepsilon_2$ then the current set of parameters satisfy the pressure condition, the Kutta condition, and the total force condition to within the prescribed tolerances.

3.3. *Determination of the Sheet Shape from the Normal Velocity Condition.*

In general the normal velocity condition (9) will not be satisfied at this stage. We assume that the changes it is necessary to make in the polar distances in order to satisfy the condition are small and that the velocity field is unaffected by them. The required values of Φ_{σ_m} and Φ_n are evaluated using equations (47) and (68) at the intermediate points in terms of the current approximation obtained as in Sections 3.1 and 3.2. Now

$$\begin{aligned} [r_1 \sin \phi_1]_{\text{jth intermediate point}} &= \left[\frac{r_1^2}{s}\frac{d\theta_1}{d\sigma}\right]_{\text{jth intermediate point}} \\ &= \frac{b_{2j-1}^3 f_{2j}}{e_{2j}(y_{2j-1}^{*2} + z_{2j-1}^{*2})}. \end{aligned} \tag{88}$$

The positive (anti-clockwise) rotation η_j $j=1,\ldots,n$ of the tangent at the jth intermediate point which is necessary if the normal velocity condition is to be satisfied is given by

$$\eta_j = \left[\frac{\Phi_n/U \tan\gamma + r_1 \sin\phi_1}{\Phi_{\sigma_m}/U \tan\gamma}\right]_{\text{jth intermediate point}} \qquad j=1,\ldots,n. \tag{89}$$

If the quantities η_j are small, as assumed, then the corresponding change δ_j to be made to the jth polar

distance d_{2j} is then given by

$$\delta_j=\frac{d_{2j}\delta_{j-1}}{d_{2j-2}}-\frac{d_{2j}^2+d_{2j-2}^2-2d_{2j}d_{2j-2}\cos(h_j-h_{j-1})}{d_{2j-2}\sin(h_j-h_{j-1})}\eta_j, \tag{90}$$

as shown in Ref. 5, for $j=1,\ldots,n$, with $\delta_0=0$ since the sheet remains fixed to the leading edge. We introduce the quantity β_m where

$$\beta_m=\max\left|\frac{\delta_j}{d_{2j}}\right| \qquad j=1,\ldots,n. \tag{91}$$

If β_m is greater than a prescribed tolerance ε_3, the pivotal distances are adjusted in the following manner.

If $\beta_m \geqslant a_m$,

$$[d_{2j}]_{\text{new}}=[d_{2j}]_{\text{old}}+\frac{a_m}{\beta_m}\delta_j$$

and if $\beta_m < a_m$,

$$[d_{2j}]_{\text{new}}=[d_{2j}]_{\text{old}}+\delta_j \qquad \Bigg\} \; j=1,\ldots,n, \tag{92}$$

where the quantity a_m is the maximum proportional change to be allowed in the polar distances. With these new values for the d_{2j} we return to the innermost stage of our iteration scheme (3.1) and repeat the whole calculation until β_m becomes less than ε_3, at which stage it is concluded that a solution has been obtained.

4. *Solution Technique.*

4.1. *Solutions Obtained.*

The value of the semi-apex angle γ was held fixed at 20 degrees for all the solutions described in this Report. This value is the same as that of the model used by Alexander[16] in his experiments, and of the model currently being tested at Cranfield by J. J. Spillman. Two different sheet representations were used, a long finite sheet of about 16 radians in angular extent specified by 39 pivotal points, and a shorter sheet of about 3 radians specified by 14 pivotal points. The program written for the longer sheet was only used for blowing angles $\beta<70$ degrees for which the jet sheet lies within the length of the finite vortex sheet. There was no facility in this program for calculating the force to be sustained on the vortex and cut, hence this force was set to zero which is correct when $\beta<70$ degrees in the particular case. The program for the shorter finite sheet could, in principle, be used for all angles of β from 20 to 200 degrees although in practice it was only used for values of β up to 120 degrees since, as already mentioned, $\Delta C_N(\beta)$ has a maximum at $\beta=110$ degrees. The jet itself was only contained on this shorter finite jet-vortex sheet for values of $\beta<35$ degrees, consequently a useful check for 35 degrees $<\beta<70$ degrees could be made between the results obtained from the two programs. In all cases the asymptotic method used for calculating the force to be sustained on the vortex and cut used in association with the 14 point program produced satisfactory agreement. Results for the 14 point and 39 point programs are given at the end of Table 1. Comparison of the normal force coefficient reveals differences of less than 1·5 per cent. The slight discrepancy in the position of the isolated vortex is similar to the discrepancy that Smith found in the no-blow case[5].

The solutions obtained can be conveniently split into two separate categories:—

(i) The 14 point program was used to obtain solutions for $a=0{\cdot}75$, $C_\mu=0{\cdot}1$, $\gamma=20$ degrees, increasing β until a maximum in the lift increment was reached. This occurred for a value of $\beta\simeq 110$ degrees so that solutions were obtained for 20 degrees $\leqslant\beta\leqslant 120$ degrees. Further solutions were found for $C_\mu=0{\cdot}025$, 0·05, 0·075 for selected values of β over the range 20 to 120 degrees.

(ii) Although earlier results indicated that the 14 point representation was an adequate model in calculating quantities like the normal force, a number of solutions had already been found from the

39 point program for an angle of $\beta = 40$ degrees. The longer 39 point program was thus used for a survey varying both a and C_μ for a fixed $\gamma (= 20$ degrees) and $\beta (= 40$ degrees). Solutions for $a \leqslant 0{\cdot}25$ proved too difficult to obtain on account of the inordinate length of time required to reach a solution, which was apparently related to an unrealistic point of inflexion which developed in the sheet shape close to the leading edge. Similar difficulties were experienced by Smith[5] for these low values of a. The 'carpet' of solutions obtained using this program extended over the range $0{\cdot}35 \leqslant a \leqslant 1{\cdot}00$, $0{\cdot}00 \leqslant C_\mu \leqslant 0{\cdot}10$.

4.2. *Tolerances.*

The value of the quantity a_m used in the outer loop, and the values of the tolerances ε_1, ε_2, ε_3 were chosen from the experience gained by Smith in his calculations. The tolerances ε_1, ε_2, ε_3 were held fixed for all solutions and were set equal to the values $2{\cdot}0 \times 10^{-4}$, $1{\cdot}0 \times 10^{-5}$, and $5{\cdot}0 \times 10^{-3}$ respectively. It is felt that these values produce a sufficiently accurate solution in a reasonable amount of computing time. The value chosen for a_m, the maximum proportional change in the pivotal distances, influenced the time in which a solution could be reached considerably. This is because changes in the shape of the sheet significantly affect the curvature of the geodesics, and hence, the force that is sustained on the vortex and cut and the pressure jump across the sheet. The value that Smith used for a_m was 0·05, this was found to be too large in the present case and was reduced to 0·01 and in some cases, for the 14 point program, to 0·005. In addition, the value of a_m was halved each time the iteration began to oscillate. These measures were largely successful in preventing oscillations in the iteration process.

4.3. *Initial Approximations.*

The first initial approximations used in the solution procedure were those obtained by Smith for $C_\mu = 0$. The values of the polar angles, held fixed throughout the procedure, were set equal to those used by Smith for his 14 point and 39 point sheet representations. For small values of C_μ or for β close to γ the solutions of Smith were adequate as initial approximations for each a. However, it was found that as the numerical procedure progressed and new solutions for larger C_μ and β were generated, the sheet shape tended to flatten out close to the leading edge. The first pivotal point, being close to the leading edge, thus moved very close to the y-axis. During certain stages of the calculation, when the vortex position was varied, this first point could be pushed below the y-axis, causing the curvature and the pressure jump to change sign at the first intermediate point. This unrealistic phenomenon made the procedure very unstable and generally caused the iteration to diverge. The problem was overcome by removing this first point altogether and making up the number (to 14 or 39) by adding an extra pivotal point to the end of the sheet, thus increasing slightly the angular extent of the finite representation.

As long as the parameters a, C_μ, β, were not altered by a large amount, it was possible to use the previous solution as an initial approximation for the new solution. In this way starting with the solution for $\beta = \gamma$, which corresponds to the no blow case of Smith, it was possible to calculate solutions for fixed a, C_μ, γ increasing β from 20 degrees in steps of 2·5 degrees. Later it was found that the step length could be increased to 5 degrees by extrapolating to the new initial approximation using the two previous solutions. Any larger step length in β either caused the procedure to diverge or increase its time length by an excessive amount. By incrementing each of the parameters a, C_μ, β in turn it was possible to calculate the solutions required. It was found that some solutions were obtained more quickly by varying particular parameters. But no universal rule emerged as to which parameter it was best to vary.

At one stage one particular solution was calculated by following two different routes in the parameter space a, C_μ and β. The two solutions agreed well, suggesting that the solutions obtained by this method are unique.

4.4. *Programming Technique and Computer Operation.*

The program was written in Fortran IV and first used on the ICL 1905E computer at the University of East Anglia. When a successful program had been developed, the 39 point version was converted to run on the SRC Atlas computer at Didcot. On the 1905E computer the compilation and consolidation of the program generally took about 6 minutes. The program was, therefore, stored on disc in a loadable

binary form, from where it could be loaded onto the computer in a few seconds using only a few punched cards. Since the time to reach a solution could vary between 15 and 60 minutes, a dump and restart procedure was used, and the program run for a specified amount of time. This meant that if the iteration did not converge within the time allowed, the program was dumped onto disc from where it could be restarted later from the point where it left off. As the program became more sophisticated it was overlaid to conserve space. The dump and restart procedure was removed and the current approximation was dumped out on cards at the end of the specified time. The iteration could be recommenced by feeding in this current approximation as the new initial approximation.

During the initial stages a Minimop on-line system was used to develop the program. Such a system allows the programmer to run his program from a console enabling him to correct and run his program 5 or 6 times during one hour. It was on this system that the program first converged to a solution.

Figs. 7 and 8 give a flow diagram of the program. Fig. 8 is the innermost loop of the program, code named DEUCE, and is shown separately for clarity.

5. *Results.*

5.1. *Normal Force.*

Due to the singularity in the complex transformation the values of the pressure and velocity fields are less accurate close to the point corresponding to the leading edge in the cross-flow plane than elsewhere. Because of this singularity the normal force calculated by integrating the pressure difference presents a difficult numerical problem. The normal force is therefore obtained by calculating the flux of downward momentum due to the presence of the wing and of the vortex system. If in the solution procedure there were no approximations, then the calculation of the normal force by this method would yield the same results as the pressure integral, because the jet leaves the leading edge tangentially to the wing. For the case in which there is no blowing Smith has shown that, although there are small unbalanced forces in the flow field, the values of the normal force obtained by the two different methods show close agreement.

Let the normal force coefficient be denoted by C_N and define L_2 such that

$$C_N = L_2 \tan^2 \gamma . \tag{93}$$

The quantity L_2 is calculated from a consideration of the flux of downward momentum produced by the wing and vortex system; in the absence of blowing, L_2 is a function of a only. Since the fluid in the jet does not mix with the mainstream, the total flux of downward momentum across the cross-flow plane is the sum of the flux of downward momentum in the main flow, denoted by L_{21}, and the flux of downward momentum in the jet, which is embedded within the main flow, denoted by L_{22}. For the main flow we have

$$L_{21} = -2\mathscr{R}\left\{ \int_C \frac{W}{Us \tan \gamma} d(Z/s) \right\} , \tag{94}$$

where C is a contour surrounding the entire system of wing, vortex sheets, isolated vortices and cuts in the cross-flow plane. The expansion of W for large Z^*/s gives

$$W = c_{-1} Z^*/s + c_0 + c_1 s/Z^* + \ldots , \tag{95}$$

and if we take the contour C to be a very large circle then equation (94) reduces to

$$L_{21} = 2\pi \mathscr{I}\{2c_1 - c_{-1}\} \tag{96}$$

where

$$c_{-1} = -ia \tag{97}$$

and

$$c_1=\frac{ig\bar{y}}{\pi}+\frac{i}{2\pi}\sum_{j=1}^{n} g_j(h_{j+1}-h_{j-1})y^*_{2j}, \tag{98}$$

in our finite difference notation.

To calculate the quantity L_{22}, let $\underline{t}^\alpha$ be the unit tangent vector of a particular jet geodesic in the conical jet-vortex sheet. Let V be the speed of the fluid in the jet, ρ_J its density, and δ the jet thickness. The rate at which downward momentum is carried across the cross-flow plane by the two leading-edge jets is then given by

$$\tilde{L}_{22}=-2\int_{C_s}\rho_J\delta V(\underline{t}^\alpha.\underline{k})V(\underline{t}^\alpha.\underline{i})d\sigma, \tag{99}$$

where C_s is a contour along the starboard jet trace in the cross-flow plane, $\underline{i}$ and $\underline{k}$ are unit vectors parallel to Ox and Oz, σ is the dimensional distance measured along this trace and $\tilde{L}_{22}=\frac{1}{2}\rho U^2 s^2\tan\gamma\, L_{22}$. Now

$$\underline{t}^\alpha=\frac{\underline{R}'(\bar{s}(\theta),\theta)}{|\underline{R}'|} \tag{100}$$

where $\underline{R}(\bar{s}(\theta),\theta)$ is defined by equations (23) and $\bar{s}(\theta)$ is defined by the differential equation (28). The flux of downward momentum, after taking the thin-jet limit, is given, from equations (99) and (100), by

$$\tilde{L}_{22}=-2\int_{C_s}\frac{J\{[\lambda_2+f\sin(\theta-\varepsilon)]\bar{s}'+[f'\sin(\theta-\varepsilon)+f\cos(\theta-\varepsilon)]\bar{s}\}\bar{s}'sd\zeta}{(a\bar{s}'^2+2b\bar{s}\bar{s}'+c\bar{s}^2)\tan\gamma} \tag{101}$$

Substituting for $\bar{s}(\theta)$ from equation (34) in (101) and using equations (20), (21), (96), (97), (98) and (I.8) we find that

$$\begin{aligned}L_2&=L_{21}+L_{22}\\&=2\pi a+4g\bar{y}+2\sum_{j=1}^{n} g_j(h_{j+1}-h_{j-1})y^*_{2j}-\\&\quad-\int_0^{\theta_m}\frac{\left\{\begin{array}{l}C\mu\cos\gamma\sqrt{c}\,ww'\{[\lambda_2+f\sin(\theta-\varepsilon)]w'\\\quad-[f'\sin(\theta-\varepsilon)+f\cos(\theta-\varepsilon)]w\}\end{array}\right\}}{2\sin(\beta-\gamma)\tan^2\gamma\,(aw'^2-2bww+cw^2)}d\theta\end{aligned} \tag{102}$$

where θ_m is the value of θ at which the pressure jump across the sheet goes to zero. For the case when the jet exceeds the finite jet-vortex sheet the functions $w(\theta)$ and $f(\theta)$ are calculated using the asymptotic method outlined in Appendix I. The integral involved in equation (102) is evaluated using the trapezium rule. The magnitude of L_{22} is about 10 per cent of the increment in L_2 due to the introduction of the jet.

We define the normal force increment ΔC_N to be equal to the normal force calculated for a particular set of parameters (a, C_μ, β, γ) minus the normal force calculated for the same configuration but with $C_\mu=0$. In Fig. 9 ΔC_N is shown as a function of β for various values of C_μ. For all values of C_μ, ΔC_N reaches

a maximum at $\beta = 110$ degrees within the numerical accuracy of the calculations. This represents an initial jet direction which is normal to the leading edge. This maximum is seen in Fig. 11 to be an increasing function of C_μ. In Fig. 10 the value of C_N is shown as a function of C_μ for various values of a at a fixed angle of $\beta = 40$ degrees. For each value of a there is, as we expect, an increase in C_N corresponding to an increase in C_μ, although there appears to be little difference with a in the rate of increase. This point is illustrated in Fig. 12 where for two values of a the value of ΔC_N is shown as a function of C_μ. Adding further curves for other values of a does not help to establish any consistent variation of ΔC_N with a. Thus over the range of values of C_μ considered, the variation of ΔC_N with C_μ is approximately independent of the value of a for $0{\cdot}35 \leqslant a \leqslant 1{\cdot}00$, at least for $\beta = 40$ degrees. The variation of $\Delta C_N / C_\mu$ with C_μ is shown in Fig. 13. The percentage gain in ΔC_N falls off as C_μ increases, a fact that is apparent for all the values of β considered.

The net effect of introducing a jet blowing air out from the leading edge, and in a direction normal to the leading edge, is to increase the normal force on the wing by as much as 25 per cent for $a = 0{\cdot}75$ with a blowing coefficient of $C_\mu = 0{\cdot}1$. The results for fixed β show that the normal force increment is largely independent of a. We note that for a value of $a = 0{\cdot}35$ the gain in normal force is about 25 per cent even for the relatively small value of $\beta = 40$ degrees with $C_\mu = 0{\cdot}1$.

5.2. *Vortex Sheet Shape and Position. Circulation.*

In Figs. 14 and 15 the effect of the jet on the shape of the jet-vortex sheet is shown. Fig. 14 shows the shape obtained, using the 39 point representation, for values of $a = 0{\cdot}35$, $1{\cdot}00$ and for $C_\mu = 0$. Fig. 15 shows the corresponding shapes for $C_\mu = 0{\cdot}1$. The larger one in each case corresponds to $a = 1{\cdot}00$. There is a considerable reduction in the curvature of the sheet near the leading edge, an effect which occurs even for smaller values of C_μ. The reduction in curvature is more marked for the lower value of a. Otherwise the jet-vortex sheet spiral expands slightly and becomes less tightly rolled as either C_μ or β is increased. This effect can be seen more clearly in Fig. 16 where the two spirals corresponding to $a = 1{\cdot}0$ in Figs. 14 and 15 have been superposed so that their centres coincide.

Corresponding to the flattening out of the sheet at the leading edge is the general outboard movement of the vortex system as a whole. This effect is demonstrated in Fig. 17 where the sheet shape and vortex positions are shown for $a = 0{\cdot}75$ and various values of β using the 14 point representation. The case $\beta = 20$ degrees corresponds to no blowing since the jet then degenerates into a straight line along the leading edge and can sustain no pressure jump. These outboard movements are demonstrated again in Figs. 18 and 19 where the vortex position is shown as a function of β, C_μ and of a, C_μ respectively. Although the vortex moves outboard and away from the wing as β increases initially, we see that as β approaches 110 degrees the vortex, although continuing its outboard movement, moves closer to the wing plane. For decreasing values of a the vortex movements become larger for given values of C_μ and β.

In Fig. 22 the total circulation about the vortex system is shown as a function of β, together with, in Figs. 20 and 21, the variation with β of the circulation about the finite outer part of the jet-vortex sheet and about the isolated vortex respectively. The 14 point representation is employed in Figs. 20–22. We see that there is an effective transfer of vorticity from the outer part of the jet-vortex sheet to the vortex core as β increases. In fact the local strength of the jet-vortex sheet close to the leading edge ultimately changes sign for the larger values of β considered, as can be seen in Fig. 23. Thus in Figs. 20 and 21 we see that the increase in circulation about the isolated vortex is counterbalanced to some extent by a decrease in circulation about the finite part of the jet-vortex sheet. This decrease arises from the introduction of vorticity by the curved jet which is opposite in sign to the vorticity usually associated with the leading-edge vortices. In order to appreciate this point we recall that $\tilde{\Delta} p_s$ is positive across the jet-vortex sheet, which implies that the speed of the fluid leaving the upper surface of the wing at the leading edge is greater than that leaving the lower surface. The consequence is a contribution to the streamwise vorticity of opposite sign to the main vortex system. The net effect on the overall circulation is to increase the circulation with β in a manner which is closely paralleled by the variation of ΔC_N with β in Fig. 9.

5.3. *Pressure and Velocity Distributions on the Wing Surface.*

To obtain the components of velocity in the cross-flow plane we use equation (46),

$$\Phi_y - i\Phi_z = \frac{dW}{dZ} = \frac{Z}{Z^*}\frac{dW}{dZ^*},$$

where dW/dZ^* is given in finite difference form from equation (68) as

$$\frac{1}{U\tan\gamma}\frac{dW}{dZ^*} = -ia + \frac{g}{2\pi i}\left(\frac{1}{Z^*/s - \bar{y} - i\bar{z}} - \frac{1}{Z^*/s + \bar{y} - i\bar{z}}\right) +$$

$$+\frac{1}{4\pi i}\sum_{j=1}^{n} g_j(h_{j+1} - h_{j-1})\left(\frac{1}{Z^*/s - y^*_{2j} - iz^*_{2j}} - \frac{1}{Z^*/s + y^*_{2j} - iz^*_{2j}}\right).$$

The velocity component Φ_x is given from equation (11) as

$$\Phi_x = \frac{1}{x}(\Phi - y\Phi_y - z\Phi_z),$$

where $\Phi = \mathscr{R}\{W\}$,

and

$$\frac{W}{Us\tan\gamma} = -ia\,Z^*/s + \frac{g}{2\pi i}\log\frac{Z^*/s - \bar{y} - i\bar{z}}{Z^*/s + \bar{y} - i\bar{z}} +$$

$$+\frac{1}{4\pi i}\sum_{j=1}^{n} g_j(h_{j+1} - h_{j-1})\log\frac{Z^*/s - y^*_{2j} - iz^*_{2j}}{Z^*/s + y^*_{2j} - iz^*_{2j}}. \tag{103}$$

In order to calculate W on the wing surface we must remove the ambiguity involved in determining the logarithm of a complex number and so we proceed as follows. Denote by $\mathrm{Log}\,Z$ the value of $\log Z$ for which the imaginary part lies in the range $(-\pi, \pi]$. Then to evaluate W on the imaginary axis of the transformed plane, at the point Z^* where $\mathscr{R}\{Z^*\} = 0$, we use the following values for the logarithms involved.

For

$$\mathscr{I}\{Z^*/s\} \geqslant \bar{z}\,, \log c = \mathrm{Log}\,c$$

for

$$\bar{z} > \mathscr{I}\{Z^*/s\} \geqslant 0\,, \log c = \mathrm{Log}\,c + 2\pi i$$

for

$$0 > \mathscr{I}\{Z^*/s\} \quad\,, \log c = \mathrm{Log}\,c\,,$$

where $c = \dfrac{Z^*/s - \bar{y} - i\bar{z}}{Z^*/s + \bar{y} - i\bar{z}}$.

Similar formulae are used when (y^*_{2j}, z^*_{2j}) replace $(\bar{y}, \bar{z})$ for the other logarithms involved in equation (103). This determination displaces the discontinuity involved in evaluating the logarithms so that it occurs as we cross the jet-vortex sheet.

From the values of Φ_x, Φ_y and Φ_z so obtained we calculate the pressure distribution from equation (10),

$$C_p/\tan^2\gamma = -2\Phi_x/U\tan^2\gamma - (\Phi_y^2+\Phi_z^2)/U^2\tan^2\gamma + a^2.$$

In Figs. 24 and 25 we see the effects on the wing-surface pressure distribution of introducing a jet with an initial direction $\beta = 40$ degrees, and a blowing coefficient $C_\mu = 0{\cdot}1$. For both the values of a shown there is an increase in the magnitude of the suction peak together with a slight outboard displacement of it. These changes are consistent with both the increase in strength of the isolated vortex and its lateral outboard movement. Fig. 26 shows the effect on the surface pressure distribution of changing the initial direction of the jet for a fixed value of the blowing coefficient. Again an increase in the suction peak is induced together with a slight outboard movement. Another effect of the jet is to reduce the drop in pressure on the lower surface of the wing as the leading edge is approached, thus maintaining the favourable pressure difference up to the leading edge. This occurs even for small C_μ which perhaps explains the larger values of $\Delta C_N/C_\mu$ obtained at the smaller values of C_μ; the effect is similar to an end-plate effect.

In Fig. 27 the lateral velocity $\Phi_y/U\tan\gamma$ on the wing surface is shown for fixed $\beta = 40$ degrees for two values of a and C_μ. Apart from the changes due to the outboard movement of the vortex system there is little difference between the cases where there is blowing and the cases where there is no blowing, except near the leading edge where the direct effects of the jet are most significant. As β is increased the increase in the lateral velocity becomes more marked as can be seen in Fig. 28. Similar effects are exhibited by the longitudinal velocity $\Phi_x/U\tan^2\gamma$ shown in Figs. 29 and 30.

Associated with the wing surface velocities Φ_x and Φ_y are the bound vortex lines which are found by integrating the differential equation

$$\frac{dy}{dx} = -\frac{\tilde{\Delta}\Phi_x}{\tilde{\Delta}\Phi_y},$$

where $\tilde{\Delta}\Phi_x$ and $\tilde{\Delta}\Phi_y$ are the differences across the wing surface of the longitudinal and lateral velocity components respectively. In Fig. 31 the bound vortex lines in the presence of edge blowing are shown for various values of a. The changes brought about in these bound vortex lines are seen to be most significant for the smaller values of a. In Fig. 32 we observe that even for large values of β the changes in the bound vortex lines brought about by blowing are still quite small for $a = 0{\cdot}75$.

6. *Comparison with Experiment.*

Comparison with experiment is difficult, since none of the experiments carried out with leading-edge blowing has produced the conical flow conditions which are assumed in the theoretical calculations. The experiments have been at subsonic speeds, for which the upstream influence of the trailing edge reduces the lift below that which would be expected on the basis of slender-body theory, whether in attached flow, separated flow, or with leading-edge blowing. On the other hand, where the experiments have employed blowing over the forward part of the leading edge only, a given blowing momentum C_μ is more effective in producing lift than when it is distributed in a conical fashion along the whole leading edge, since the momentum blown from near the trailing edge has little chance to influence the wing.

The only experimental results which cover variations in β as well as in C_μ and a are those of Alexander[16], who used a cropped delta wing. In Fig. 33 the variation with β of ΔC_N from both theory and experiment, is compared for $a = 0{\cdot}75$. The conclusion drawn by Alexander was that, for blowing angles not too close to the leading edge, the normal force increment is approximately constant. The present theory conflicts with this conclusion since the normal force increments attain a well-defined maximum at $\beta = 110$ degrees. An additional point from the experimental work of Trebble[19] is also shown in Fig. 33 and corresponds to $\beta = 110$ degrees. In Trebble's model air was blown, as far as was possible, from the whole length of the leading edge in a conical fashion, unlike Alexander's cropped delta wing model which had a large section at the rear from which no air was blown. As mentioned above, this section would experience the beneficial effects of the jet as it is swept back over the wing surface. Except for Alexander's results for $\beta = 30$ and 40 degrees the experimental values of ΔC_N are lower than the predictions for a given β and C_μ. This probably arises because the theory does not take into account the trailing edge effect, and hence

overestimates the normal force on the wing. The fact that Alexander's results appear to be less sensitive to variations in the angle β is probably due to the large section at the rear of the model from which no air is blown. For small values of β much of the air that is emitted near the trailing edge of the wing is rapidly swept away downstream and hence makes a smaller contribution to the local flow properties than air blown at a larger angle. Moreover the conical nature of the jet in our model enhances this effect since more air is blown out as we approach the trailing edge. In Alexander's model the unblown section at the rear will experience the effects of this 'lost' air even for low values of β, and the variation of ΔC_N with β will be much less than if blowing had occurred along the whole length of the leading edge.

In Fig. 34 ΔC_N is shown as a function of C_μ, for various values of a, with $\beta = 110$ degrees. These may be compared with the experimental results obtained by Trebble which are also displayed. Since, as we have already mentioned, air was blown conically from as much of the leading edge as possible in Trebble's experiments, we may anticipate that the difference between these experiments and the present theory may be traced to the trailing edge effect referred to above. To test this hypothesis we have also included in Fig. 34 the variation of ΔC_N^* with C_μ where

$$\Delta C_N^* = \Delta C_N \left[\frac{C_{NE}}{C_{NT}}\right].$$

Here C_{NE} and C_{NT} are the experimental and theoretical results obtained, in the absence of blowing, by Kirby[20] and Smith[5], respectively, at the appropriate value of a. We believe that we are justified in concluding that the trailing edge effect accounts for most of the discrepancy between the present theory and a finite wing experiment with conical full-edge blowing.

As we have already indicated, the experimental investigations have concentrated upon total force measurements. However, Alexander[16] presents surface pressure measurements sufficiently close to the apex of the wing for the flow field to simulate, approximately, the conditions of the present theory. Alexander's results for the spanwise pressure, on both the upper and lower surfaces of the wing, are shown in Fig. 35 where a comparison is made with the theoretically predicted pressure distribution. It should be noted that in this particular comparison we have allowed a factor of two between the blowing coefficient used by Alexander and that used here. This is because in Alexander's model the edge blowing terminated at a point which divided the area of the wing into equal parts. The agreement between theory and experiment on the upper surface of the wing is better than that in analogous comparisons made by Smith[5], in the absence of blowing. This is because the secondary separation close to the leading edge is less in evidence when there is edge blowing. The agreement is less good on the lower surface and the normal force coefficients calculated from the theoretical and experimental pressure distributions differ by 10 per cent. This is probably due to the thickness of the forward part of Alexander's model.

For various reasons, comparison between theory and experiment is not easy in these situations. However, the agreement obtained, with the trailing edge correction, between the theory and Trebble's total force measurements, and between the theory and Alexander's pressure measurements at a forward station, encourage us to believe that the theoretical results indicate the main features of the flow which may be expected in practice.

Acknowledgement.

The advice and help of Dr. N. Riley of the University of East Anglia, who supervised this research, and of Mr. J. H. B. Smith, of the Royal Aircraft Establishment, who monitored the research agreement, are gratefully acknowledged.

LIST OF SYMBOLS

$a(\theta)$	Conical sheet function, *see* equation (27)
a	$=\alpha/\tan\gamma$
a_m	Maximum proportional change allowed in d_{2j}
a_0, a_1, a_2, a_3	Real and imaginary parts of $Z_V/s, Z_E/s$
$b(\theta)$	Conical sheet function, *see* equation (27)
b_j	Values of r_1 at points on sheet
$c(\theta)$	Conical sheet function, *see* equation (27)
c_j	Values of θ_1 at points on sheet
C_N	Normal force coefficient
C_N^*	$=C_N\times\left(\frac{C_{NE}}{C_{NT}}\right)$
C_{NE}	Experimental normal force coefficient for $C_\mu=0$
C_{NT}	Theoretical normal force coefficient for $C_\mu=0$
C_p	Pressure coefficient
C_μ	Blowing coefficient
c_{-1}, c_0, c_1	Coefficients in expansion of W for large Z^*
d_j	Values of r^*/s of sheet in transformed plane
e_j	Sheet derivatives, *see* equations (66)
f	Function of sheet shape in cross-flow plane
f_j	Sheet derivatives, *see* equations (66)
F	Non-dimensional force sustained by inner jet sheet
F^y, F^z	y and z components of F
g	$=\Gamma/Us\tan\gamma$ non-dimensional circulation of vortex
g_j	$=\left[\frac{d\Delta\Phi}{d\theta^*}\Big/ Us\tan\gamma\right]$ at the n pivotal points
h_j	Polar angles of pivotal points in transformed plane
J	$=\lim_{\delta\to 0}\delta\rho_J V^2$ momentum flux of jet
k	Index of point on sheet beyond which sheet moves with vortex
L_{jk}	Matrix used in satisfying pressure condition
L_2	$=C_N/\tan^2\gamma$
L_{21}	Contribution to L_2 from flow field
L_{22}	Contribution to L_2 from jet
$\tilde{L}_{22}$	Dimensional contribution to L_2 from jet

M	$=J/s_0$, conical jet constant
n	Number of pivotal points specifying finite sheet
$\underline{n}$	Normal to trace of jet vortex sheet in cross-flow plane
$\underline{n}^\alpha$	Unit principal normal to geodesic
N	Component of velocity normal to line vortex
p_s	Pressure
$p(\theta)$	Conical sheet function, *see* equation (29)
P	Excess force on vortex and cut
$q(\theta)$	Conical sheet function, *see* equation (29)
$\delta P^y, \delta P^z$	y and z components of P
r	$=f(\theta)$, non-dimensional distance from trace of sheet in cross-flow plane to the vortex
r^*	Non-dimensional distance of trace to the origin in the transformed plane
r_1	Non-dimensional distance of trace to the origin in the cross-flow plane
$\tilde{r}_1$	$=r_1 s$ dimensional distance of trace to the origin in the cross-flow plane
r^0, r^I	Values of r at θ, $\theta+2\pi$ near the centre of the core region
$\underline{R}$	Vector specifying conical sheet
s	Wing semi-span of a particular cross-flow plane
s_0	Wing semi-span of the point where a particular geodesic originates
$\bar{s}$	Wing semi-span of any cross-flow plane
S	Equation of conical surface
$\underline{t}^\alpha$	Tangent of geodesic
T	Geodesic shape function
U	Speed of undisturbed flow
v	Angle in 'unrolled' vortex sheet, *see* Fig. 2
V	Speed of jet fluid
$\underline{V}$	$=\nabla\Phi$, velocity vector
V_1, V_2	Speed of fluid in core region
w	$=s_0/\bar{s}$, function determining geodesics
W	$=\Phi+i\psi$, complex potential
x, y, z	Cartesian coordinates
$\bar{y}, \bar{z}$	Non-dimensional coordinates of starboard vortex
$\bar{y}, \bar{z}_j$	Trial positions used to find a new vortex position
y_j^*, z_j^*	Non-dimensional coordinates of sheet point in transformed plane

LIST OF SYMBOLS—*continued*

Z	$=y+iz$, complex representation of cross-flow plane
Z^*	Complex representation of transformed plane
Z_E	Position of end of the starboard vortex sheet
Z_V	Starboard vortex position
α	Wing incidence
α_j	Quantity used in linearization of the pressure equation
β	Angle of jet with wing centre line
β_j	Pressure jump across the sheet at the intermediate points
β_m	$=\max \frac{\delta_j}{d_{2j}}$
γ	Wing semi-apex angle
γ_j	Strength of the sheet at the intermediate points
Γ	Circulation of starboard vortex
δ	Width of jet
δ	Angle of constant flow through core region, *see* Fig. 6
Δ	Increment due to blowing
$\tilde{\Delta}$	Difference operator across the sheet and wing surface
δ_j	Changes in d_{2j}
∇	Laplacian operator
ε	Angle between line joining vortex to leading edge and the y-axis
$\varepsilon_1, \varepsilon_2, \varepsilon_3$	Tolerances
ζ	Non-dimensional arc length of trace in cross-flow plane
η_j	Required rotation of tangent to sheet
θ	Polar angle of trace with vortex as origin in cross-flow plane
θ^*	Polar angle of trace with vortex as origin in transformed plane
θ_1	Polar angle of trace with centre line as origin in cross-flow plane
θ_0	Value of θ at end of finite jet-vortex sheet
θ_m	Value of θ at end of inner jet spiral
ϑ	*see* Fig. 4
κ	Curvature of geodesic
λ	Angle of outward normal of sheet with y-axis, *see* Fig. 6
λ_1, λ_2	Real and imaginary parts of Z_V/s
ρ	Density of freestream fluid
ρ_J	Density of jet fluid

σ	Dimensional arc length of trace in cross-flow plane
σ^*	Dimensional arc length of trace in transformed plane
σ^a	Dimensional arc length of geodesic
τ	Geodesic parameter
ϕ	Angle between radius r and tangent of trace
ϕ_1	Angle between radius r_1 and tangent of trace
Φ	Velocity potential
ψ	Angle between y-axis and tangent of trace

REFERENCES

No.	*Author(s)*	*Title, etc.*
1	R. Legendre	Écoulement au voisinage de la point avant d'une aile à forte flèche aux incidences moyennes. *8th Int. Cong. Th. Appl. Mech.*, Istanbul (1952). Rech. aéro., 30 (1952) and Rech. aéro., 31 (1953).
2	R. Legendre	Écoulement au voisinage de la point avant d'une aile à forte flèche. Rech. aéro., 35 (1953).
3	C. E. Brown and W. H. Michael	On slender delta wings with leading-edge separation. *J. Aero. Sci., 21*, 690-694 and 706 (1954). NACA Tech. Note 3430, April 1955.
4	K. W. Mangler and .. .. J. B. H. Smith	Calculation of the flow past a slender delta wing with leading-edge separation. RAE Report Aero 2593 (1957). *Proc. Roy. Soc. A., 251*, 200-217 (1959).
5	J. H. B. Smith	Improved calculations of leading-edge separation from slender delta wings. RAE Technical Report 66070 (1966). *Proc. Roy. Soc. A., 306*, 67-90 (1968).
6	K. Stewartson and M. G. Hall	The inner viscous solution for the core of a leading-edge vortex. *J. Fluid Mech., 15*, 306-318 (1963).
7	K. W. Mangler and J. Weber..	The flow field near the centre of a rolled-up vortex sheet. *J. Fluid Mech., 30*, 177-196 (1967).
8	M. G. Hall	A theory for the core of a leading-edge vortex. *J. Fluid Mech., 11*, 209-228 (1961).
9	S. N. Brown	The compressible inviscid leading-edge vortex. *J. Fluid Mech., 22*, 17-32 (1965).
10	D. Küchemann and J. Weber	Vortex motions. ZAMM, *45*, 457-474 (1965).
11	D. A. Spence	The lift coefficient of a thin, jet flapped wing. *Proc. Roy. Soc., 238*, 46-68 (1965).
12	C. M. P. Morgado and .. A. H. Craven	A theory for slender delta wings with leading-edge blowing. COA Report Aero 169, Cranfield (1963).
13	E. C. Maskell	Discussion at the symposium on vortex motions organised by IUTAM in 1964. *Progress in Aeronautical Sciences 7*, 44, Pergamon (1966).

REFERENCES—*continued*

No.	*Author(s)*	*Title, etc.*
14	F. J. Warner	On the solution of 'Jury problems' with many degrees of freedom. *Math. Tab., Wash., 11*, 268-271 (1957).
15	E. S. Levinsky and M. H. Y. Wei	Non-linear lift and pressure distribution of slender conical bodies with strakes at low speeds. NASA CR-1202 (1968).
16	A. J. Alexander	Experimental investigation on a cropped delta wing with leading-edge blowing. COA Report *162*, Cranfield (1963).
17	T. J. Willmore	*An introduction to differential geometry.* Oxford University Press (1959).
18	E. C. Maskell	On the asymptotic structure of a conical leading-edge vortex. Paper presented at the symposium organised by IUTAM in 1964. *Progress in Aeronautical Sciences 7*, 40 (1966).
19	W. J. G. Trebble	Exploratory investigation of the effects of blowing from the leading edge of a delta wing. A.R.C. R. & M. 3518 (1966).
20	D. A. Kirby	An experimental investigation of the effect of planform shape on the subsonic longitudinal stability characteristics of slender wings. A.R.C. R. & M. 3568 (1967).

APPENDIX I

Force on the Vortex and Cut, Using the Asymptotic Method of Mangler and Smith[4].

The problem is to calculate the shape of a tightly rolled jet-vortex sheet that carries a pressure jump across it. The conditions which must be satisfied on the sheet are those already outlined in Section 2.1, namely

$$\Phi_n = -U \tan\gamma \, r_1 \sin\phi_1 , \tag{9}$$

$$\frac{\tilde{\Delta}\Phi}{Us\tan\gamma} = \frac{\tilde{\Delta}\Phi_\sigma(r_1\cos\phi_1 - \Phi_{\sigma_m}/(U\tan\gamma))}{U\tan\gamma} + \frac{\kappa s_0 C_\mu \cos\gamma}{2\sin(\beta-\gamma)\tan^2\gamma} . \tag{22}$$

With reference to Fig. 4, let $s\lambda_0$ be the length of the line between the vortex and the origin in the cross-flow plane, and let ϑ be the angle it makes with the y-axis. Let the polar coordinates of a point on the trace of the sheet in this cross-flow plane relative to the origin and with the y-axis as initial line be $r_1 s$ and θ_1, and relative to the vortex with the y-axis as initial line be rs and $\bar{\theta}$. Let ϕ_1 and ϕ be the corresponding angles between the corresponding radial vectors and the tangent of the trace of the sheet in the cross-flow plane. Let ψ be the angle between this tangent and the positive y-axis. Now

$$\left.\begin{aligned} r_1\cos\theta_1 &= \lambda_0\cos\vartheta + r\cos\bar{\theta} , \\ r_1\sin\theta_1 &= \lambda_0\sin\vartheta + r\sin\bar{\theta} \\ \phi_1 + \theta_1 &= \psi , \\ \phi + \bar{\theta} &= \psi . \end{aligned}\right\} \tag{I.1}$$

and

Therefore we have

$$\left.\begin{aligned} r_1\cos\theta_1 &= r_1\cos\phi_1\cos\psi + r_1\sin\phi_1\sin\psi \\ r_1\sin\theta_1 &= r_1\cos\phi_1\sin\psi - r_1\sin\phi_1\cos\psi . \end{aligned}\right\} \tag{I.2}$$

and

From an equation similar to equation (7) we have that

$$\cot\phi = f'(\bar{\theta})/f(\bar{\theta}) \tag{I.3}$$

for a plane curve $r = f(\theta)$, and hence

$$\cos\phi = f'/\sqrt{(f^2+f'^2)} , \sin\phi = f/\sqrt{(f^2+f'^2)} . \tag{I.4}$$

From equations (27) we can write

$$c(\bar{\theta}) = f^2(\bar{\theta}) + f'^2(\bar{\theta}) . \tag{27}$$

Thus it can be shown that

$$\left.\begin{aligned} r_1\cos\phi_1 &= c^{-\frac{1}{2}}(\lambda_0 f'\cos(\theta-\vartheta) - \lambda_0 f\sin(\bar{\theta}-\vartheta) + f'f) \\ r_1\sin\phi_1 &= c^{-\frac{1}{2}}(\lambda_0 f\cos(\theta-\vartheta) + \lambda_0 f'\sin(\bar{\theta}-\vartheta) + f^2) . \end{aligned}\right\} \tag{I.5}$$

and

The curvature κs_0 is calculated using the spherical approximation which is outlined in Appendix II and is given by

$$\kappa s_0 = \frac{(f^2 - ff'' + 2f'^2)\sin^3(\beta - \gamma(1+\zeta))}{\sin(\beta-\gamma)} \frac{}{c^{3/2}} \tag{II.13}$$

where ζ is the non-dimensional arc length along the trace of the sheet.

With reference to Fig. 6, let V_1 be the effect of the outside flow field on the core region and let it be taken as a parallel uniform flow at angle δ to y-axis. Let V_2 be the transverse component of velocity where V_2 is assumed to be a slowly varying function of r only. If r^1 and r^0 are the radii of the trace at angles $\theta + 2\pi$ and θ respectively, then the amount of fluid flowing across the arc ABC in Fig. 6 equals the amount flowing out of AC. Thus,

$$\int_{\bar\theta}^{\bar\theta+2\pi} \frac{\partial\Phi}{\partial n} s d\zeta = -\int_{r^1}^{r^0} (V_2 - V_1 \sin(\bar\theta - \delta)) s dr\,, \tag{I.6}$$

which can be written using equations (9) and (I.5)

$$-\int_{\theta}^{\bar\theta+2\pi} U\tan\gamma\,(\lambda_0 f\cos(\bar\theta-\vartheta) + \lambda_0 f'\sin(\bar\theta-\vartheta) + f^2) s d\bar\theta$$

$$= -\int_{r^1}^{r^0} (V_2 - V_1\sin(\bar\theta-\delta)) s dr\,, \tag{I.7}$$

where we have used the fact that

$$\frac{d\zeta}{d\bar\theta} = \sqrt{(f^2+f'^2)} = \sqrt{c(\bar\theta)}\,. \tag{I.8}$$

We now assume that the non-oscillatory terms in equation (I.7) must cancel, so that

$$-\int_{\theta}^{\bar\theta+2\pi} U\tan\gamma\, f^2 d\bar\theta = -\int_{r^1}^{r^0} V_2 dr\,. \tag{I.9}$$

Since we are close to the centre of an infinite angular spiral we assume f to be a slowly varying function of $\bar\theta$. Thus if we assume that f^2 and V_2 are constant over their respective ranges of integration then equation (I.9) reduces to

$$-(\bar\theta + 2\pi - \bar\theta) U\tan\gamma\, f^2(\bar\theta) = -(f(\bar\theta) - f(\bar\theta+2\pi)) V_2\,, \tag{I.10}$$

from which we deduce that

$$V_2 = -U\tan\gamma\, f^2(\bar\theta)/f'(\bar\theta)\,, \tag{I.11}$$

$$2\zeta'^4\zeta''^2=\zeta'^5\zeta'''+\frac{C_\mu\zeta''^3\sin^3(\beta-\gamma(1+\zeta))}{4\pi\tan^2\gamma\sin^2(\beta-\gamma)}. \tag{I.18}$$

Thus equation (I.18) defines the shape of the inner part of the jet-vortex sheet. Three boundary conditions are necessary to solve for $\zeta(\bar{\theta})$. Since this inner asymptotic representation is required to join onto the finite outer representation of the jet-vortex sheet, we apply the initial conditions for equation (I.18) at this point. If ζ_0, f_0, f_0', $\bar{\theta}_0$ are the values of ζ, f, f', $\bar{\theta}$ at the end of the finite outer part of the vortex sheet, they can be calculated from the current approximation to the solution for the finite sheet shape. Hence the conditions used in the solution of equation (I.18) are

$$\left.\begin{aligned}\zeta(\bar{\theta}_0)&=\zeta_0\,,\\ \zeta'(\bar{\theta}_0)&=f_0\,,\\ \zeta''(\bar{\theta}_0)&=f_0'\,.\end{aligned}\right\} \tag{I.19}$$

The shape of the asymptotic inner jet sheet has now been determined.

In Fig. 6 let the angle between the outward normal to the trace and the y/s axis be λ. Let θ_m be the value of θ at the point where the curvature κs_0 goes to zero. Then the force $\tilde{F}$, per unit length in the x-direction, sustained by the inner part of the jet-vortex sheet is equal to the following integral.

$$\tilde{F}=\int_{\theta=\theta_0}^{\theta=\theta_m}\tfrac{1}{2}\rho U^2\tilde{\Delta}C_p(\cos\lambda+i\sin\lambda)d(s\zeta)\,. \tag{I.20}$$

From equation (II.13) in Appendix II and equations (19), (20), (21) we have

$$\tilde{\Delta}C_p=-\frac{C_\mu(f^2-ff''+2f'^2)\sin^3(\beta-\gamma(1+\zeta))}{\sin^2(\beta-\gamma)c^{3/2}}. \tag{I.21}$$

We now define a force coefficient F as

$$F=\frac{\tilde{F}}{\frac{1}{2}\rho U^2\tan^2\gamma s} \tag{I.22}$$

and hence, using (I.8),

$$F=-\frac{C_\mu}{\tan^2\gamma}\int_{\theta}^{\theta_m}\frac{(f^2-ff''+2f'^2)\sin^3(\beta-\gamma(1+\zeta))e^{i\lambda}}{c\sin^2(\beta-\gamma)}d\theta\,. \tag{I.23}$$

Now

and

$$\left.\begin{aligned}\cos\lambda=\ \ \sin\psi=\ \ &\sin(\theta-\varepsilon)\cos\phi+\cos(\theta-\varepsilon)\sin\phi\,,\\ \sin\lambda=-\cos\psi=-&\cos(\theta-\varepsilon)\cos\phi+\sin(\theta-\varepsilon)\sin\phi\,.\end{aligned}\right\} \tag{I.24}$$

Using expressions (I.4) it can be shown that

$$e^{i\lambda}=c^{-\frac{1}{2}}(f-if')e^{i(\theta-\varepsilon)}\,. \tag{I.25}$$

Assuming again that $f'^2 \ll f^2$ and $f'' \ll f$ and using equations (I.25), the force equation (I.23) reduces to

$$F = -\frac{C_\mu}{\sin^2(\beta-\gamma)\tan^2\gamma}\int_{\theta_0}^{\theta_m}\sin^3(\beta-\gamma(1+\zeta))\,(1-if'/f)e^{i(\theta-\varepsilon)}d\theta\,. \tag{I.26}$$

The value θ_m is the value of θ at which $\beta=\gamma(1+\zeta)$, at which point it can be shown (*see* Appendix II) that the curvature of the jet streamlines has gone to zero. The value of F in equation (I.26) is the value used in Section 2.3 to establish the total force condition. The force F is a complex quantity and a typical value calculated for it is (0·43, 0·16).

APPENDIX II

Geodesic Lines on a Conical Surface.

If $\underline{R}=\underline{R}(\bar{s}, \theta)$ is the equation of the conical jet-vortex sheet, then $\underline{R}=\underline{R}(s_0 w(\theta), \theta)$ is the equation for a geodesic line in this sheet, where $w(\theta)$ is the solution of the differential equation (35). The function $w(\theta)$ may be obtained in an alternative geometrical manner by considering the jet-vortex sheet to be 'unrolled' into a plane surface. Thus in Fig. 2 let C and C' be neighbouring points on the 'unrolled' trace of the sheet. If v is the angle between OC and the leading edge OB, and $sh(v)$ is the length of OC, the distance, measured along the trace, from C to C' is given by $\delta\sigma$ where

$$\delta\sigma^2=s^2(h^2\delta v^2+\delta h^2)\,. \tag{II.1}$$

Since distances measured along a path remain unchanged when a developable surface is 'rolled' or 'unrolled', we find from Fig. 4 that

$$\delta\sigma^2=s^2\left(f^2+\left(\frac{df}{d\theta}\right)^2\right)\delta\theta^2\,. \tag{II.2}$$

where we use the fact that $r=f(\theta)$.

Now in Fig. 2 the line OC is a generator of the conical surface and thus remains a straight line when the surface is 'rolled' up. Thus on the conical surface the line OC forms part of a right-angled triangle OAC, the base of which, AC, can be seen in Fig. 4. Hence we have

$$s^2h^2=x^2+s^2r_1^2\,. \tag{II.3}$$

The connection between the two sets of polar coordinates (r, θ) and (r_1, θ_1) yields the result

$$\begin{aligned} r_1^2&=\lambda_1^2+\lambda_2^2+2f(\lambda_1\cos(\theta-\varepsilon)+\lambda_2\sin(\theta-\varepsilon))+f^2 \\ &=a(\theta)-\cot^2\gamma \end{aligned} \tag{II.4}$$

where λ_1, λ_2 can be found in Fig. 4 and $a(\theta)$ is defined by equations (27). Substitution of equations (II.4) into (II.3) gives

$$h=\sqrt{a}\,. \tag{II.5}$$

From equations (II.1) and (II.2) we deduce, in taking the limit as $\delta\theta\to 0$ that

$$f^2+\left(\frac{df}{d\theta}\right)^2=h^2\left(\frac{dv}{d\theta}\right)^2+\left(\frac{dh}{d\theta}\right)^2, \tag{II.6}$$

and substituting in (II.6) the value of h given in equation (II.5) we find, using the identity $da/d\theta=2b$, that

$$\frac{dv}{d\theta}=\sqrt{q}/a\,, \tag{II.7}$$

where $q(\theta)$ is given by equation (29).

From the triangle DCO in Fig. 2 we see, using the sine rule, that

$$\frac{OC}{\sin(\beta-\gamma)}=\frac{OD}{\sin(\beta-\gamma-v)},$$

or

$$\frac{\widehat{sh}}{\sin(\beta-\gamma)}=\frac{s_0\operatorname{cosec}\gamma}{\sin(\beta-\gamma-v)},$$

and consequently, using (II.5)

$$w(\theta)=\frac{s_0}{\bar{s}}=\frac{\sin\gamma}{\sin(\beta-\gamma)}\sqrt{a(\theta)}\sin(\beta-\gamma-v(\theta)). \tag{II.8}$$

Thus equation (II.8) is an expression for $w(\theta)$ in terms of the function $v(\theta)$, which itself is determined by integrating equation (II.7) using the condition that $v(0)=0$. The expression for $w(\theta)$ given by equation (II.8) may be substituted directly into the equations (35), (36) and (37) to confirm that it is the appropriate solution of the differential equation satisfied by w.

If the quantity $w(\theta)$ given in (II.8) is substituted into the expression (43) for κs_0, we have

$$\kappa s_0=\frac{\cos\gamma}{\sin(\beta-\gamma)}(2f'^2-ff''+f^2)\left(\frac{a}{q}\right)^{3/2}\sin^3(\beta-\gamma-v(\theta)). \tag{II.9}$$

For very small apex angles γ, since

$$a(\theta)\simeq\cot^2\gamma, \tag{II.10}$$

$$q(\theta)\simeq\cot^2\gamma\, c(\theta), \tag{II.11}$$

we can simplify the expression for the curvature κs_0. The arc length along the trace of the jet-vortex sheet in the cross-flow plane made dimensionless using s is

$$\zeta(\theta)=\int_0^\theta c^{\frac{1}{2}}(\theta)d\theta,$$

and, using the fact that γ is small, we find from equation (II.7) that

$$v(\theta)=\zeta\tan\gamma\simeq\gamma\zeta(\theta). \tag{II.12}$$

Thus substituting equations (II.10), (II.11) and (II.12) into equation (II.9), we have

$$\kappa s_0\simeq\frac{1}{\sin(\beta-\gamma)}(2f'^2-ff''+f^2)c^{-3/2}\sin^3(\beta-\gamma-\gamma\zeta). \tag{II.13}$$

Thus the curvature falls to zero, marking the end of the jet-vortex sheet, when the non-dimensional arc length ζ reaches a value ζ_m given by

$$\zeta_m=\beta/\gamma-1. \tag{II.14}$$

TABLE 1

					Vortex-Position		*Circulation*
N	a	C_μ	β	C_N	y/s	z/s	
14	0·75	0·000	—	1·0219	0·7591	0·1809	3·3454
		0·025	40	1·0594	0·7714	0·1856	3·4651
			50	1·0719	0·7784	0·1860	3·4920
			80	1·0989	0·7888	0·1871	3·5741
			100	1·1085	0,7934	0·1870	3·6024
			110	1·1084	0·7950	0·1858	3·6072
			120	1·1082	0·7945	0·1856	3·6098
		0·050	40	1·0798	0·7794	0·1886	3·5230
			50	1·1032	0·7862	0·1910	3·5898
			80	1·1496	0·8056	0·1931	3·7208
			100	1·1658	0·8103	0·1933	3·7791
			110	1·1673	0·8130	0·1923	3·7847
			120	1·1651	0·8144	0·1907	3·7817
		0·075	40	1·0978	0·7841	0·1923	3·5823
			50	1·1296	0·7940	0·1954	3·6703
			80	1·1960	0·8169	0·1999	3·8577
			100	1·2151	0·8246	0·1996	3·9180
			110	1·2176	0·8265	0·1985	3·9333
			120	1·2157	0·8278	0·1970	3·9320
		0·100	40	1·1142	0·7890	0·1954	3·6370
			50	1.1524	0·8024	0·1990	3·7319
			60	1·1872	0·8117	0·2026	3·8319
			70	1·2162	0·8193	0·2052	3·9162
			80	1·2371	0·8253	0·2066	3·9783
			90	1·2518	0·8306	0·2068	4·0206
			100	1.2620	0·8345	0·2067	4·0534
			110	1·2667	0·8363	0·2059	4·0771
			120	1·2635	0·8385	0·2035	4·0733
		0·0643	60	1·1413	0·8010	0·1949	3·6913
		0·1286	60	1·2222	0·8196	0·2089	3·9332
		0·1928	60	1·2899	0·8332	0·2220	4·1265
		0·0866	80	1·2146	0·8217	0·2026	3·9101
		0·1732	80	1·3452	0·8464	0·2256	4·2728
		0·1182	100	1·2948	0·8399	0·2122	4·1478
		0·1970	100	1·4168	0·8608	0·2334	4·4767
		0·1200	110	1·3020	0·8428	0·2116	4·1782
		0·2000	110	1·4272	0·8644	0·2327	4·5176
		0·1182	120	1·2970	0·8433	0·2091	4·1751
14	0·75	0·1970	120	1·4212	0·8645	0·2295	4·5196
39	0·35	0·0000	40	0·3939	0·8662	0·0783	1·3990
		0·0171		0·4189	0·8819	0·0849	1·5058
		0·0342		0·4320	0·8885	0·0887	1·5587
		0·0513		0·4497	0·8961	0·0944	1·6271

TABLE 1—*continued*

					Vortex-Position		*Circulation*
N	a	C_μ	β	C_N	y/s	z/s	
39	0·35	0·0684	40	0·4644	0·9003	0·0995	1·6869
		0·0855		0·4776	0·9042	0·1042	1·7367
		0·1026		0·4895	0·9072	0·1086	1·7843
	0·40	0·0000		0·4619	0·8511	0·0904	1·6248
		0·0171		0·4888	0·8666	0·0965	1·7334
		0·0342		0·5025	0·8731	0·1000	1·7855
		0·0513		0·5177	0·8792	0·1042	1·8467
		0·0684		0·5317	0·8839	0·1088	1·8993
		0·0855		0·5444	0·8883	0·1130	1·9514
		0·1026		0·5562	0·8911	0·1169	1·9944
	0·50	0·0000		0·6063	0·8233	0·1146	2·0965
		0·0171		0·6356	0·8379	0·1199	2·2015
		0·0342		0·6519	0·8435	0·1238	2·2599
		0·0513		0·6634	0·8500	0·1262	2·2993
		0·0684		0·6740	0·8545	0·1295	2·3465
		0·0855		0·6848	0·8584	0·1326	2·3878
		0·1026		0·6983	0·8613	0·1355	2·4308
	0·75	0·0000		1·0122	0·7684	0·1767	3·3435
		0·0171		1·0404	0·7793	0·1796	3·4293
		0·0342		1·0594	0·7863	0·1819	3·4919
		0·0513		1·0735	0·7913	0·1841	3·5365
		0·0684		1·0857	0·7948	0·1864	3·5767
		0·0855		1·0958	0·7988	0·1879	3·6097
		0·1026		1·1060	0·8019	0·1901	3·6417
	1·00	0·0000	40	1·4730	0·7300	0·2348	4·7067
		0·0171		1·4976	0·7373	0·2370	4·7710
		0·0342		1·5176	0·7434	0·2388	4·8280
		0·0513		1·5340	0·7478	0·2407	4·8756
		0·0684		1·5473	0·7521	0·2418	4·9139
		0·0855		1·5583	0·7559	0·2430	4·9470
		0·1026		1·5692	0·7581	0·2449	4·9808
14	0·75	0·0000	—	1·0219	0·7591	0·1809	3·3454
39		0·0000	—	1·0122	0·7684	0·1767	3·3435
14	0·75	0·0174	30	1·0381	0·7630	0·1830	3·3981
39		0·0174	30	1·0253	0·7745	0·1778	3·3875
14		0·0342	40	1·0682	0·7740	0·1871	3·4898
39		0·0342	40	1·0596	0·7863	0·1819	3·4919
14		0·0423	45	1·0852	0·7801	0·1891	3·5353
39		0·0423	45	1·0776	0·7915	0·1846	3·5428
14		0·0500	50	1·1034	0·7862	0·1910	3·5898
39		0·0500	50	1·0952	0·7984	0·1864	3·5894
14	0·75	0·0574	55	1·1215	0·7939	0·1928	3·6372
39		0·0574	55	1·1138	0·8039	0·1888	3·6431

TABLE 1—*continued*

					Vortex-Position		*Circulation*
N	a	C_μ	β	C_N	y/s	z/s	
14	0·75	0·0643	60	1·1413	0·8010	0·1949	3·6913
39		0·0643	60	1·1338	0·8096	0·1915	3·6966
14		0·0707	65	1·1628	0·8060	0·1974	3·7587
39		0·0707	65	1·1529	0·8152	0·1942	3·7445
14		0·0766	70	1·1807	0·8116	0·1993	3·8113
39		0·0766	70	1·1733	0·8199	0·1971	3·8002

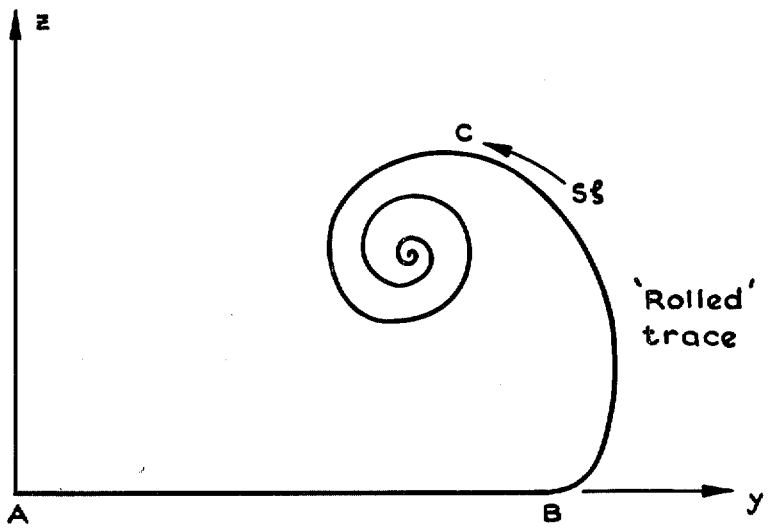

FIG. 1. . Vortex sheet spiral in cross-flow plane.

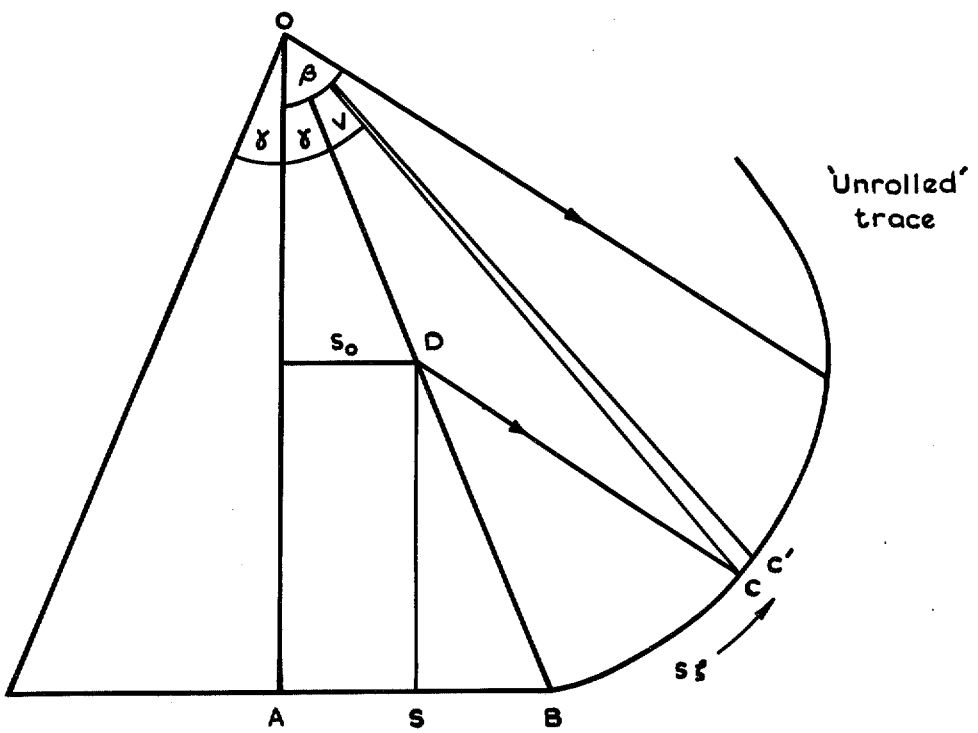

FIG. 2. 'Unrolled' vortex sheet in plane of wing.

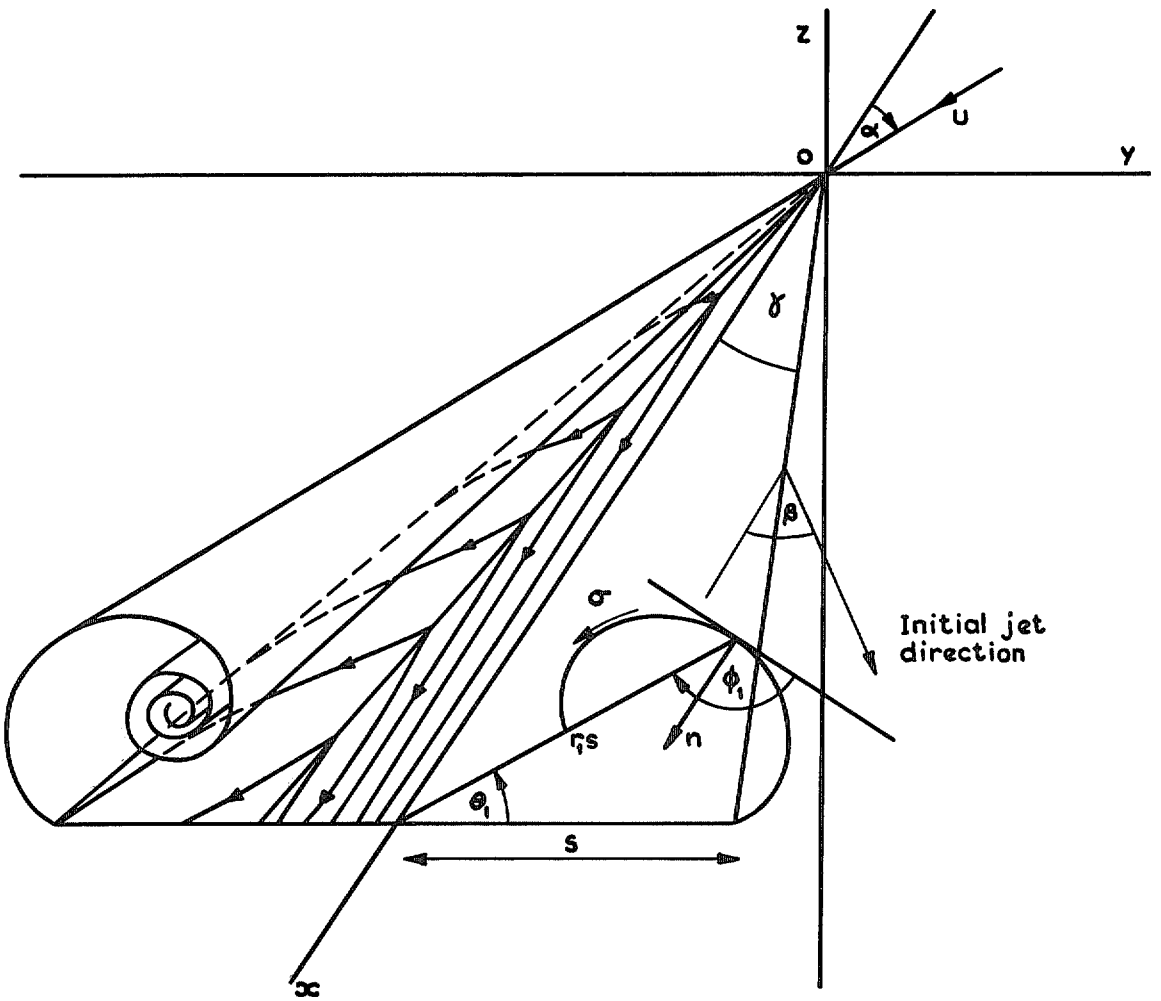

FIG. 3. Delta wing with vortex sheets.

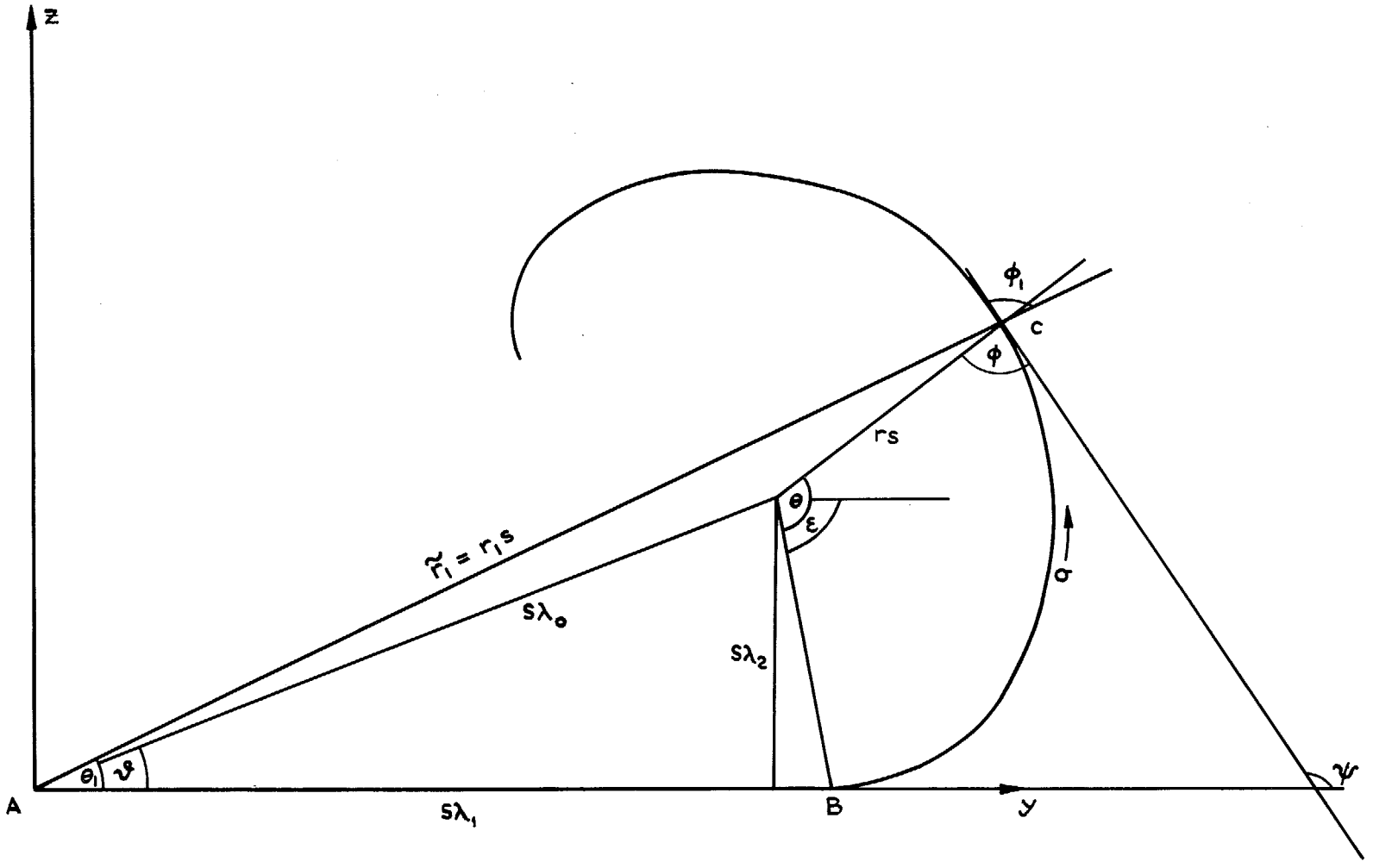

FIG. 4. Cross-flow plane. Axes and coordinates.

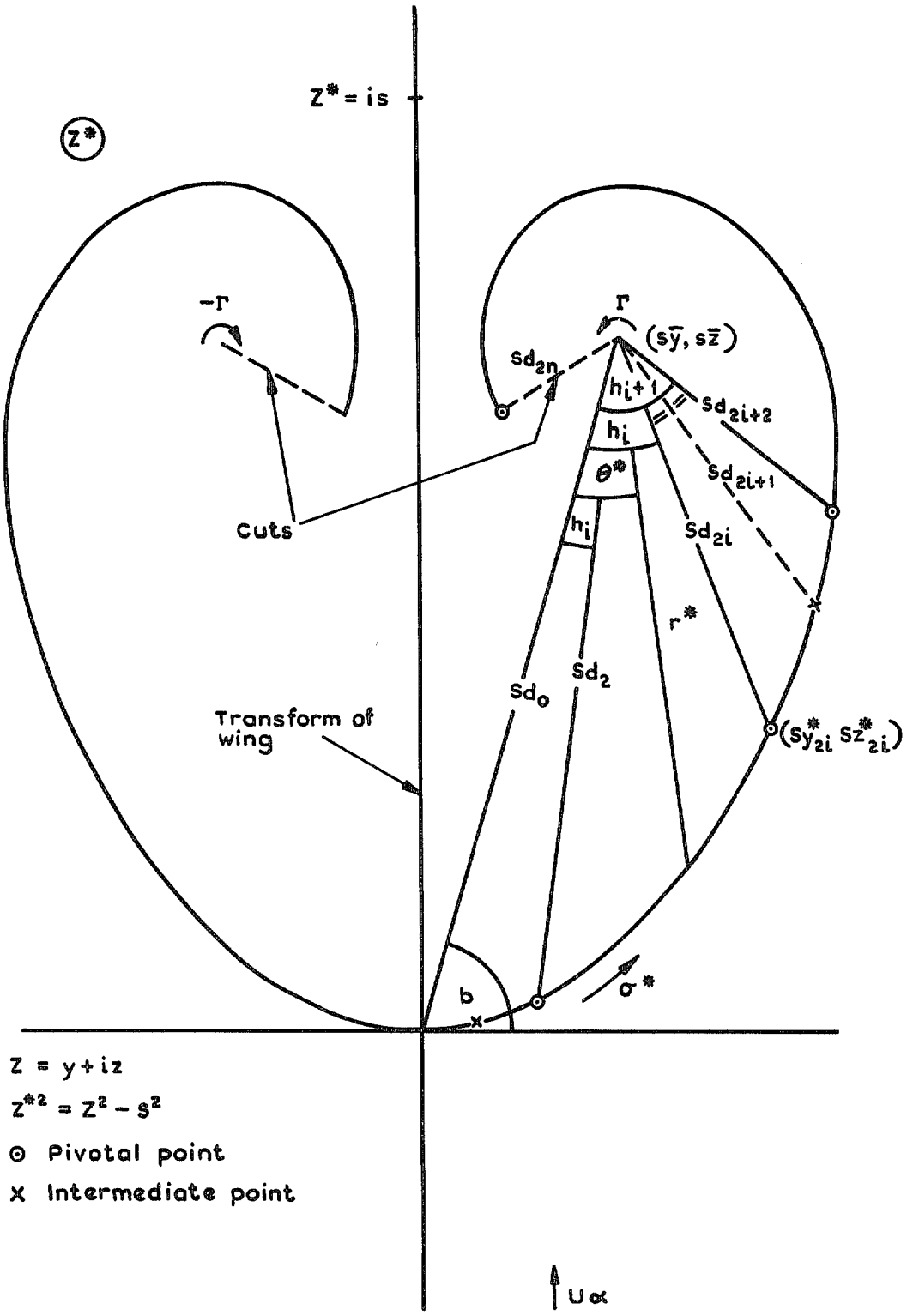

FIG. 5. Configuration in transformed plane.

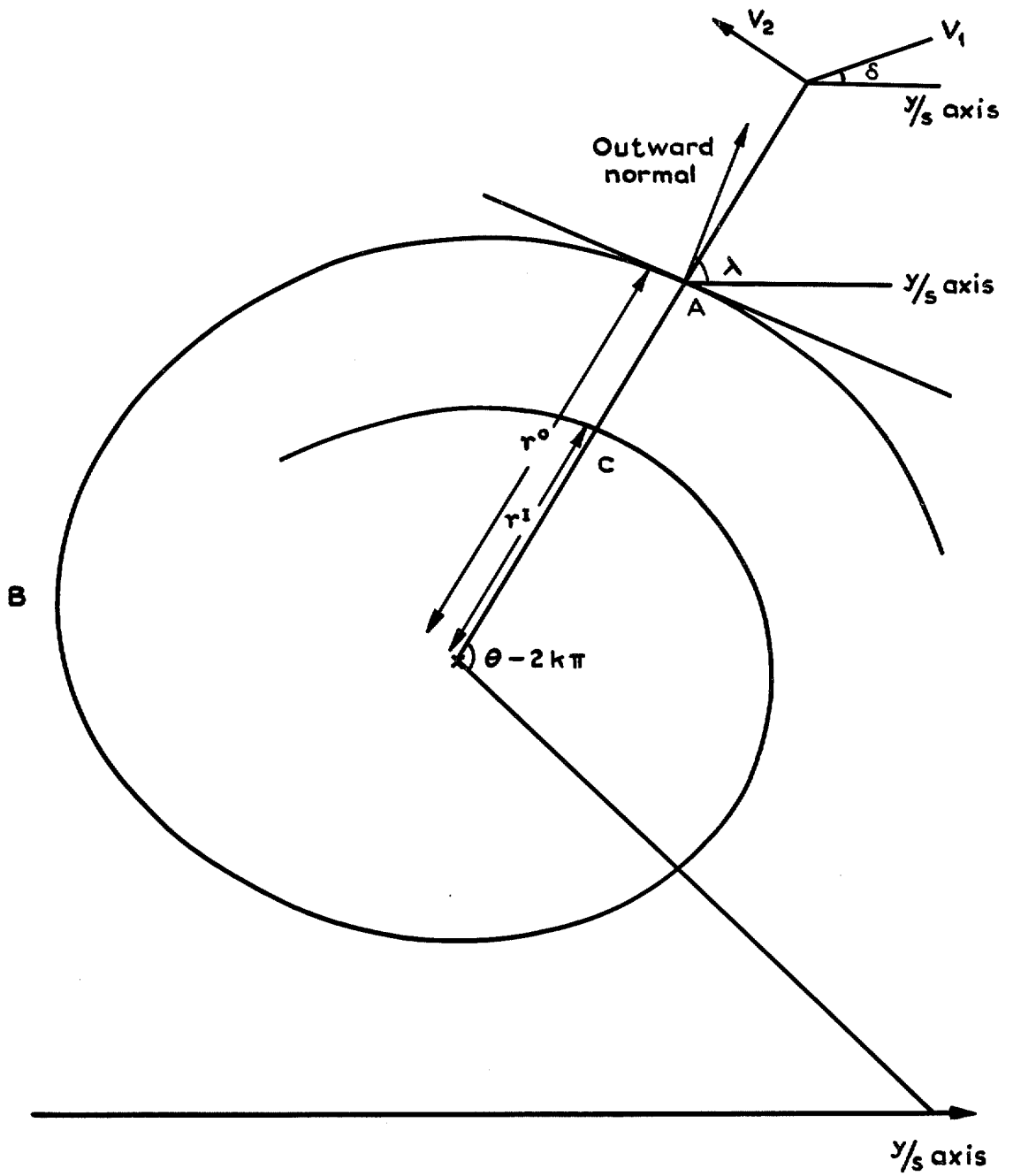

FIG. 6. Trace of asymptotic sheet in cross-flow plane.

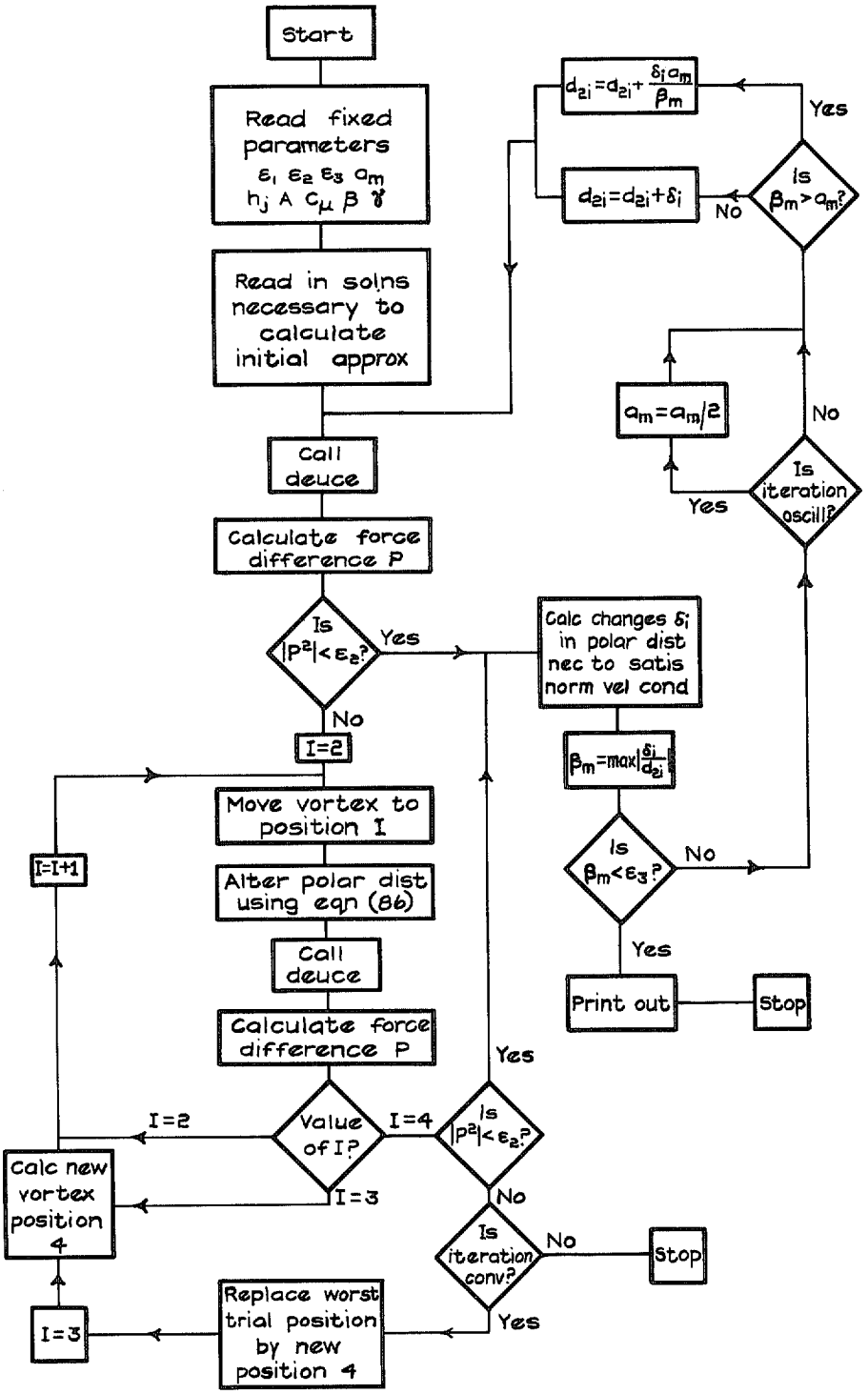

FIG. 7. Flow diagram of computer program.

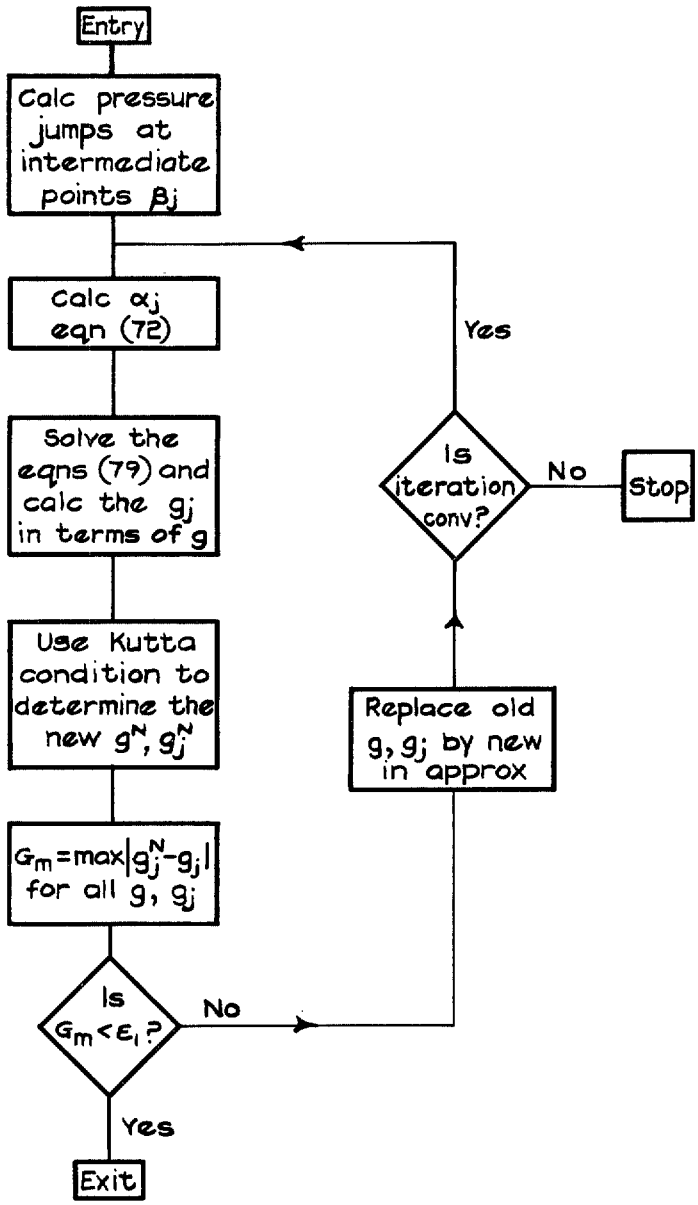

FIG. 8. Flow diagram for subroutine code-named 'Deuce'.

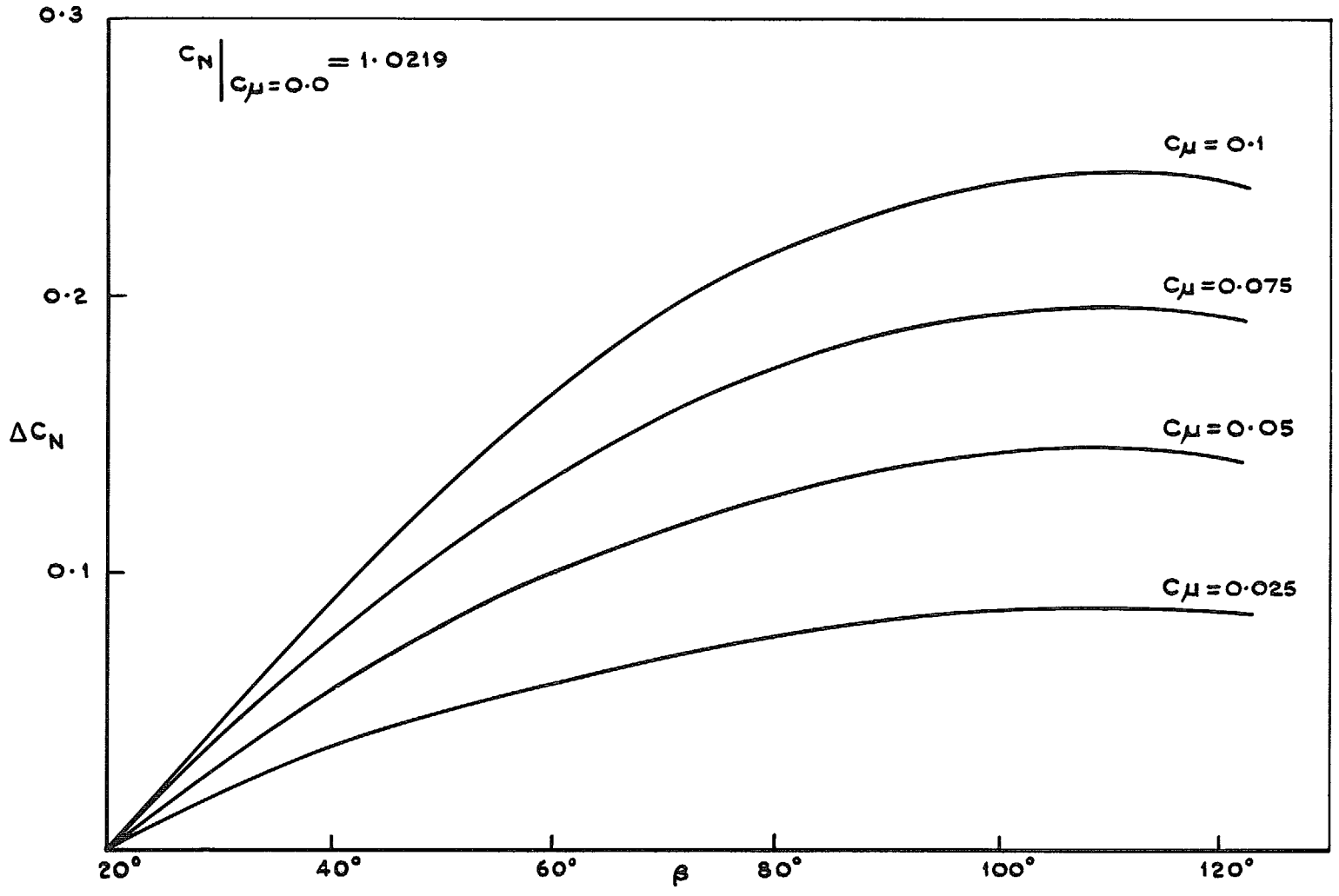

FIG. 9. Normal force increments, $a = 0.75(\gamma = 20°)$, $N = 14$.

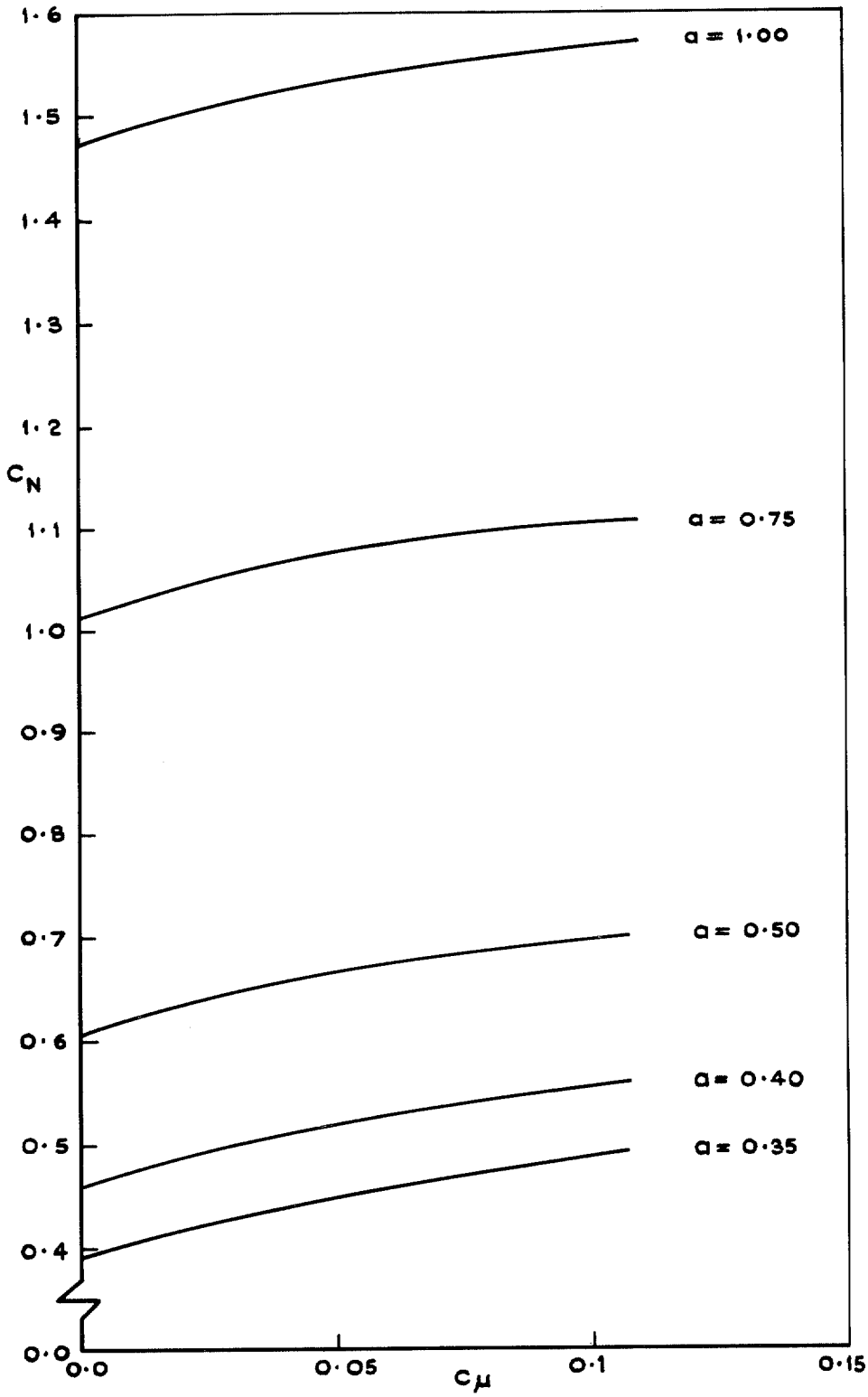

FIG. 10. Normal force, $\beta = 40°(\gamma = 20°)$ $N = 39$.

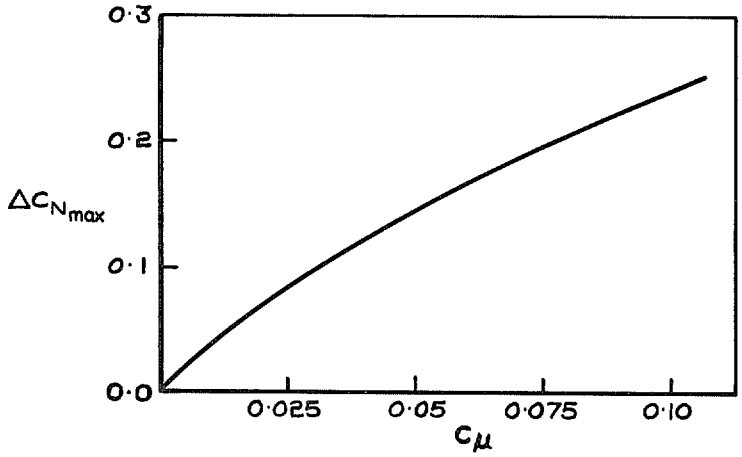

FIG. 11. Maximum normal force increments, $a=0{\cdot}75$ ($\gamma=20°$), $N=14$.

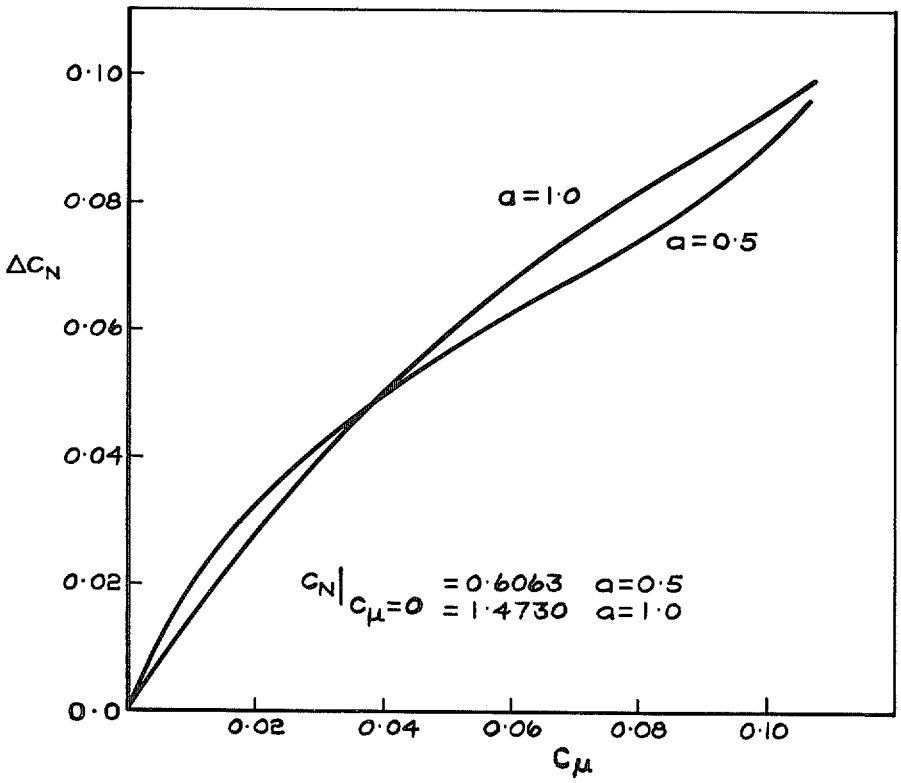

FIG. 12. Normal force increments, $a=0{\cdot}5$, $1{\cdot}0$ ($\gamma=20°$), $\beta=40°$, $N=39$.

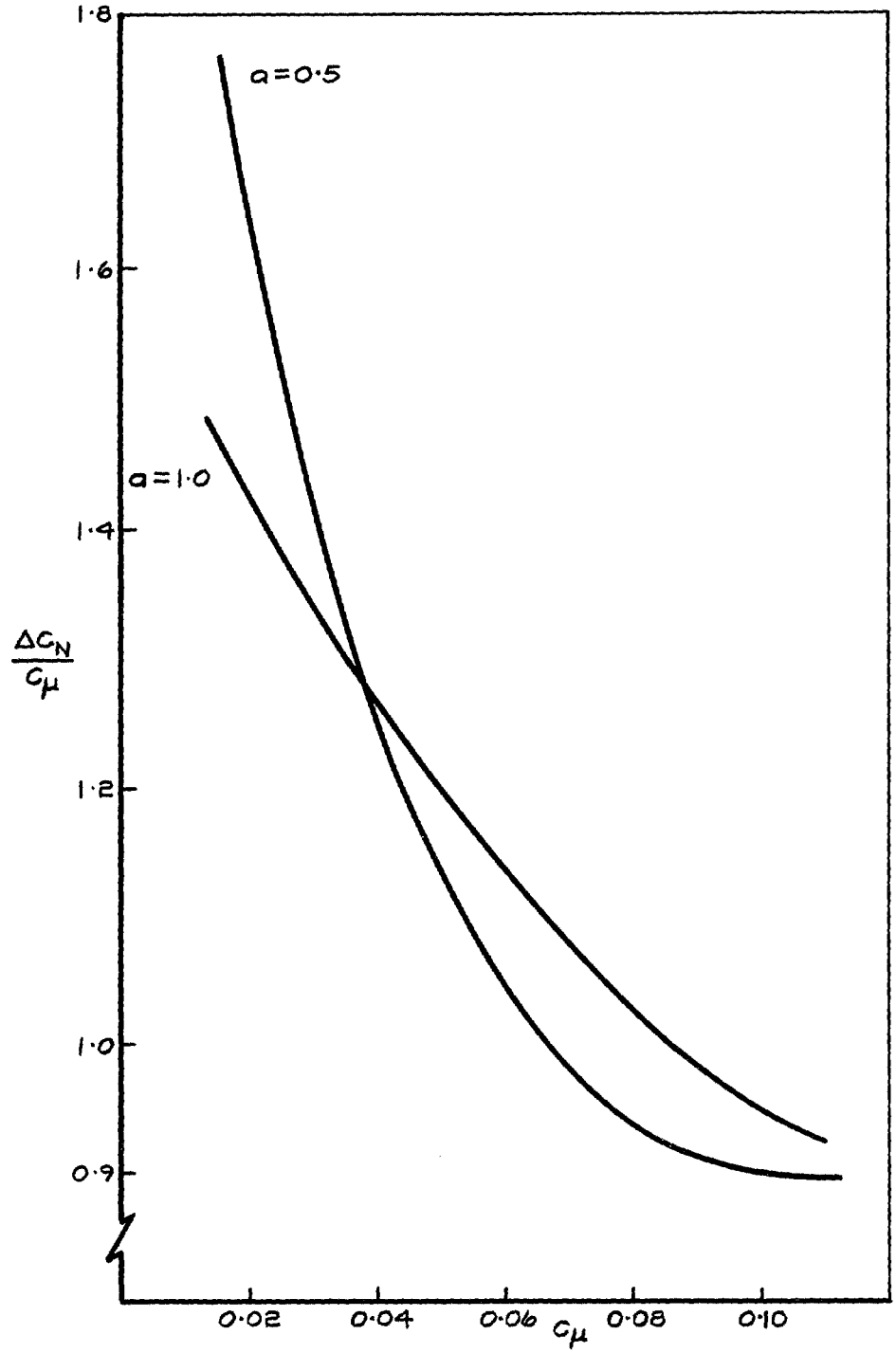

FIG. 13. Variation of $\Delta C_N/C_\mu$, $a=0{\cdot}5$, $1{\cdot}0$ ($\gamma=20°$), $\beta=40°$, $N=39$.

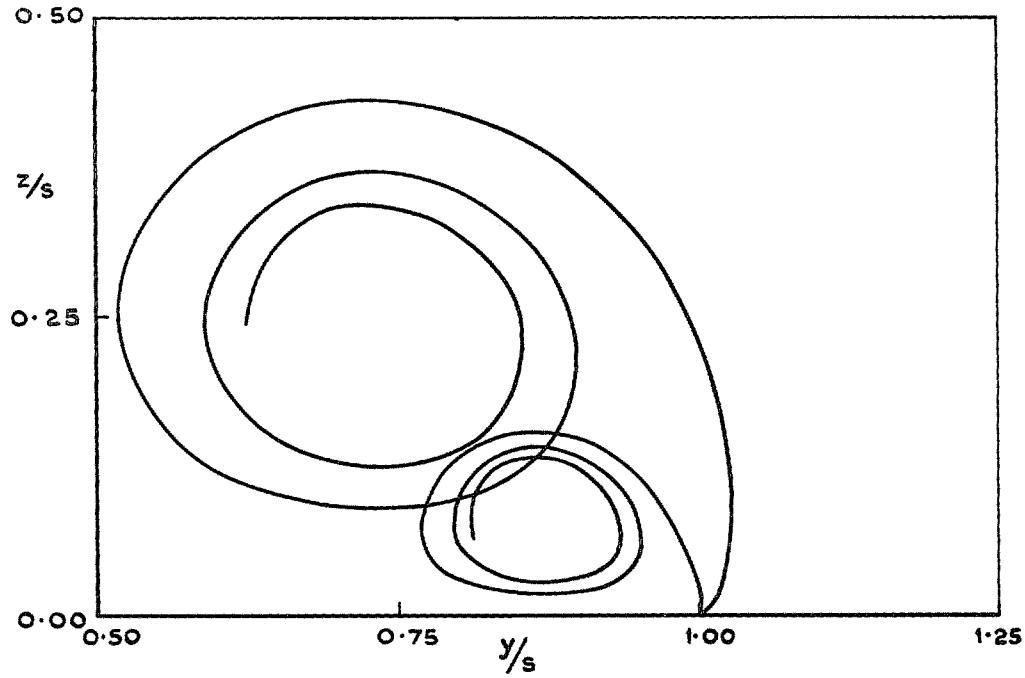

FIG. 14. 39 pt sheet shapes, $a=0{\cdot}35$, $1{\cdot}00$ ($\gamma=20°$), $C_\mu=0{\cdot}0$, $\beta=40°$.

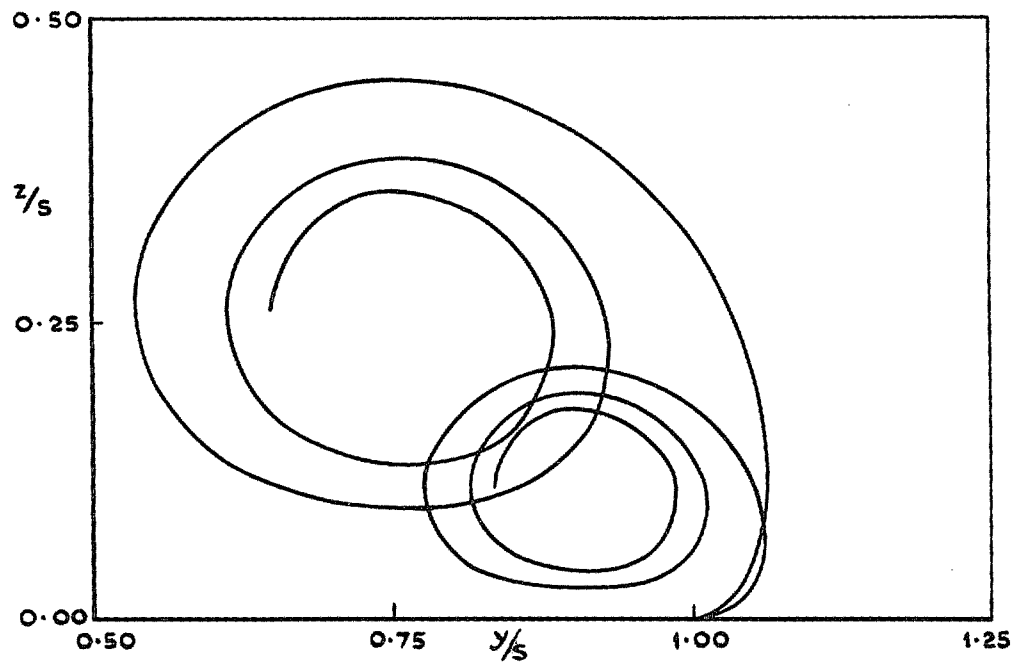

FIG. 15. 39 pt sheet shapes, $a=0{\cdot}35$, $1{\cdot}00$ ($\gamma=20°$), $C_\mu=0{\cdot}1$, $\beta=40°$.

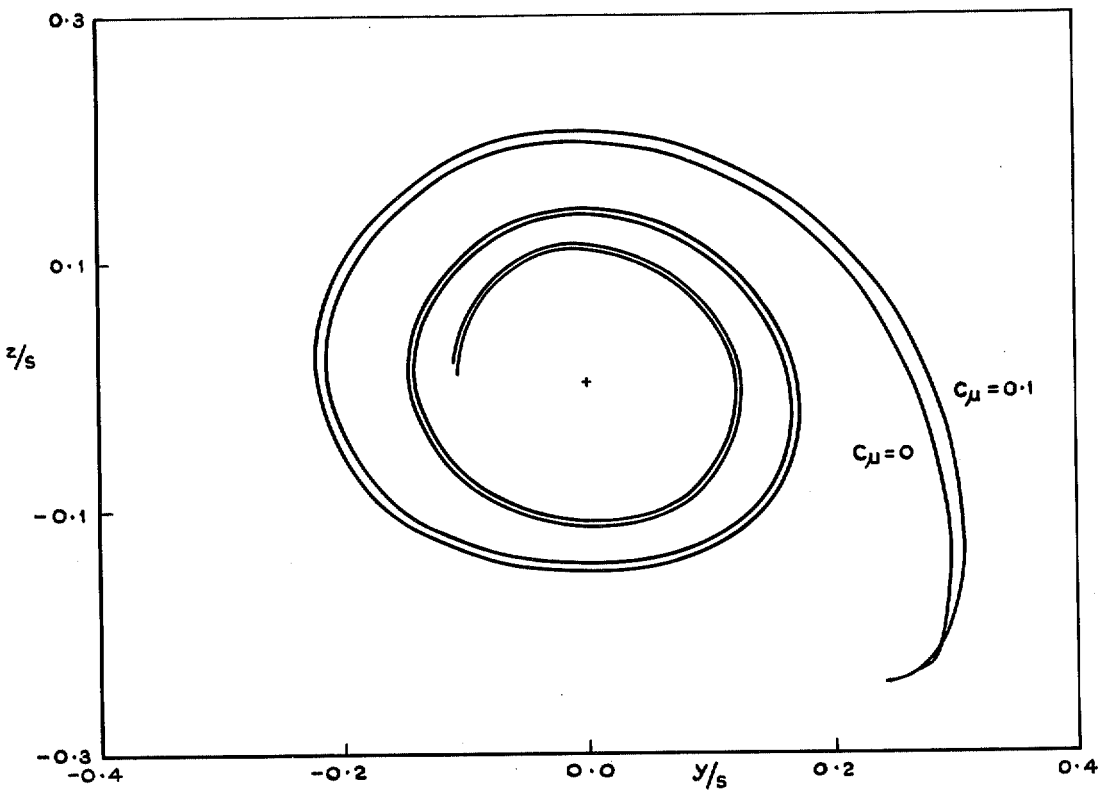

FIG. 16. Superimposed 39 pt sheet shapes, $a = 1·0$ ($\gamma = 20°$), $C_\mu = 0·0, 0·1$, $\beta = 40°$.

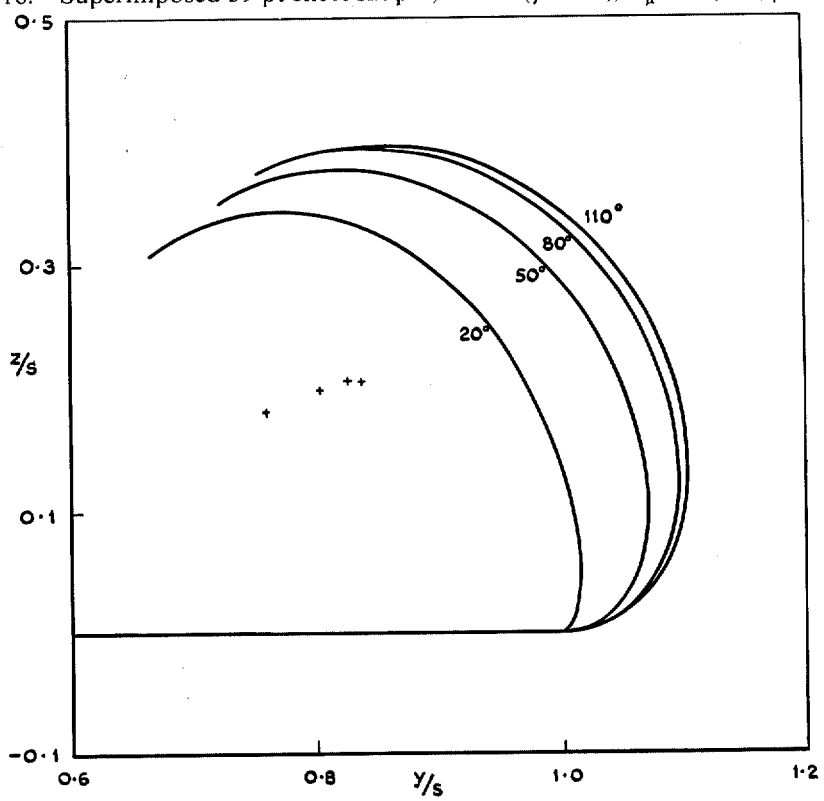

FIG. 17. 14 pt sheet shapes, $a = 0·75$ ($\gamma = 20°$), $C_\mu = 0·1$, $\beta = 20°, 50°, 80°, 110°$.

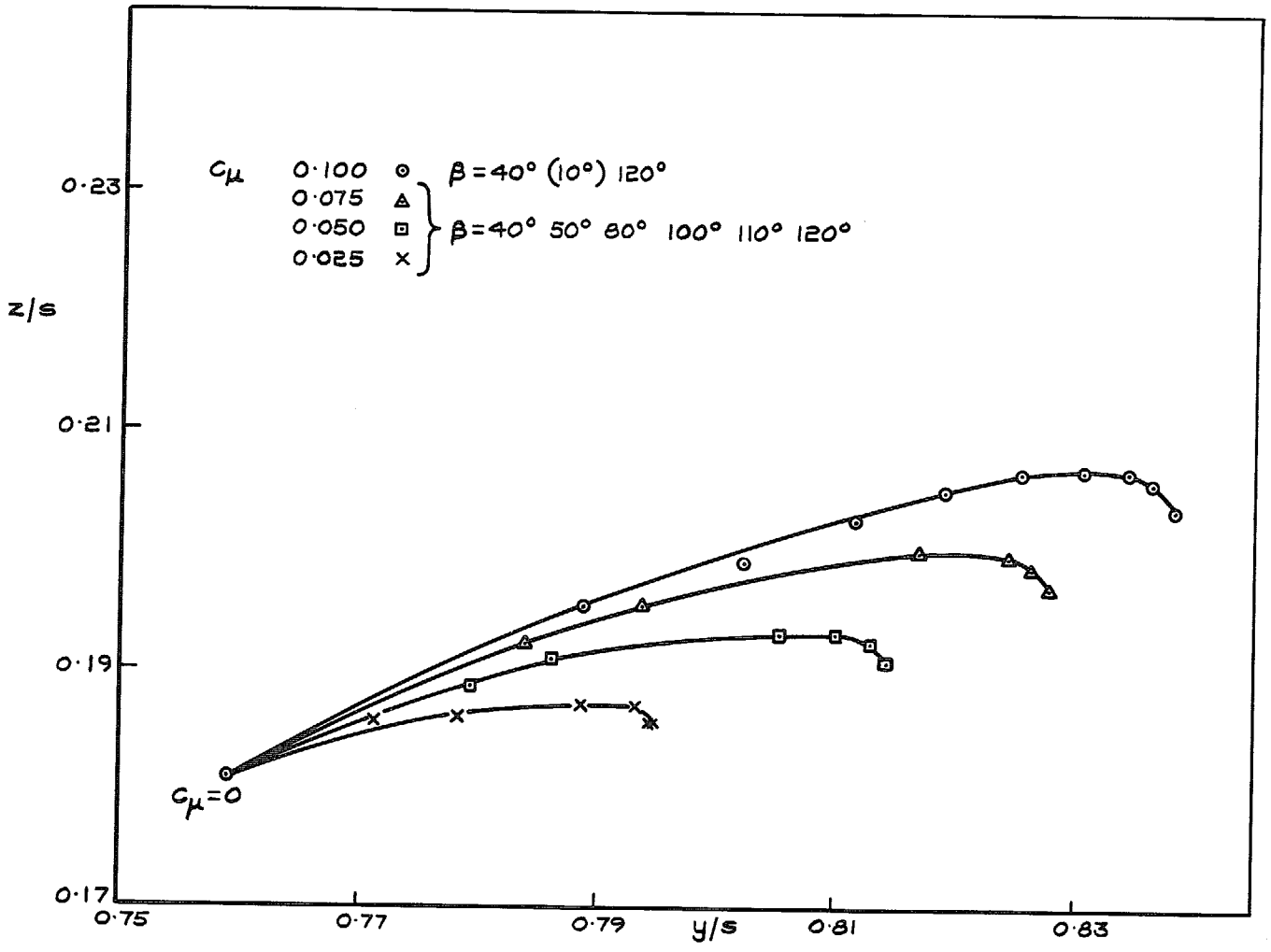

FIG. 18. Vortex position $a = 0{\cdot}75$ ($\gamma = 20°$), $N = 14$.

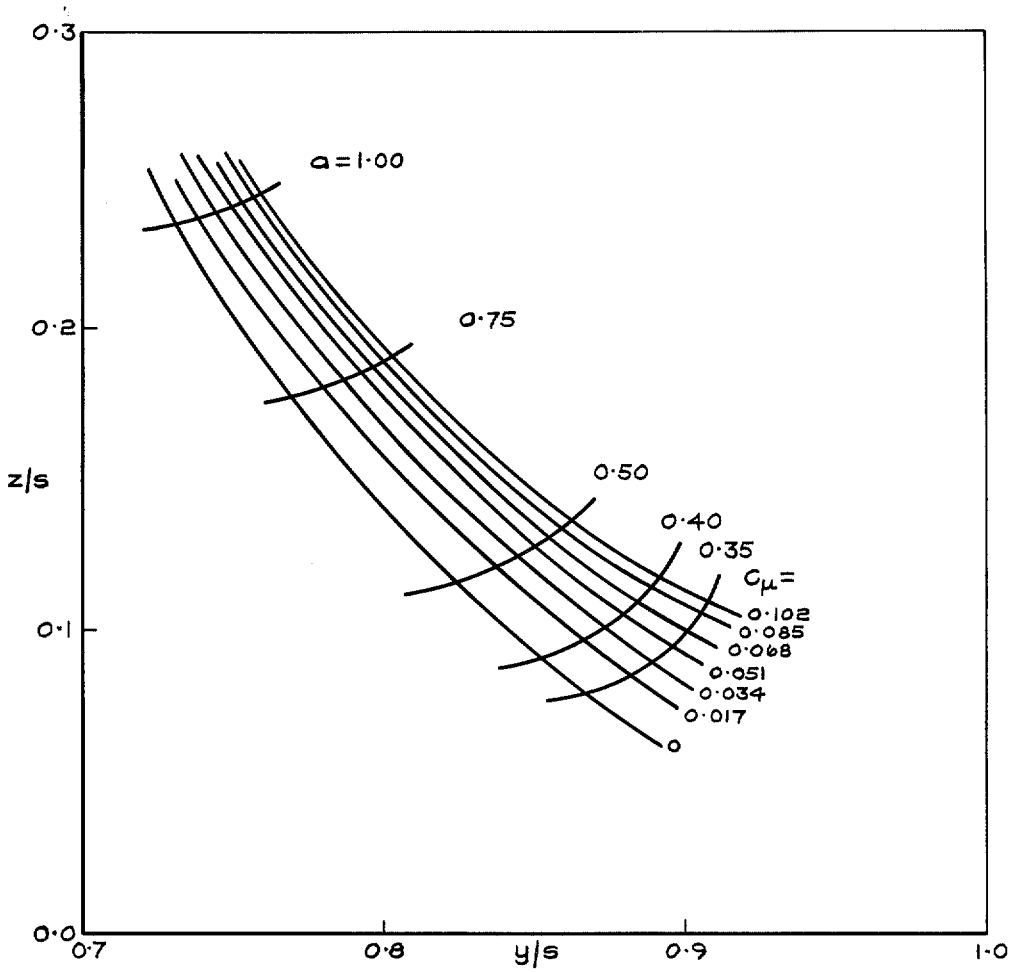

FIG. 19. Vortex position, $\beta = 40°$ ($\gamma = 20°$), $N = 39$.

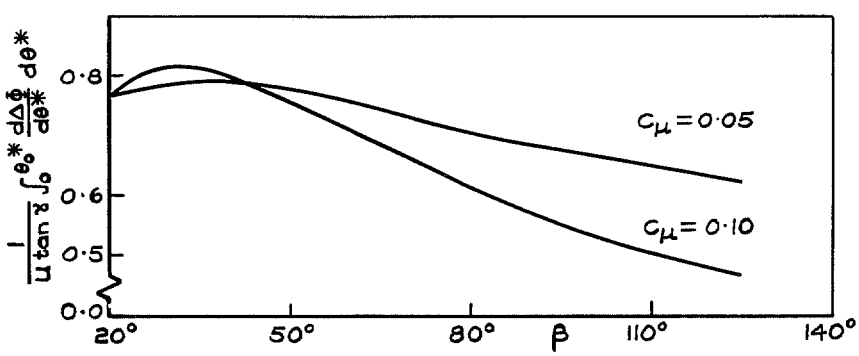

FIG. 20. Sheet circulation $a = 0{\cdot}75°$ ($\gamma = 20°$), $N = 14$.

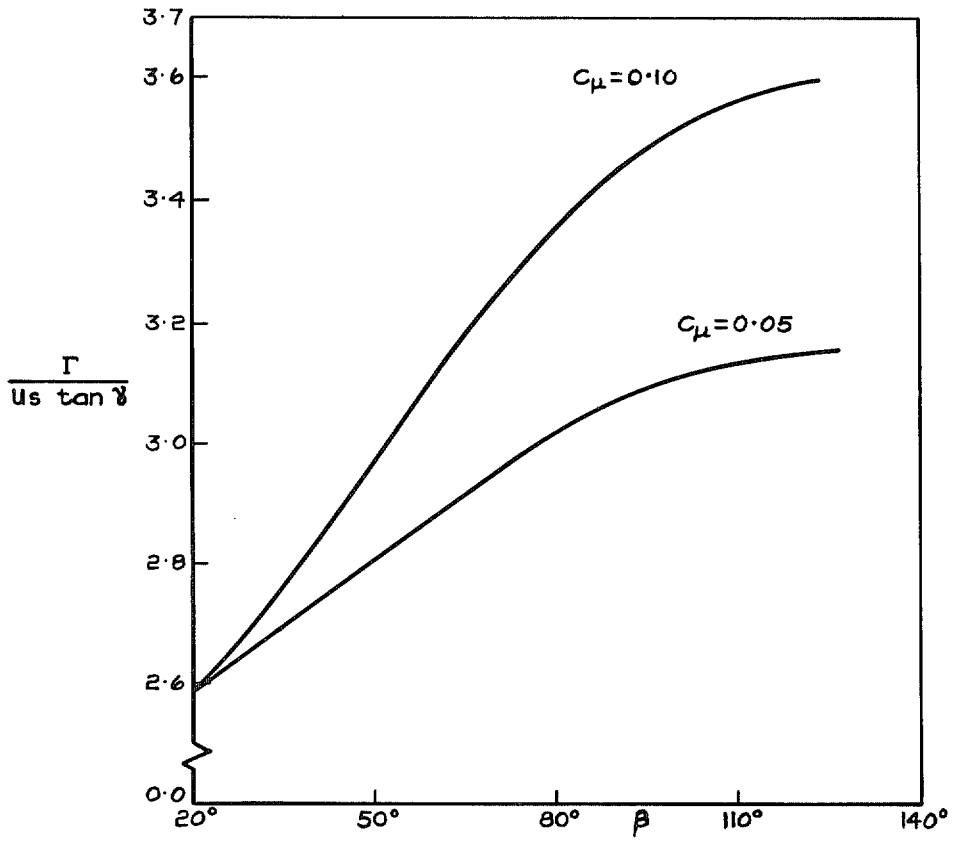

FIG. 21. Vortex circulation, $a=0{\cdot}75$ ($\gamma=20°$), $N=14$.

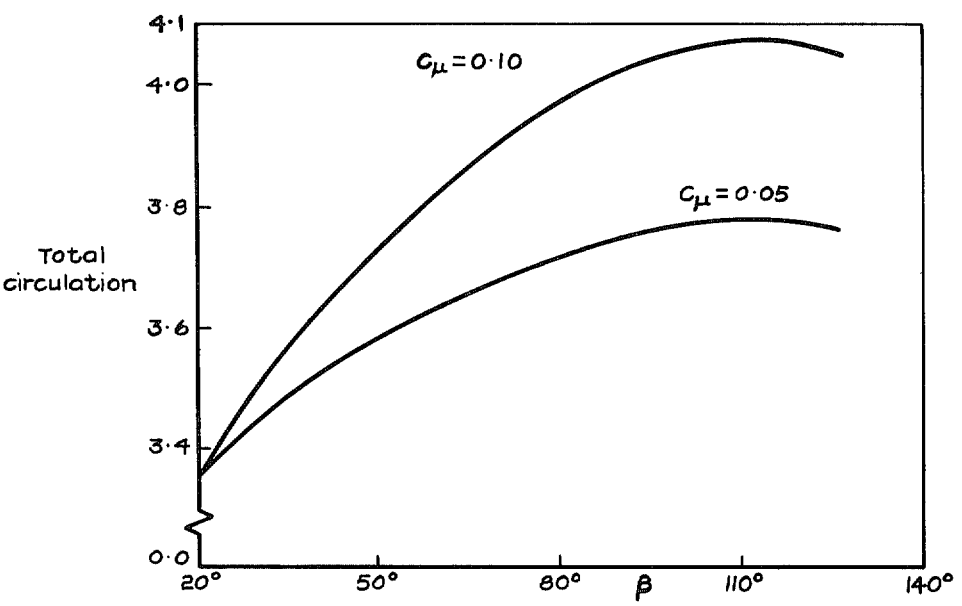

FIG. 22. Total circulation, $a=0{\cdot}75$ ($\gamma=20°$), $N=14$.

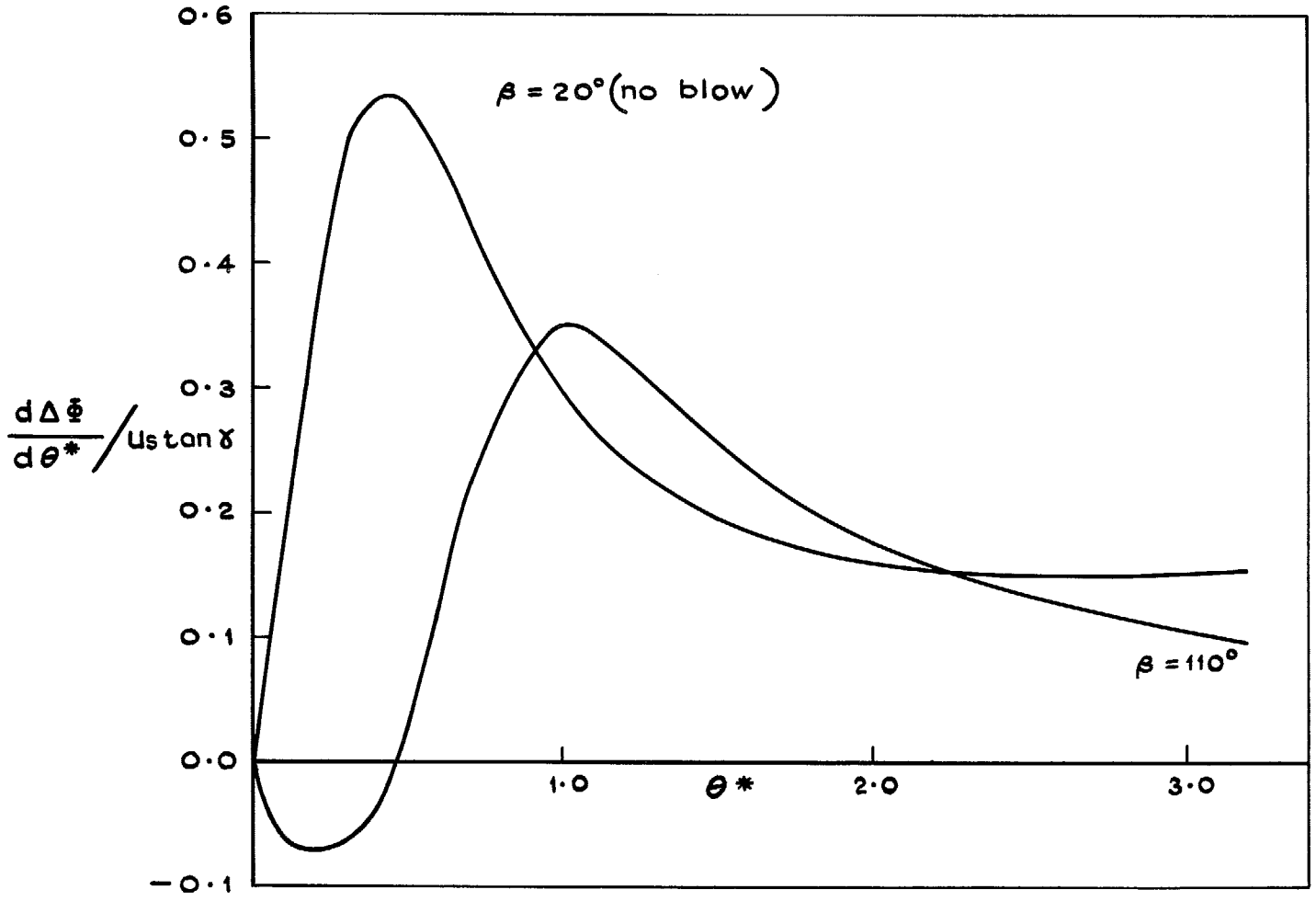

FIG. 23. Sheet strength $\frac{d\Delta\Phi}{d\theta^*}$ $U\ s\ \tan\gamma$, $a=0{\cdot}75$ ($\gamma=20°$), $C_\mu=0{\cdot}1$, $N=14$.

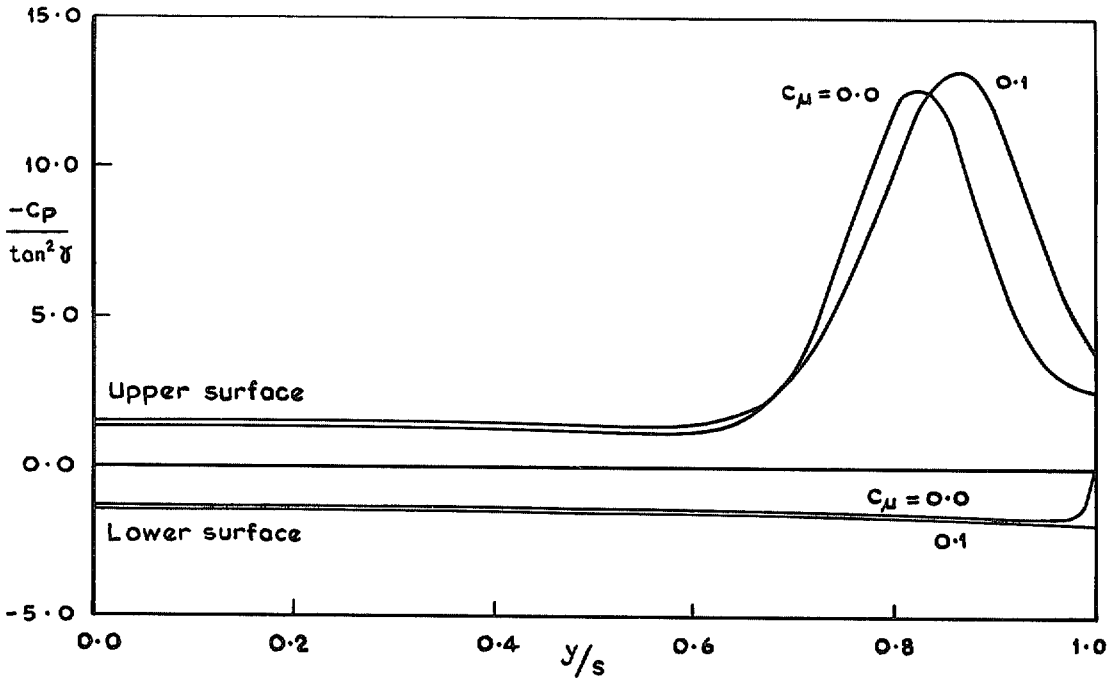

FIG. 24. Pressure distribution on wing surface, $a=0{\cdot}5$ ($\gamma=20°$), $\beta=40°$, $N=39$.

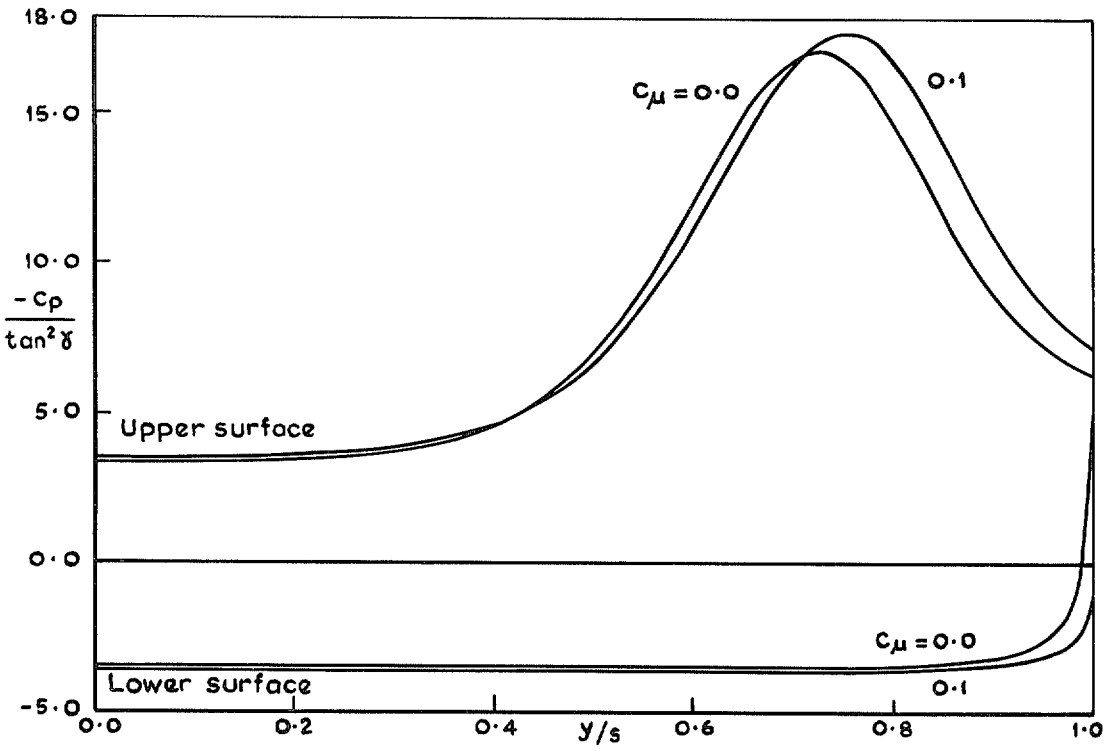

FIG. 25. Pressure distribution on wing surface, $a=1{\cdot}0$ ($\gamma=20°$), $\beta=40°$, $N=39$.

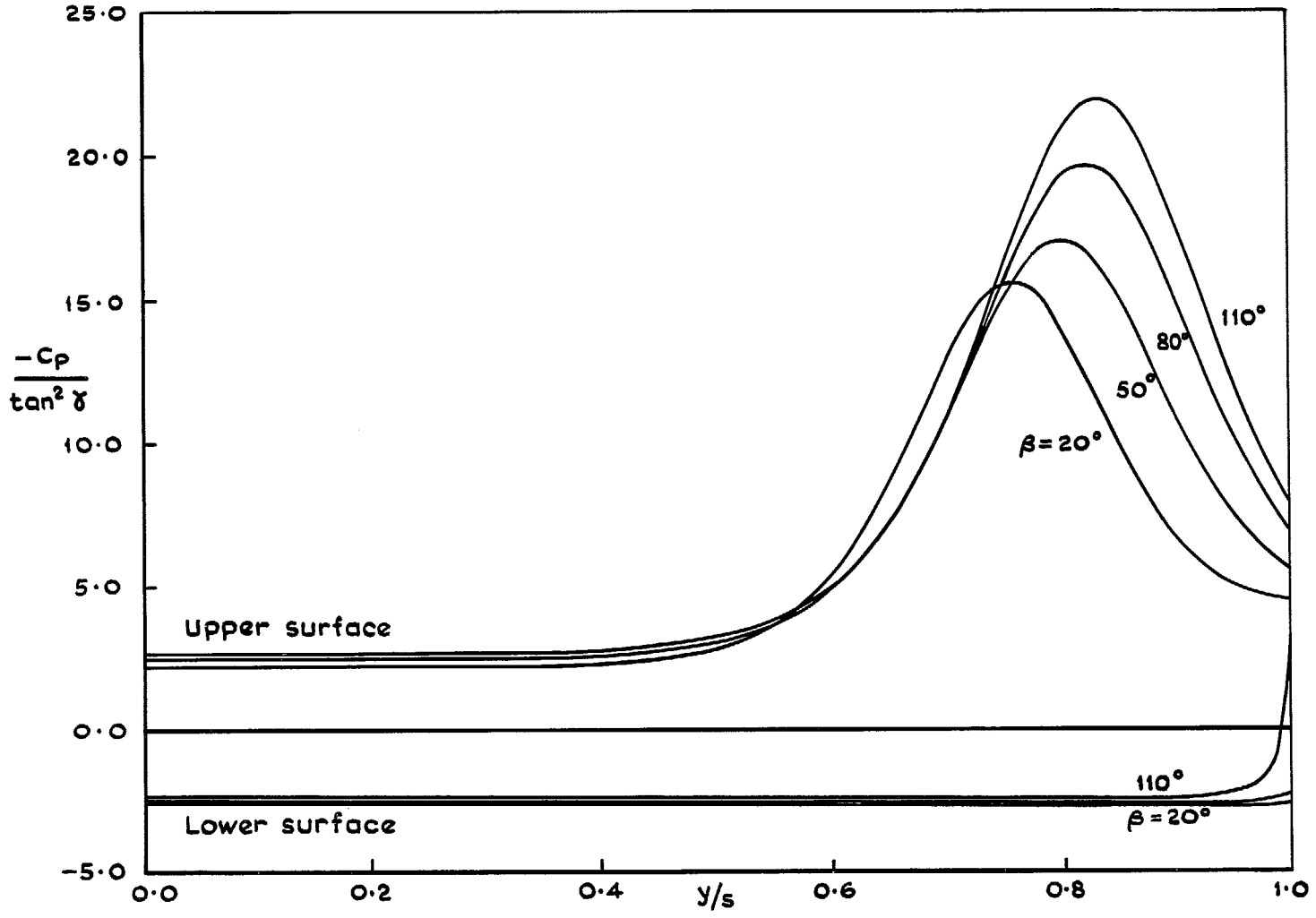

FIG. 26. Pressure distribution on wing surface, $a=0{\cdot}75$ ($\gamma=20°$), $C_\mu=0{\cdot}1$, $N=14$.

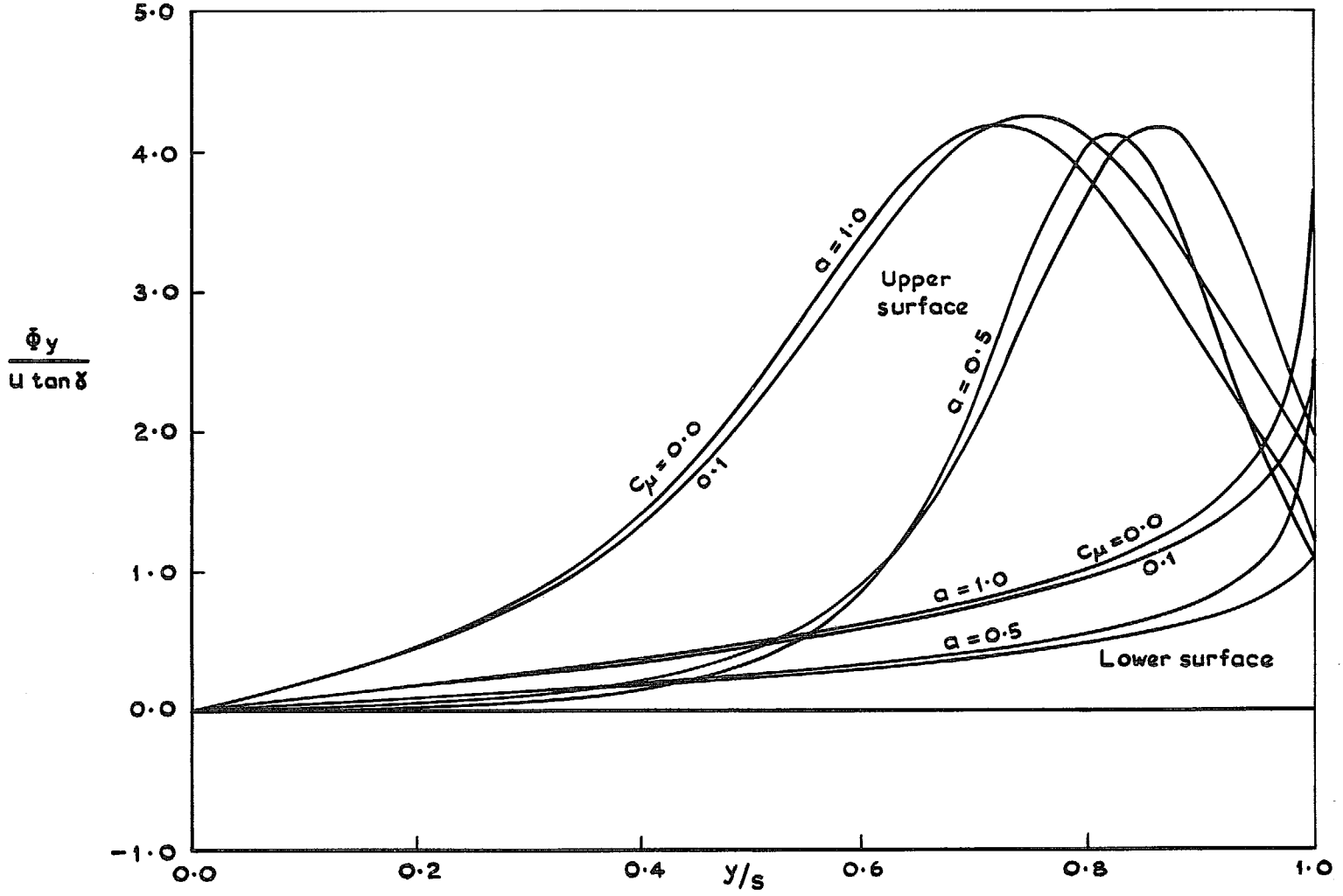

FIG. 27. Lateral velocities on wing surface, $\beta = 40°$ ($\gamma = 20°$), $N = 39$.

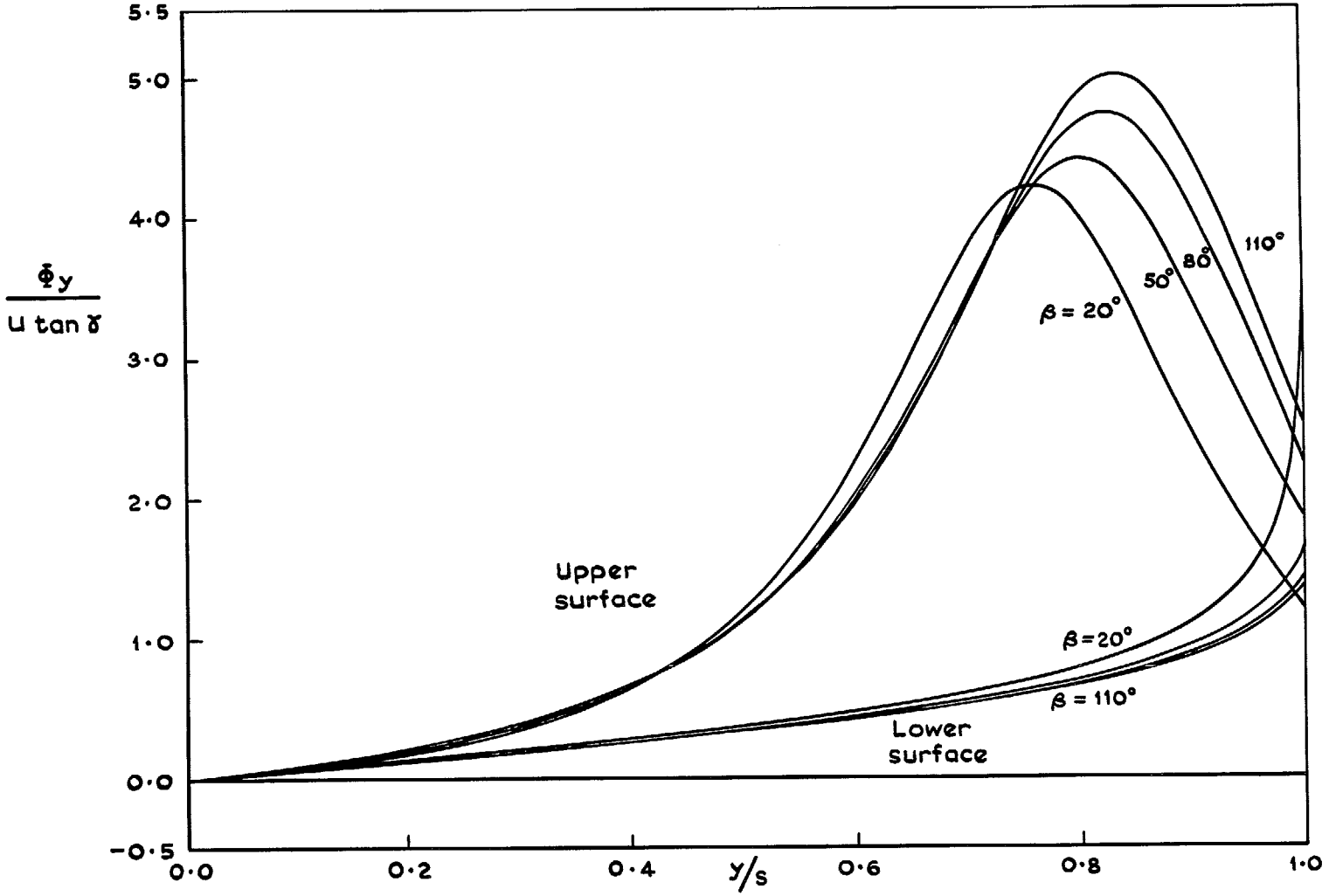

FIG. 28. Lateral velocities on wing surface, $a=0{\cdot}75$ ($\gamma=20°$), $C_\mu=0{\cdot}1$, $N=14$.

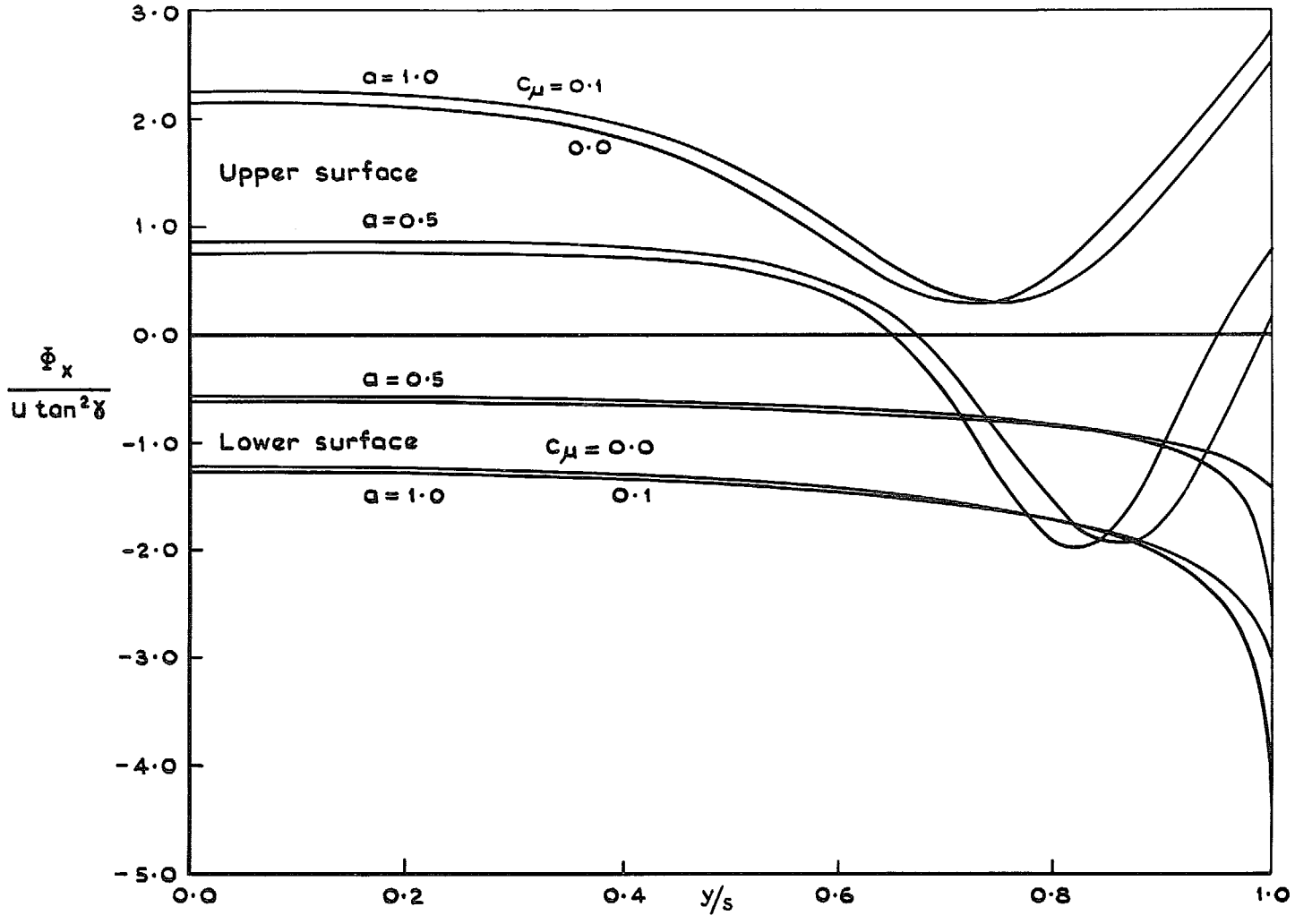

FIG. 29. Longitudinal velocities on wing surface, $\beta = 40°$ ($\gamma = 20°$), $N = 39$.

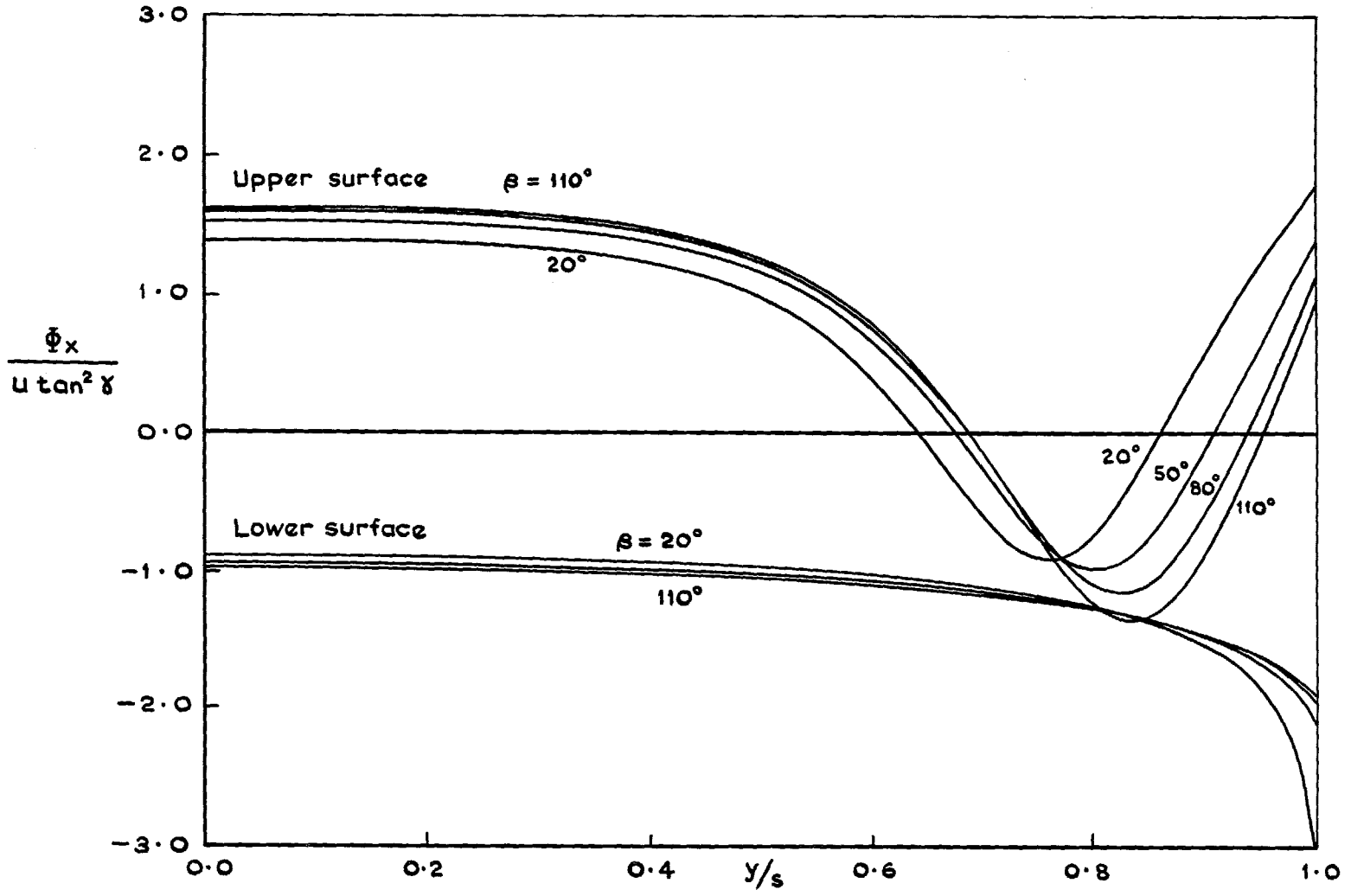

FIG. 30. Longitudinal velocities on wing surface, $a = 0{\cdot}75$ ($\gamma = 20°$), $C_\mu = 0{\cdot}1$, $N = 14$, $\beta = 20°, 50°, 80°, 110°$.

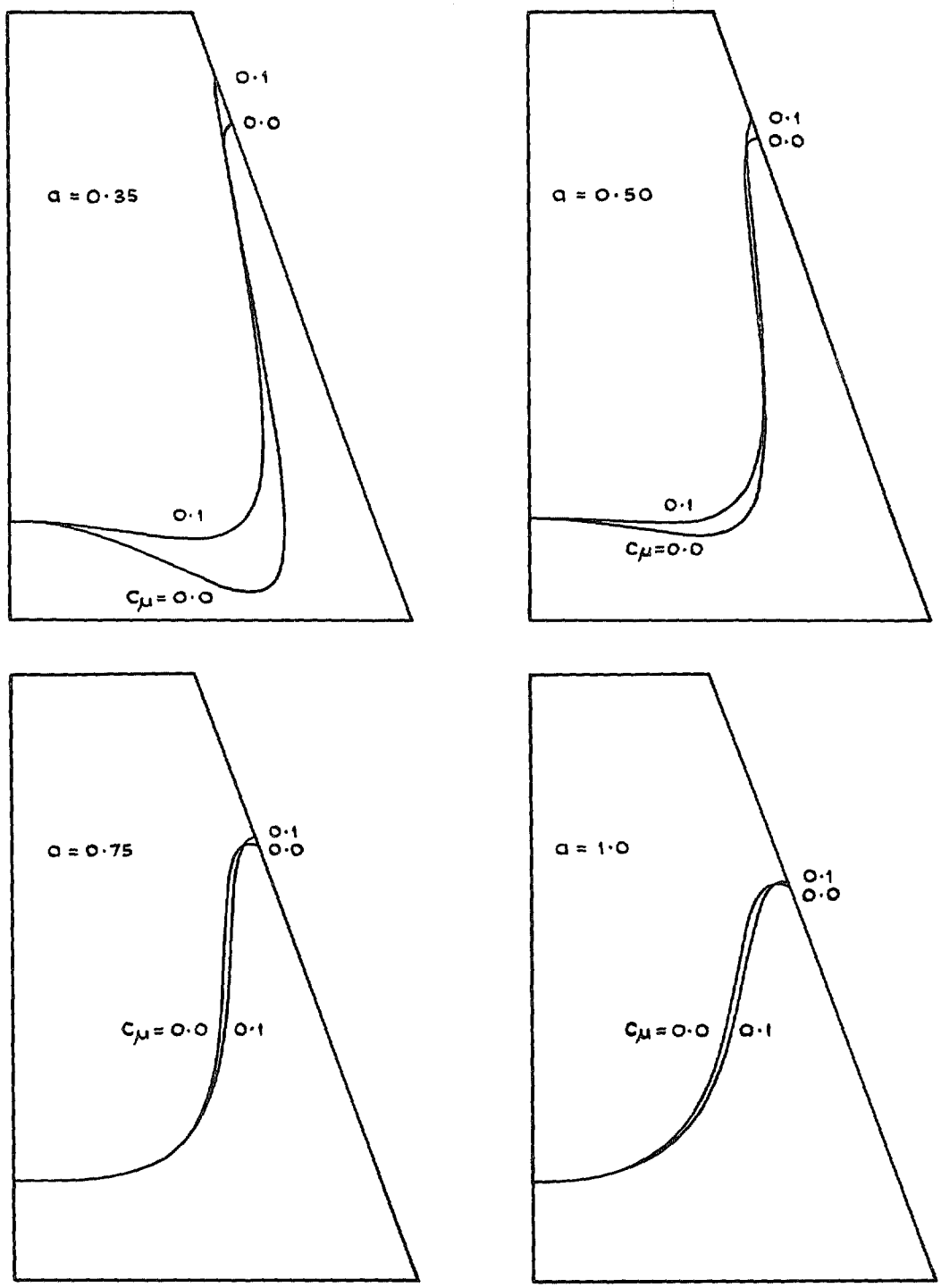

FIG. 31. Bound vortex lines, $\beta = 40°$ ($\gamma = 20°$), $N = 39$.

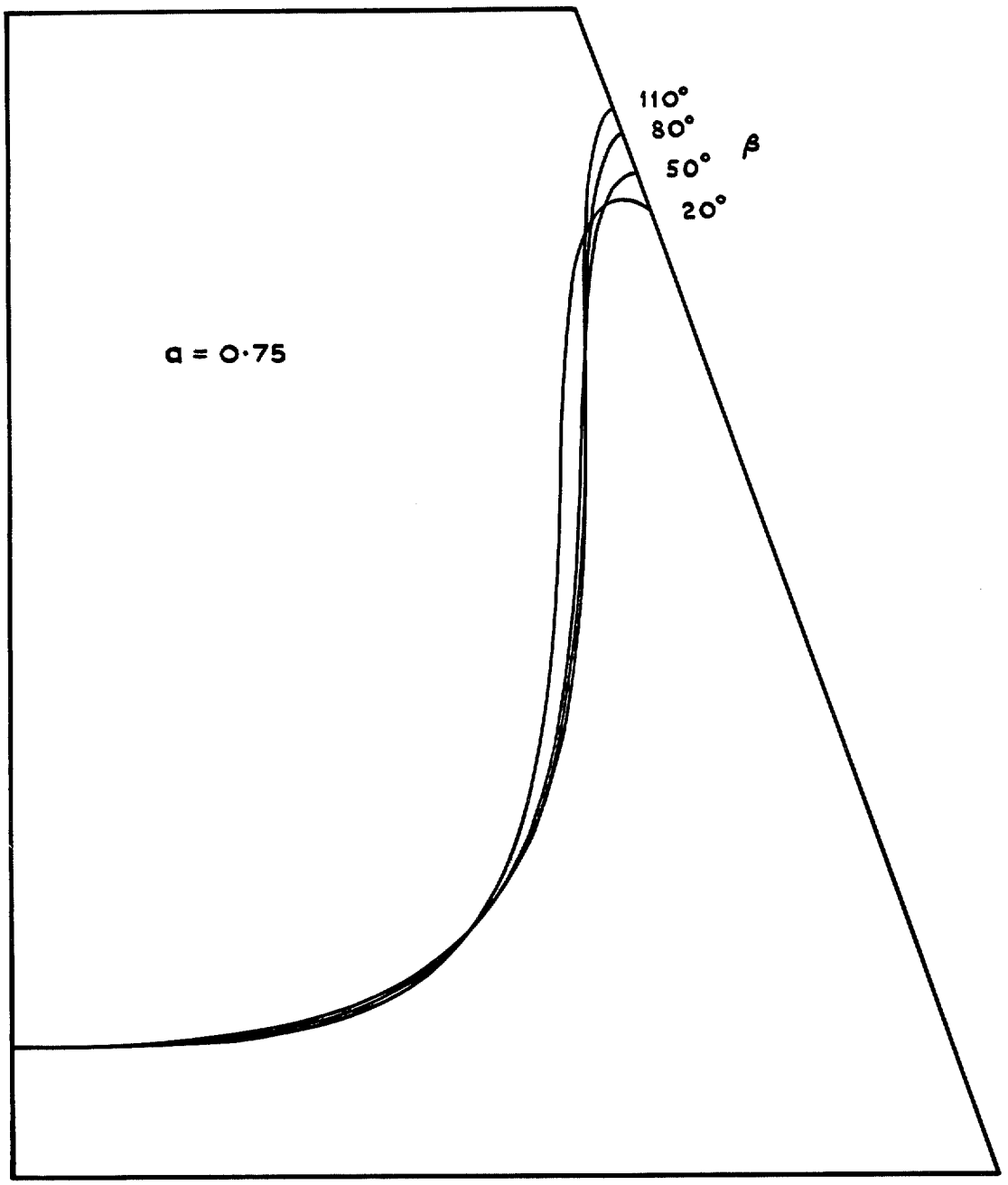

FIG. 32. Bound vortex lines, $a=0{\cdot}75$ ($\gamma=20°$), $C_\mu=0{\cdot}1$, $N=14$.

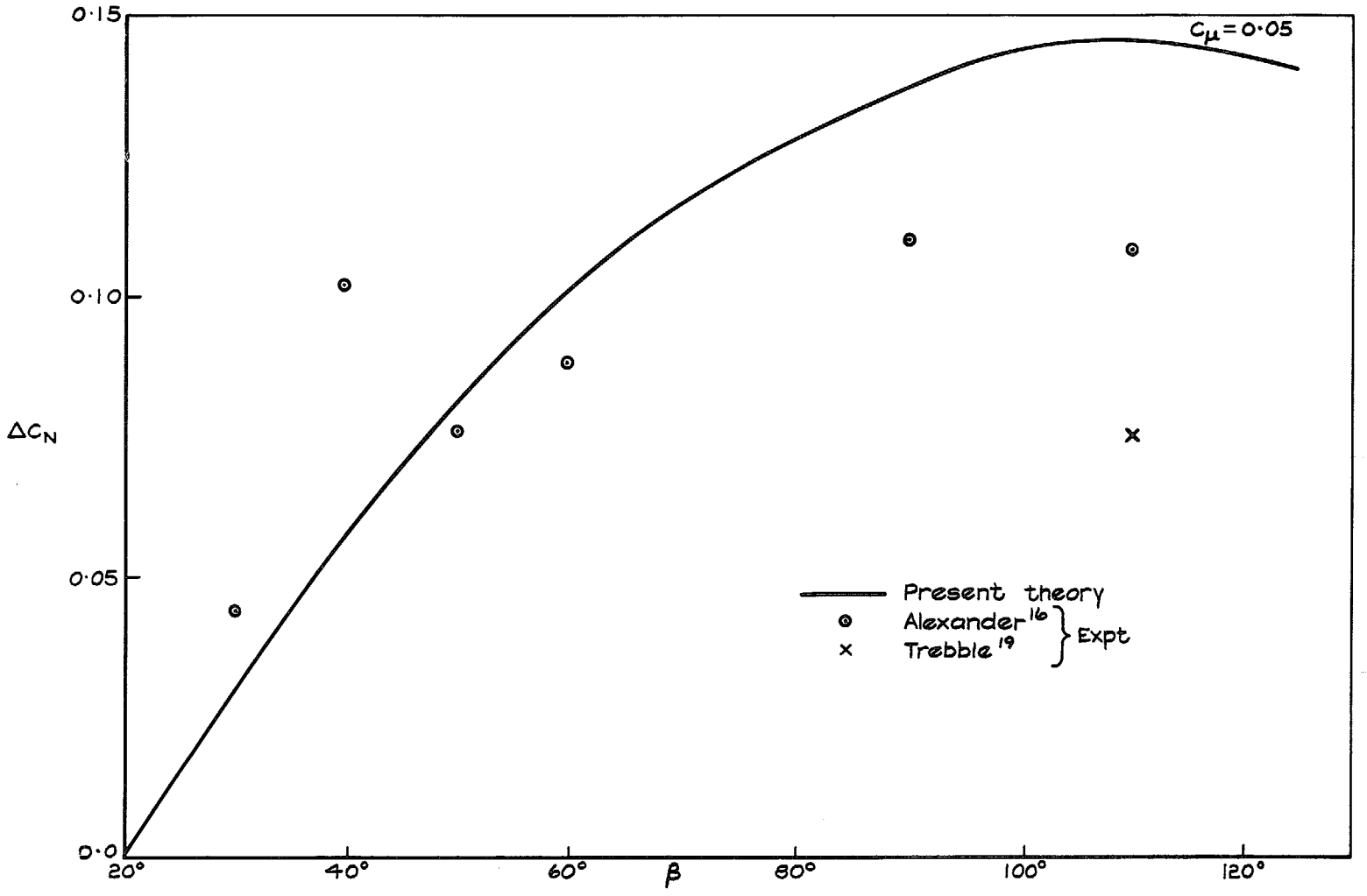

FIG. 33. Normal force increment comparison with experiment, $a = 0{\cdot}75$ ($\gamma = 20°$), $C_\mu = 0{\cdot}05$, $N = 14$.

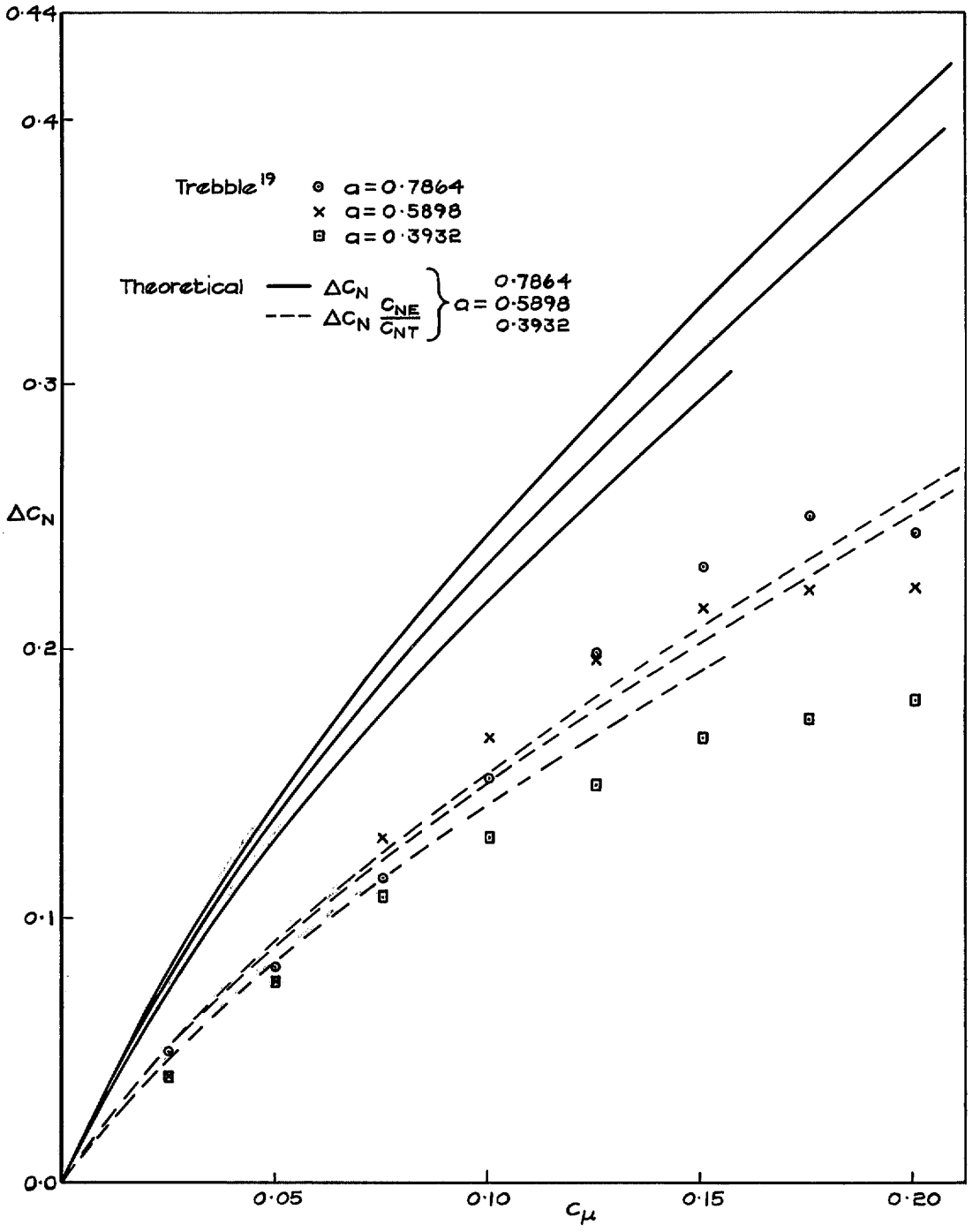

FIG. 34. Comparison of ΔC_N and $\Delta C_N \frac{C_{NE}}{C_{NT}}$ with Trebble's experimental results. $\beta = 110°$, $\gamma = 20°$.

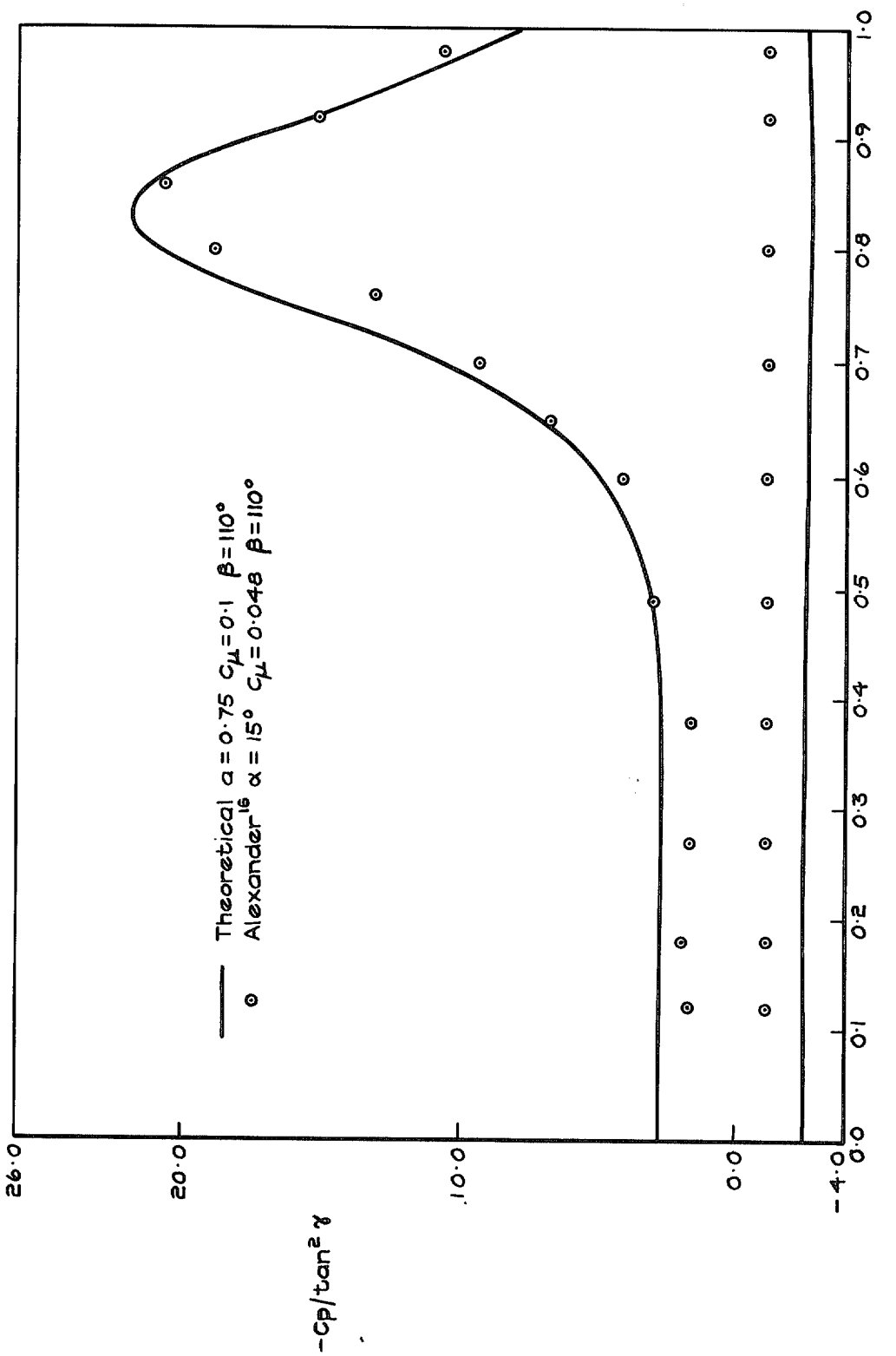

FIG. 35. Comparison of wing surface pressures with Alexander's experimental results. ($\gamma = 20°$).

Printed in Wales for Her Majesty's Stationery Office by Allens Printers (Wales) Ltd.

Dd. 502110 K.5 6/72

Published by
HER MAJESTY'S STATIONERY OFFICE

To be purchased from
49 High Holborn, London WC1V 6HB
13a Castle Street, Edinburgh EH2 3AR
109 St. Mary Street, Cardiff CF1 1JW
Brazennose Street, Manchester M60 8AS
50 Fairfax Street, Bristol BS1 3DE
258 Broad Street, Birmingham B1 2HE
80 Chichester Street, Belfast BT1 4JY
or through booksellers

R. & M. No. 3692

SBN 11 470492 9*